THE UNIVERSITY OF MICHIGAN

INDUSTRY PROGRAM OF THE COLLEGE OF ENGINEERING

A STUDY OF PRESSURE DROPS AND VOID FRACTIONS IN HORIZONTAL TWO-PHASE FLOWS OF POTASSIUM (8 PER CENT SODIUM)

Lowell R. Smith

A dissertation submitted in partial fulfillment
of the requirements for the degree of
Doctor of Philosophy in the
University of Michigan
Department of Chemical and Metallurgical Engineering
1964

April, 1964

IP-668

ACKNOWLEDGEMENTS

This study was made possible by support from The United States Air Force, Aeronautical Systems Division, Contracts AF33(616)-8277 and AF33(657)-11548, under the direction of Professor R. E. Balzhiser.

The author is grateful to the cochairmen of the doctoral committee, Professors R. E. Balzhiser and M. R. Tek, for their encouragement and advice during the course of this work. The other members of the doctoral committee, Professors J. A. Clark, D. L. Katz, and J. Louis York, gave freely of their time and made several helpful suggestions.

The author also wishes to specially acknowledge Robert E. Barry, whose determined efforts in design, startup and operation of the boiling potassium test loop were of immeasurable aid in the culmination of this study.

Since appreciation and thanks also go to:

Professor G. L. Gyorey of the Department of Nuclear Engineering for loaning the scaler used in the void fraction measurements.

Radiation Control Service for aid in procurement and handling of the gamma-ray source.

The shop personnel of the Department of Chemical and Metallurgical Engineering for assistance in construction of the void fraction equipment.

The University of Michigan Computing Center for donation of computing time.

Many individuals, too numerous to mention, who assisted in operation of the boiling potassium test loop; Dennis R. Twining and Stephen P. Werenski for assistance with calculations.

Mrs. Elaine Fritz for her conscientious efforts in preparation of the manuscript.

The Industry Program of the College of Engineering for cooperation in assembling this dissertation in its final form.

Finally, the author dedicates this work jointly to his wife, Dorothy, and his parents, in recognition of their unceasing devotion and encouragement.

TABLE OF CONTENTS

LIST OF TABLES

LIST OF TABLES (Continued)

LIST OF FIGURES

LIST OF APPENDICES

NOMENCLATURE

A	Cross sectional area of flow channel
a	Linear regression constant in Equation (F-3)
B	Constant in Andrade equation for liquid viscosity, Equation (A-3)
b	Linear regression constant in Equation (F-3)
C	Specific heat of pure liquid potassium or sodium; constant in equation for Fanning friction factor, used in Equation (14); constant defined by Equation (I-18); or constant in Andrade equation for liquid viscosity, Equation (A-3)
Cp	Specific heat
D	Diameter
E	Millivolt signal from flowmeter
f	Two-phase friction factor defined by Equation (7)
f_g	Moody single-phase friction factor for all-vapor flow at conditions of same total flow rate and temperature as two-phase flow
f_I	Two-phase friction factor for isothermal flow
f_ℓ	Moody single-phase friction factor for all-liquid flow
f_{sp}	Moody single-phase pipe flow friction factor, given by Equation (28)
G	Mass velocity based on flow channel cross section, $\dot{m}/A$. When unsubscripted denotes total value for two-phase mixture.
g	Acceleration of gravity
g_c	Gravitational conversion constant, 32.17 lbm ft/lbf sec^2
h_ℓ	Enthalpy of saturated liquid
I	Emergent intensity of radiation beam
I_g	Emergent intensity of radiation beam for all-vapor flow
I_ℓ	Emergent intensity of radiation beam for all-liquid flow
I_o	Incident intensity of radiation beam

K	Bankoff's two-phase flow parameter (8); or flowmeter calibration factor
L	Length along flow channel
M	Molecular weight of saturated vapor, given by Equation (A-15)
$\dot{m}$	Total mass flow rate
N	True gamma-ray count rate; or Ros (75) two-phase flow parameter, defined by Equation (26)
N_ℓ	Ros (75) dimensionless liquid viscosity influence number, defined by Equation (38)
n	Number of lamina in an absorbing slab; or number of data points
P	Absolute pressure; or vapor pressure
p_k^o	Vapor pressure of pure potassium
ΔP	Two-phase pressure drop
$-dP_a$	Differential pressure drop due to acceleration effects
$-dP_f$	Differential pressure drop due to friction
$\Delta P/\Delta L$	Two-phase pressure gradient
Q_1	Rate of heat transfer to preheater
Q_2	Rate of heat loss from preheater
Q_3	Rate of heat loss from heat transfer test section
Q_4	Rate of heat loss from pressure drop test section
R	Constant in perfect gas law; or Ros (75) two-phase flow parameter, defined by Equation (27)
r	Observed gamma-ray count rate
Re	Reynolds number, DG/μ
S	Velocity slip ratio given by Equation (5)
S^2	Variance operator in Equations (F-2), (F-4), (F-12) and (F-13)
T	Temperature
T_a	Absolute temperature
T_o	Reference temperature for gamma-ray calibration measurements
t	Thickness of gamma-ray absorber
U_g	Superficial vapor velocity

V	Local superficial two-phase mixture velocity
V_g	Average vapor velocity, based on cross-sectional area occupied by vapor
V_ℓ	Average liquid velocity, based on cross-sectional area occupied by liquid
V_o	Cross-sectional mean velocity for flow as total liquid
V_{sg}	Superficial gas velocity for two-phase flow
$V_{s\ell}$	Superficial liquid velocity for two-phase flow
v	Specific volume, $1/\rho$
W	Weight fraction in liquid of component denoted by subscript
X	Lockhart-Martinelli (53) two-phase flow parameter defined by Equation (12)
X_{tt}	Lockhart-Martinelli X parameter for liquid turbulent-vapor turbulent flow, defined by Equation (13)
X_{vt}	Lockhart-Martinelli X parameter for liquid viscous-vapor turbulent flow, defined by Equation (14)
x	Quality (vapor mass fraction); or when subscripted by chemical symbol, denotes mol fraction of indicated species in liquid
$\hat{x}_i$	General independent variable, used in Equations (F-2), (F-3) and (F-4)
y	Coordinate direction; or when subscripted by chemical symbol, denotes mol fraction of indicated species in vapor
$\hat{y}_i$	General dependent variable, used in Equations (F-2), (F-3) and (F-4)
z	Coordinate direction
α	Void fraction (vapor volume fraction)
Θ	Angle of inclination of flow channel from horizontal
λ	Latent heat of vaporization; or Baker (3) two-phase flow pattern parameter, defined by Equation (24)
μ	Viscosity; or linear gamma-ray absorption coefficient
μ'_K	Vapor viscosity for pure potassium; also used for sodium
(μ/ρ)	Mass gamma-ray absorption coefficient

ρ	Density
$\bar{\rho}$	Local mean density of two-phase mixture
σ	Surface tension
σ^2	Variance operator in Equations (F-7), (F-9) and (F-10)
τ	Dead time of gamma-ray detection system; or wall shear stress for two-phase flow
τ_{sp}	Wall shear stress if flow were all-liquid at same total flow rate and temperature as the two-phase flow
ϕ	Lockhart-Martinelli (53) two-phase frictional pressure drop parameter defined by Equation (1)
Ψ	Baker (3) two-phase flow pattern parameter defined by Equation (25)

Subscripts

bkg	Gamma-ray background
coll	Gamma-ray collimated beam
g	Vapor (gas) phase
K	Potassium
ℓ	Liquid phase
Na	Sodium
prop	Fluid properties
s	Solid phase
TPF	Two-phase frictional
1	Inlet to pressure drop section
2	Outlet of pressure drop section
25	Temperature indicated by thermocouple TC25. This notation is also used to refer to readings from thermocouples TC26 through TC31.

Superscript

$-$	Average value

I. INTRODUCTION

The importance of studies to provide insight into the nature of two-phase flow cannot be overemphasized. Theoretical developments are necessary to the establishment of general methods, while the gathering of reliable experimental data is essential for verification of theory and development of empirical correlations in the absence of adequate theory. Liquid-vapor flows commonly occur in boilers, evaporators, refrigerators, heat exchangers, and chemical reactors. Of recent interest are the two-phase flows which occur in atomic power plants and proposed space electrical power generation systems. The very accurate designs required in these latter applications necessitate the ability to predict two-phase flow phenomena to a high degree of accuracy.

In addition to their adaptation as coolants in atomic power reactors, liquid metals are being proposed for use as heat transfer media in space power generating systems. Although a voluminous literature exists on the subject of two-phase fluid flow, few investigations have been reported on metallic two-phase flows, and the need for such experimental studies has therefore been widely recognized.

For two-phase flow in a pipe, the pressure drop between two points in general is the summation of losses due to friction, acceleration effects, and hydrostatic head. The complex interactions between vapor and liquid, when added to the drag of the fluid phases on the pipe wall, usually lead to greater pressure losses than are experienced in single-phase flow. Such frictional losses occur for any orientation of the flow channel and for isothermal or heated conditions. The acceleration losses occur primarily in

forced-circulation boiling flows, where the continuous phase change causes the mixture density to vary along the tube. Hydrostatic head terms are present only for vertical or inclined pipes.

Knowledge of the mean density of the two-phase mixture is necessary in predicting acceleration losses and hydrostatic head. In gas-liquid flow, the mean velocities of the two phases based on the cross sectional area of each generally are not equal. Because of this inequality of velocities, referred to as "slip," the true fraction of the pipe cross section occupied by either phase differs from that calculated on the basis of the volumes of gas and liquid entering the tube. As a result of this situation, the mean mixture density cannot be calculated on the basis of quality (vapor mass fraction) alone, and knowledge of the void fraction (fraction of the channel cross section occupied by vapor) is also necessary. The void fraction, then, is an important parameter in predicting the hydraulics of many two-phase flow systems, since without it the accelerative and hydrostatic contributions to the pressure drop cannot be obtained.

The scarcity of information concerning two-phase flows of metallic systems prompted this experimental study of two-phase flows of potassium. The primary objectives of this investigation have been the following: (a) to obtain reliable pressure drop and void fraction data for potassium; (b) to present such data in a form suitable for engineering use; and (c) to determine whether any of the existing two-phase flow correlations adequately predict the potassium results.

Potassium two-phase pressure drop and void fraction data were obtained from a boiling heat transfer test loop. Two-phase mixtures were generated in a preheater section, and the pressure drops were measured over a horizontal three-foot length of 0.495-inch ID tube. The total flow rate and mixture qualities at the entrance and exit of this test section were measured. Void

fractions were measured at the middle of the pressure drop section using the gamma-ray attenuation technique.

The potassium heat transfer test loop also includes a heat transfer test section in which sodium vapor from an auxiliary pool boiler is condensed in an annulus, thereby transferring heat to two-phase potassium flowing in the central tube. Prior to making experimental runs a leak developed in this test section, allowing sodium to enter the potassium system. Although this failure prevented the accomplishment of heat transfer measurements, it did not prevent making two-phase flow runs. The result of the sodium leak is that the data reported are for flows of a potassium-sodium mixture containing 8 per cent sodium by weight. For the sake of ease in expression, the fluid will usually be referred to as potassium in this dissertation.

II. LITERATURE REVIEW

It is not possible here, nor is it the purpose, to make an exhaustive review of the two-phase flow literature. This literature is voluminous, to say the least, representing a large technical endeavor. The treatments of two-phase flow are generally empirical in nature and lend little insight into the prevailing physics of the problem. It is further noteworthy that of all the papers written on this subject, few represent fresh approaches to the problem. These facts arise from the complexity of the phenomena encountered, and do not depreciate the competence of workers in the field.

In examining the literature one finds that the majority of investigations have been concerned with two-component two-phase flows, such as occur in the air-water system. Considerably less work has been done in single-component systems, although quickening interest has led recently to intensified efforts in this area.

Although a tremendous amount of data on gas-liquid pipe flows has been published, only four basic methods of analysis have been used. The most satisfying but also most difficult approach is the analytical one. Because of the complexities encountered in two-phase flow, only two relatively simple flow regimes have been attacked by this method. Anderson and Mantzouranis (1) and Calvert and Williams (16) performed theoretical analyses of annular upward flow in vertical pipes, applying the classical von Karman-Prandtl-Nikuradse work on turbulent velocity profiles. Dukler (20) performed a similar but more advanced analysis which yielded only numerical solutions for downward annular

flows. Hewitt (34) extended Dukler's work to upward annular flows. Street (79) performed an accurate analysis of the vertical slug flow regime.

Bankoff (8) recently analyzed the bubble flow regime for vertical upward flows, proposing a variable density single-fluid model. His model supposes that the mixture flows as a suspension of bubbles in the liquid, where radial gradients exist in the concentration of the bubbles. The bubble concentration is maximum at the center of the pipe, decreasing to zero at the wall. The slippage at any point is considered negligible, and the mixture thus may be considered as a single fluid with density varying radially in the pipe. It was not possible to obtain the radial void distribution, since information on turbulent diffusivities of bubbles was lacking. Nevertheless, the model's predictions of void fractions and frictional pressure drops compared very favorably with data obtained from steam-water flows. Bankoff's approach has received wide attention since it represents a high level of creative thinking.

The second basic approach to two-component two-phase flow problems was first developed by Lockhart, Martinelli, et al. (53, 54, 56). The method predicts pressure drops and void fractions occurring in horizontal, isothermal gas-liquid flows. The authors assumed that the frictional pressure loss is the same for each phase and is equivalent to the static pressure drop, i.e., momentum losses are not considered. An empirical correlation of the following form was developed.

$$\frac{(\Delta P/\Delta L)_{TPF}}{(\Delta P/\Delta L)_g} = \phi_g^2(X) \qquad (1)$$

$$\frac{(\Delta P/\Delta L)_{TPF}}{(\Delta P/\Delta L)_\ell} = \phi_\ell^2(X)$$

where $(\Delta P/\Delta L)_{TPF}$ = two-phase frictional pressure gradient

$(\Delta P/\Delta L)_{g \text{ (or } \ell)}$ = pressure gradient computed for gas (or liquid) flowing alone in the tube at the same mass rate as in the two-phase stream

X = ratio of single-phase pressure gradients,

$$\left[\frac{(\Delta P/\Delta L)_{\ell}}{(\Delta P/\Delta L)_{g}}\right]^{0.5}$$

The Martinelli procedure utilizes a notion of "flow type" based on whether laminar ($Re < 1000$) or turbulent ($Re > 2000$) flow would exist if the phases were flowing alone. The ϕ parameters, therefore, are correlated as a function of X in four curves corresponding to the four possible flow types. Although the correlation leaves a great deal of scatter in the data, the method has been perhaps most widely used of all available correlations.

Several attempts have been made to improve the Lockhart-Martinelli approach. Hoogendoorn (37) and Chenoweth and Martin (17) presented improved correlations for high gas densities. Chisolm and Laird (18) made corrections for pipe roughness to the Martinelli correlation, and Hughmark and Pressburg (40) indicated that total mass velocity appears to be an important variable in two-phase flow. Earlier, Levy (51) in an analytical effort established that the ϕ parameters do have theoretical significance.

The third type of approach to two-phase flow is through the friction factor concept, which has been used for both horizontal and vertical cases. Govier and co-workers (14, 15, 28, 29, 30) treated the two-phase system as a single phase and presented plots of friction factor as a function of Reynolds number with gas-liquid ratio taken as a parameter. Bertuzzi, Tek, and Poettmann (13) used the same general technique to achieve a correlation for horizontal flows which they claimed to be independent of flow pattern. Their correlation curves did show a shift with liquid phase Reynolds number.

The fourth basic approach is illustrated by the work of Ros (75) who performed a general dimensional analysis on vertical two-phase pipe flow. He considered twelve independent variables which account for geometry, liquid and gas physical properties, flow properties, and interactions between phases. Using pressure gradient and liquid holdup as dependent variables, he obtained ten dimensionless groups. Some groups were eliminated because they were physically insignificant in the subsequent experiments. After treating 20,000 experimental points, Ros found only four of the original nine groups had significant effect on pressure drop. His resulting correlation for frictional pressure gradient and liquid holdup involve a rather large number of constants. Although the method is strictly empirical, Ros' correlation does give impressive accuracy.

Most of the literature mentioned so far has been concerned with two-component flows. Linning (52) and Pike (66) performed analyses of horizontal, adiabatic flows of pure evaporating fluids in pipes. The flows were assumed to be in the annular regime, and the authors achieved excellent agreement with their steam-water experiments. Pike's void fraction predictions were within $\pm$ 10 per cent of measured values. His model produced a series of non-linear differential equations which took into account different phase velocities, fluid accelerations, wall shear forces, interface shear forces, and mass and energy transfer between the phases. Pike's analysis is similar to Linning's, but Pike's model did not require information concerning flow variables at some point downstream from the point of initial vaporization, as was the case with Linning's model.

It must be recognized that the pressure drop occurring in the flow of a pure fluid which is boiling or flashing includes, in addition to the frictional loss, a loss resulting from rate of increase of momentum. Such momentum losses are often quite significant, and in order to predict them one needs to know the true gas velocity, demanding in turn knowledge of void fractions. The analyses of Linning (52) and Pike (66) accounted for the momentum effects. A very early

attempt to predict boiling pressure drops resulted in the still widely used method of Martinelli and Nelson (55). Their correlation is based on few data and is strictly valid only for steam-water flows. The correlation resulted from an integration of the Lockhart-Martinelli correlation (53), thus accounting for changing quality. However, since the Lockhart-Martinelli method was based primarily upon air-water data, an empirical extrapolation was necessary to make predictions agree with expectations at the critical pressure. Working charts are given which can be used in making rough pressure drop estimates. Goldmann (27) recently extended the Martinelli-Nelson method to sodium flows. His results are purely computational and have yet to be verified by experiment.

Soviet workers have been interested in two-phase flow in boiling systems. Armand (2) correlated the ratio of two-phase pressure gradient as a function of volumetric steam content, taking the ratio of volumetric steam content to void fraction as a parameter. Kutateladze, et al. (48) report the results of Lozhkin, Krol, and Gremilov who studied two-phase mercury flow. They report that wetting has negligible effect on two-phase mercury flow systems, and they propose the following equation for pressure drop.

$$\Delta p = \frac{f_\ell V_o^2 \rho_\ell L}{2 g_c D} \left[1 + \left(1 - \frac{\rho_g}{\rho_\ell} \right) \frac{U_g}{V_o} \right] \qquad (2)$$

The discussion thus far has said little about void fractions, although it was recognized that this parameter appears to be fundamental in the correlation and interpretation of two-phase phenomena. Indeed, most of the analytical approaches produce void fraction as a variable. The Martinelli methods (53, 55) give empirical correlations for void fractions occurring in horizontal flows, and Ros' work (75) gives values for vertical flows based on his empirical treatment. Linning (56), Pike (66), and Bankoff (8), paid particular attention to prediction of void fraction values in their analytical treatments. Hughmark

(39) recently published a method for determination of liquid holdup (one minus the void fraction) in gas-liquid flow.

Levy (49, 50) in some high-level analytical work has tried to predict void fractions (as well as pressure drops). One of his efforts resulted in a momentum model (50) for predicting slip phenomena--the condition, due to unequal density and viscosity between gas and liquid, in which the gas flows at a higher relative velocity than the liquid. The model gave reasonably good agreement with available experimental results for steam-water horizontal and vertical flows with and without heat transfer, at pressures from 12 to 2000 psia. In a very recent paper (49), Levy treated the two-phase system as a continuous medium and applied to it the single-phase turbulent mixing length methods. Two-phase density and velocity distributions as well as pressure drops were thus derived analytically. Good agreement was found between theoretical predictions and available data.

A number of papers have presented void fraction data, at the same time emphasizing the experimental techniques used. Radiation (primarily gamma-ray) attenuation has been the most widely utilized technique for obtaining void fractions. Maurer(58), Petrick (65), Hooker and Popper (38), and Richardson (74) all give good developments of the theory of gamma-ray attenuation as applied to measuring void fractions. Petrick (65) and Richardson (74) developed a traversing technique in which a narrow gamma beam is passed across the pipe. This technique was shown to be superior to the "one-shot" method, especially for wide flow channels. These authors present void fraction data for flows in vertical and horizontal rectangular channels. They also determined the effect of a sudden change in flow area on significant parameters and present pressure drop measurements as well. Hooker and Popper (38), in addition to developing the basic theory for void fraction measurements by radiation attenuation, analyze the principal sources of error inherent in the method and evaluate

their magnitude for a specific test facility. Maurer (58) presents an excellent review of the method, summarizing the apparatus used by many previous workers. Egen, Dingee, and Chastain (23) obtained void fractions occurring in forced circulation boiling of water in a vertical rectangular test section at 2000 psia. Their paper also furnished an excellent discussion of temperature effects on the gamma-ray attenuation method.

Other methods are available for measuring void fractions, although they are less widely employed. Heineman, Marchaterre and Mehta (33) have used electromagnetic flowmeters to measure void fractions in two-phase metallic flows. The flowmeters must be calibrated before use, and the method is applicable to vertical flow channels in which the quality is less than 0.01. This restricts the void fractions to values below about 0.65. It should be mentioned that the gamma-ray method is good up to qualities of about 0.15. Neal and Bankoff (63) developed an electrical resistivity probe which allows high-order resulution of local void fraction, bubble frequency, and bubble size distribution function in two-phase flows in the bubble regime. The probe was satisfactorily tested in a mercury-nitrogen system. This technique is good only for two-phase flows where the liquid phase is electrically conducting.

Of the several papers cited so far, few have included work in metallic systems. Indeed, few investigations to date have been involved with metallic fluids. As previously mentioned, Kutateladze, et al. (48) summarize the results of Gremilov and co-workers who studied the vapor-liquid flows of mercury. Kutateladze (48) also presents Siryi's results for the mercury-mercury vapor system as well as those of Korneev who worked with a magnesium amalgam-mercury vapor system. These workers obtained void fraction values and correlated them against the ratio of superficial vapor velocity to total liquid velocity, using an all-liquid Froude number as a parameter. Froude numbers were between 1 and 20. Smith, Tang, and Walker (78) obtained void fractions occurring in two-phase

flows of mercury. The Froude numbers reported in this investigation were of the order of 10^{-4}. A correlation similar to Gremilov's was given. Tang, Smith, and Ross recently extended this work to the potassium-mercury amalgam system (80). They found that their potassium amalgam data did not correlate with the mercury data of reference (78) when the original method of correlation was attempted. However, a satisfactory correlation of the Martinelli type (53) was obtained.

Neal (62) describes the same electrical probe as in reference (63) and also discusses development of an impact probe for measuring local liquid velocity. These instruments were used to measure local parameters in cocurrent mercury-nitrogen flow. A concomitant photographic study showed that the structure of mercury-nitrogen flow is much different from air-water flow, rendering inapplicable the air-water correlations.

Recently Baroczy (9) presented a generalized void fraction correlation and proposed its use for all fluid systems, including liquid metals. The correlation is based on water-air and mercury-nitrogen data. Verification of the correlation with single-component metallic systems was not possible, due to a lack of data. The correlation, which is of the Martinelli type, predicted other steam-water data and data for an organic coolant quite accurately. On the basis of this agreement, calculated values are offered for single-component flows of sodium, potassium, rubidium, and mercury.

This discussion, as mentioned at the outset, does not provide an exhaustive review of the two-phase flow literature. It was intended to cite work which is pertinent to the potassium studies. More and more experimental work in liquid metals is reaching the reporting stage (70, 71). Some work involving several aspects of two-phase flow was presented in a recent symposium (72), but none of the studies was specifically concerned with metallic systems. Several bibliographies are available which may be referred to for a more complete coverage of the two-phase flow literature (7, 11, 31, 41, 57, 87).

III. DESCRIPTION OF EQUIPMENT

1. The Potassium Test Loop

Initial design studies for the boiling potassium test loop resulted in the specification of the following operating conditions:

Fluid operating temperatures	1400-1800°F
Design pressure	200 psia
Flow rate	0.2 - 2.0 gpm
Total electrical power input	40 KW
Heat flux at the heat transfer test section	1×10^6 Btu/(hr)(sq ft)
Nominal ID of heat transfer and two-phase pressure drop sections	0.5 inch

Because of widespread interest in its forced circulation boiling heat transfer and two-phase flow characteristics, potassium had been chosen as the working fluid. Availability and low cost were also influential in its choice. The 1800°F maximum operating temperature was specified to permit use of Haynes-25 alloy* in the critical sections, rather than a refractory metal. The latter material would have necessitated enclosing the loop in an evacuated chamber and added substantially to the cost. The specified operating conditions were to allow the attainment of 100 per cent quality in the heat transfer section at 2 gpm total flow, assuming no losses.

The most critical component of the loop was the heat transfer test section where extremely high heat fluxes were desired. Several possible

---

* This alloy is also referred to as L-605 metal. Nominal composition in weight per cent is 10-Ni, 20-Cr, 3 (maximum)-Fe, 15-W, 0.1-C, 1.0 (maximum)-Si, 2-Mn, and 48.9-Co.

types of heating were considered: resistance heating, radiant heating, induction heating, liquid-liquid heat exchange, and condensing vapor. A detailed account of the advantages and disadvantages inherent in the above methods is available (7). It was decided to provide the high heat fluxes to potassium by condensing sodium vapor on a very thin walled tube. This method had the advantage of low cost and elimination of a possible burnout problem since the flux was controlled by the temperature differential. A major disadvantage was the inability to place a thermocouple in the thin tube wall. This design choice thus led to the utilization of two separate fluid circuits.

The two-phase pressure drop test section is of primary concern in the study reported here. The design of this section was in no way critical, but a system of impractical dimensions was to be avoided. The major consideration was to specify a test section that would not limit the other necessary operating characteristics of the loop--i.e., not to cause pressure drops which would be a large fraction of the pump's output head. At the same time, it was necessary to provide a test section whose length-to-diameter ratio would assure measurable two-phase pressure drop values for the conditions of quality, flow rate and absolute pressure level anticipated. Two-phase pressure drop values were estimated using the well-known correlation of Lockhart and Martinelli (53) . These predictions led to the specification of a test section having an overall length of 3 feet and an ID of 0.495 inches.

Cost considerations restricted the measurement in the two-phase flow test section to an overall pressure drop value rather than a pressure profile. The latter experimental measurements would require several pressure taps and would lead to a much more complicated transducing system than was finally employed. The disadvantage in only measuring overall pressure drops was more than offset by the fact that a commercially available direct-reading differ-

tial pressure gauge could be used. The differential gauge was available with suitable modifications for this high-temperature application.

Mine Safety Appliance Research Corporation (referred to as MSAR), Callery, Pennsylvania, did much of the design and all of the construction of the loop.

1.1 Loop Flow Scheme

A schematic flow diagram of the entire boiling liquid metal system is shown in Figure 1. In this system two separate fluid circuits are employed. The primary circuit contains potassium as the working fluid, and the secondary circuit contains sodium. The liquid metal in the primary circuit is pumped by an electromagnetic pump through a throttle valve and an electromagnetic flowmeter. The flow is then equally distributed into the three parallel heating sections of the preheater and exits into a common header at the heat transfer test section inlet. The liquid metal flows through the tube side of the heat transfer section and passes through the pressure drop test section which is horizontal. The flow then continues into a condenser section and into a hot well. From the hot well the liquid is returned to the pump after passing through a subcooler. In the secondary circuit, the sodium is vaporized in the boiler section, condensed in the shell side of the heat transfer section, and returned by gravity to the boiler.

Each circuit is equipped with a supply tank from which the system can be charged and into which liquid metal can be dumped. The supply tanks may be evacuated or pressurized with argon. Each circuit is also equipped with a diffusional cold trap for maintenance of low oxide concentration. Valves and auxiliary lines are located in each circuit for bleeding, pressurizing, venting, levelling, and draining.

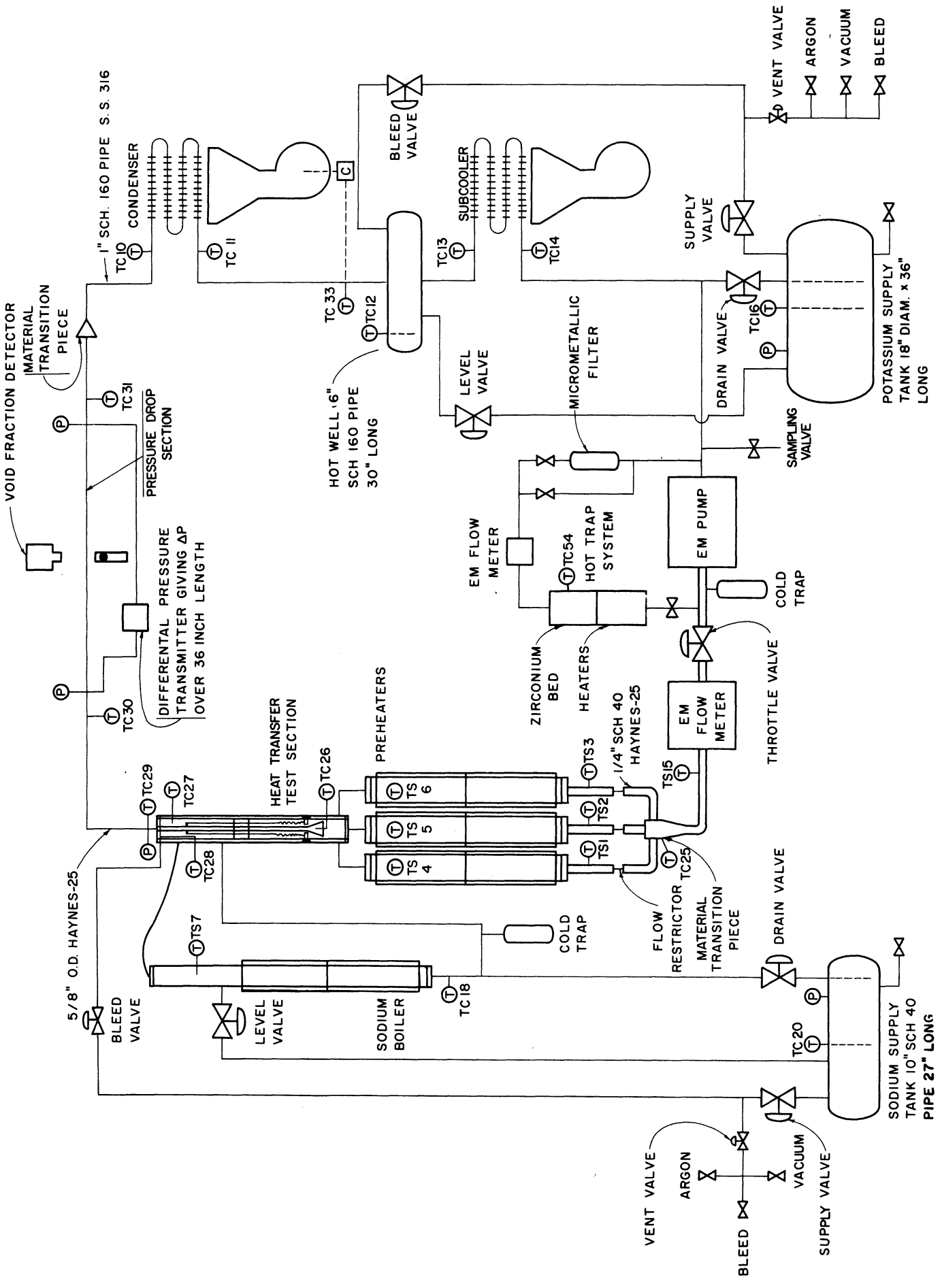

Figure 1. Flow Schematic--Boiling Liquid Metal System

1.2 Important Loop Components

Major components of the primary fluid circuit are discussed here, with the exception of the pressure drop measurement section. The secondary system is not of major concern in this study and will not be discussed. Thorough descriptions of it are available (6, 60). Most of the major primary circuit components are shown in Figures 2, 3 and 4.

Pump: This is an MSAR Style II electromagnetic conduction pump, shown in Figures 2 and 3. Alternating current passes through the liquid metal at right angles to a magnetic field. The resultant force, perpendicular to both the electric and magnetic fields, causes the liquid metal to flow through the pump and develop the head necessary to transport it through the circuit.

The pumping section consists of a 1-foot length of 3/8-inch stainless tube flattened to provide an inside width of 1/16 inch. The developed pressure is rated at 100 psi at no flow and 80 psi at 2 gpm. The flow rate is controlled by varying the applied voltage from 0 to 270 V with a variable transformer or by regulating the throttle valve. A 10 KVA capacitor is connected across the pump to correct the power factor and reduce the required line current. The pump is equipped with two blowers for cooling the magnetic field coils.

Throttle Valve: This valve is a 1/4-inch Hi-100 stainless steel control valve manufactured by the General Kinetics Corporation. It is a bellows sealed ball valve. The variable ball position is obtained from response to a 3-15 psig air signal. The valve is shown in Figures 3 and 4.

Flowmeter: The flow rate in the potassium circuit is measured by an MSAR style FM-2 magnetic flowmeter, which is shown in Figure 4. Two voltage tabs are diametrically mounted on a 3/8-inch by 0.050-inch wall stainless steel tube and perpendicular to the field of a permanent magnet. The flowing liquid metal cuts the lines of force of the magnet and generates a

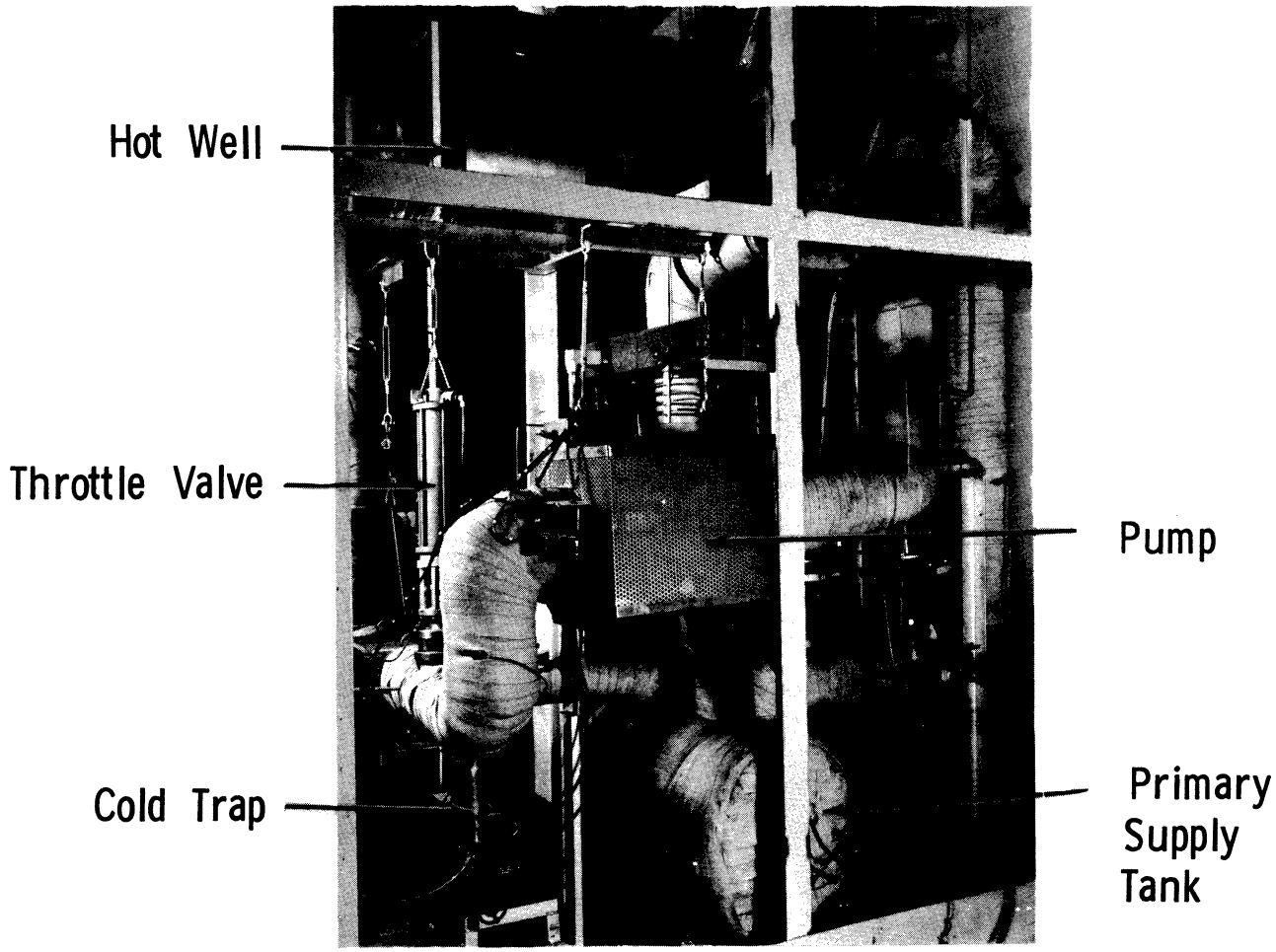

Figure 2. Potassium Boiling Heat Transfer Test Loop, North Elevation

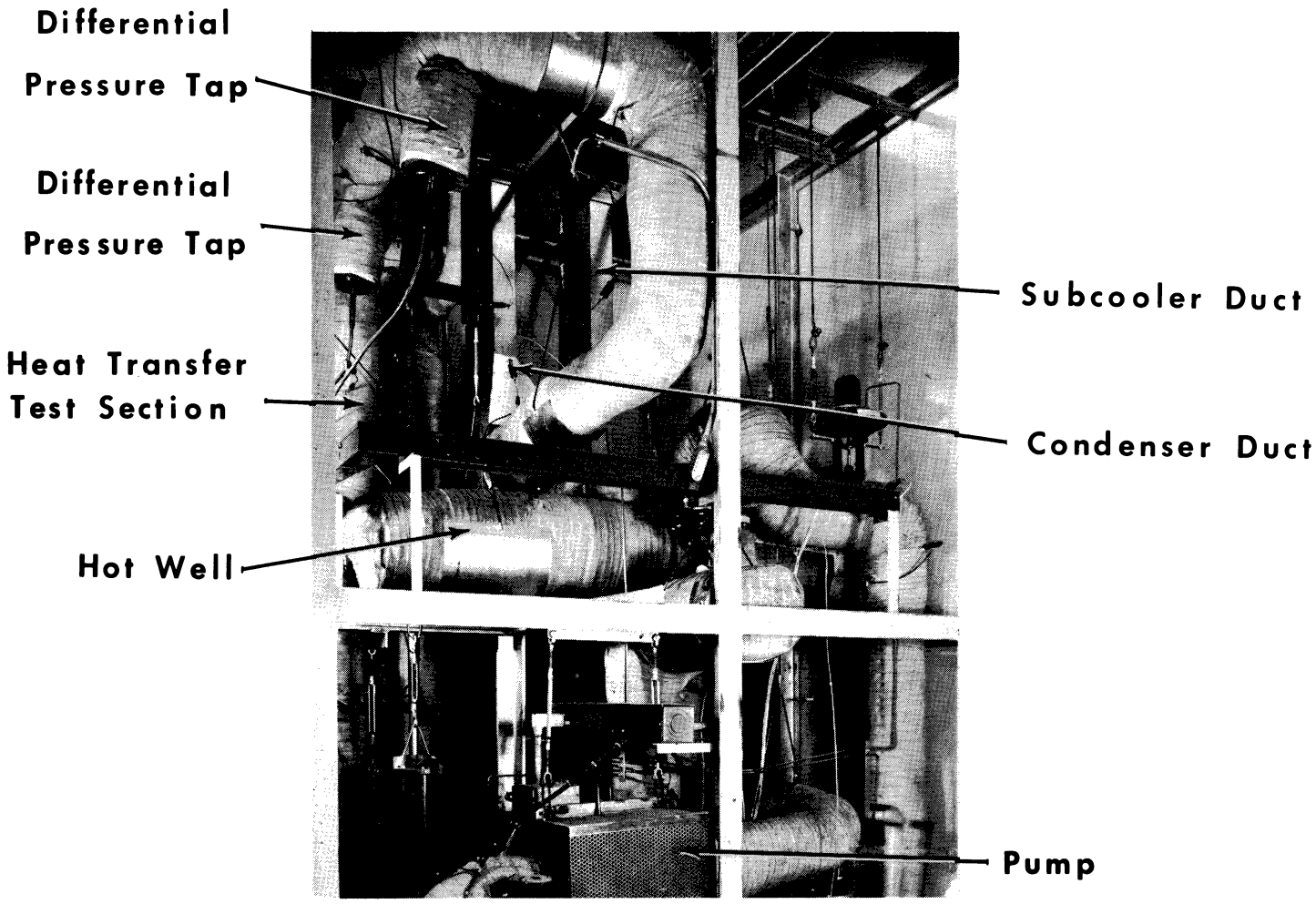

Figure 3. Potassium Boiling Heat Transfer Test Loop, North Elevation

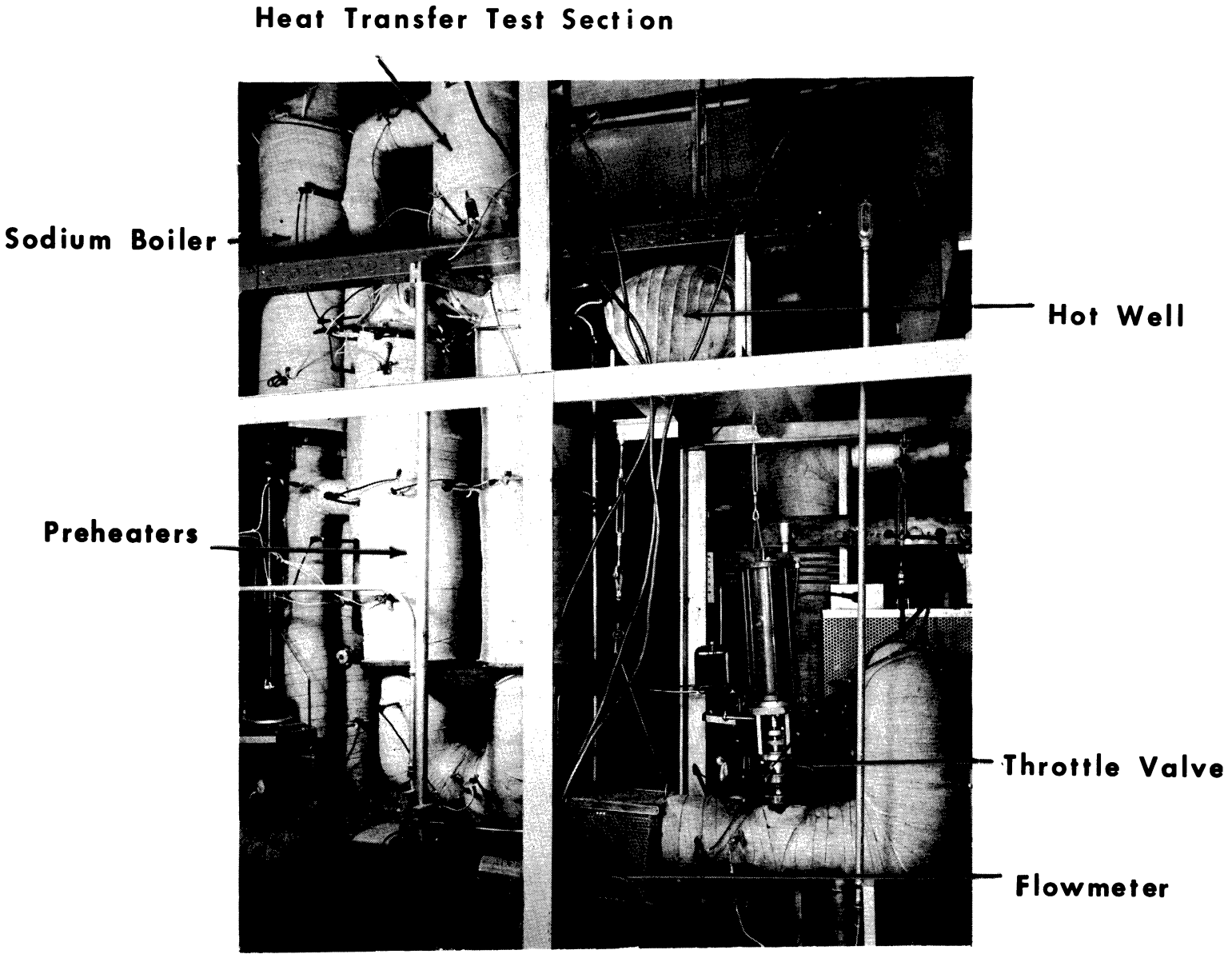

Figure 4. Potassium Boiling Heat Transfer Test Loop, East Elevation

voltage which is proportional to the flow rate. A calibration curve for converting millivolt readings to gpm, as a function of metering temperature, was supplied with the meter. Metering temperature was measured by a chromel-alumel thermocouple mounted on the meter tube surface (Thermocouple TS 15).

A discussion of the calibration and accuracy of the flowmeter is given in Appendix B.

Preheater: This is shown in Figure 4 and consists of three sections of 4-inch OD by 3-inch ID by 45-inches long Haynes-25 pipe mounted in parallel. Approximately 3 feet of each section are heated by four radiant heaters. These are half circular Hevi-Duty Type 5718 KSP heaters, each rated at 2.5 KW at 230 V and with an allowable element temperature of 2200°F. The twelve units provide for a total of 30 KW rated power. To help maintain uniform flow in each section, an orifice is located in each inlet line.

The preheater pipes were mounted in parallel to reduce the height of the unit. An experimental program was conducted on a full scale plexiglas model of this arrangement using air and water (5). It was demonstrated that such an arrangement would provide reasonably stable flow (as opposed to slug type flow) in the test section if a funnel was placed above the point where the three streams merge prior to entering the test section.

As indicated in Figure 1, entrance, exit, and exterior wall temperatures of the preheaters are monitored.

Heat Transfer Test Section: The location of this section is indicated in Figures 3 and 4. The mechanical design is quite complicated, the details of which are available elsewhere (6, 60). Figure 1 shows the essential features. This test section was designed to deliver heat fluxes up to 1×10^6 Btu/(hr)(sq ft) to a 2-inch long section of 1/2-inch OD by 0.010-inch wall Haynes-25 tube. The flows from the preheater (which may be two-phase or single-phase) tangentially enter the bottom of a 4-inch OD by 3-inch ID by

36.5-inches long Haynes-25 pipe. The fluid next enters a funnel leading to 23 inches of the 1/2-inch OD tube. All but 2 inches of this tube are enclosed in a heat shield consisting of 1-inch pipe welded to the 1/2-inch tube at the top and connected to the 4-inch pipe by means of a bellows assembly. The exposed 2 inch length of 1/2-inch tube functions as the heat transfer test section.

In operation, sodium vapor tangentially enters the top of the 4-inch pipe and condenses on the exposed 2 inches of tubing. The condensate runs down the annular space between the 1-inch and 4-inch pipes, exits through an overflow pipe (half way up the 4-inch pipe), and returns by gravity to the sodium boiler.

A total of six temperature readings are made in the heat transfer section. Two of these are made with chromel-alumel thermocouples near the bellows, in order to monitor process conditions there. The remaining four are platinum/platinum plus 10 per cent rhodium thermocouples which give readings pertinent to the heat transfer experiments. These four thermocouples are indicated in Figure 1. Readings from thermocouple TC26 are also important in the two-phase flow study, as will be shown later. A short discussion of the temperature measurement facilities, together with a tabulation of important thermocouples (Table I), will be given subsequently.

Absolute pressure is read at the test section outlet by means of a Taylor Instrument Company diaphragm type sensing element, back filled with sodium-potassium eutectic alloy leading to a pneumatic transmitter.

Condenser and Subcooler: The condenser, indicated in Figure 3, is fabricated from 10 feet of 1-inch, schedule 160, stainless steel finned tube and encased in a blower duct. Air is supplied by an 800 scfm blower, and the condenser is sized to remove a load of 105,000 Btu/hr (potassium vapors at 1500°F) with an air exit temperature of 500°F. Air flow is controlled

by adjustable louvres at the discharge of the blower. The louvre may be positioned by an automatic controller or else manually.

The subcooler, indicated in Figure 3, is identical in design to the condenser, except that it is used in all-liquid service. The subcooler's specific function is to cool hot liquid to 1400°F before it enters the pump. The louvre position for the subcooler is set manually.

Inlet and outlet temperatures for both these heat exchange units are monitored by well type chromel-alumel thermocouples, as indicated in Figure 1.

Hotwell: The hotwell is a horizontal 54-inches long section of 6-inch, schedule 160, stainless steel pipe. It is shown in Figures 2, 3 and 4. It is located between the condenser and subcooler and serves a number of purposes. Primarily, it assures an all-liquid flow through the sub-cooler and thus a liquid level above the pump even in the event of large flow rate instabilities. It also acts as an accumulating chamber for non-condensibles and as an expansion tank for liquid, the total volume of which may vary with temperature changes and vapor fraction changes in the loop.

As indicated in Figure 1, the loop may be pressurized with argon in the hot well, by means of the primary vent and bleed valves, for non-boiling operation. The loop may also be evacuated in this way. Other auxiliary piping connects the hot well with the supply tank via two separate routes. The bleed line runs from the top of the hot well to the bleed valve, then down to the supply valve and supply tank. The level line, which extends 1 inch up from the hot well bottom, runs straight down to the level valve and continues to the supply tank.

The temperature in the middle of the hot well is monitored with a chromel-alumel thermocouple.

Valves: In addition to the throttle valve, the primary circuit has five air-operated valves: the bleed, drain, level, supply and vent valves.

These are 1/2-inch bellows sealed globe valves, Model HY473, manufactured by Hoke, Inc. They are designed for liquid metal service at 1500°F and 50 psig.

Three other valves--in the hot trap system--may be noted in Figure 1. These also are Hoke bellows sealed 1/2-inch globe valves, manually operated.

Piping: The preheater, test section, and pressure drop section are constructed of Haynes-25 alloy. From the pressure drop section to the subcooler 1-inch, schedule 160, 316 stainless steel pipe is used. From the subcooler to the preheater inlet 1/2-inch pipe of the same material and schedule is used. All lines are traced with electrical warm-up heaters which are controlled by switches at the loop control panel. A complete resume of the trace heater ratings and circuitry is given in reference (60) . Surface thermocouples to measure system temperatures during heat-up and operation are furnished at many points in the piping system. Full details of the loop piping assembly are given in reference (60).

Hot Trap System: Extreme difficulties in startup of the test loop were experienced due to oxide plugging of the pump, flowmeter, and throttle valve. It was eventually determined that the only way to eliminate the oxide problem was to install a hot trap assembly for "gettering" the oxygen out of the system. This assembly is indicated in Figure 1.

The hot trap consists of a 4-foot bed of zirconium chips connected in parallel with the main line of the primary circuit, across the inlet and outlet of the pump. A portion of the loop flow can be recycled through the hot trap at 1200°F (heating accomplished by Hevi-Duty heaters similar to those in the preheater) where the zirconium removes the oxygen from the potassium. The hot trap system includes an MSAR magnetic flowmeter and a micrometallic filter. The latter component removes large particles from the system and may be included or excluded from operation by means of a valving assembly. Operation of the hot trap satisfactorily solved the oxide plugging problem.

1.3 Control and Safety Features

The loop control panel, shown in Figure 5, was assembled by R. T. Brokaw and Company, Ann Arbor, Michigan. It is located in an adjoining room. In normal circumstances, the control panel has all facilities necessary for complete remote operation of the loop.

Superior Electric Company Powerstat variable transformers control the voltage to the preheaters, sodium boiler, and pump. Electrical power to the preheaters and sodium boiler is read on General Electric AC Kilowatt meters. The positions of the throttle valve, subcooler louvre, and both drain valves are controlled by manually operated air pressure regulators. As mentioned previously, the condenser louvre may be controlled either automatically or manually. All the air-operated valves (including the drain valves) are controlled by solenoids actuated by switches on the control panel. A 12-point recorder for the chromel-alumel monitoring thermocouples and the instruments for the Pt/PtRh thermocouple read-outs are located on the panel. The millivolt signal from the flowmeter can be read on a millivoltmeter, read on a potentiometer, or recorded on the Taylor Transcope recorder. Many of the major panel components can be distinguished in Figure 5.

The hazards of working with boiling alkali metals are well known, and several safety features of the loop are worthy of mention. It was noted that absolute pressure in the loop is monitored at the heat transfer section outlet. A safety interlock is provided to shut off the preheater power in the event of high loop pressure. Thermocouples on the walls of the preheaters are connected to a Wheelco temperature indicator equipped with a high temperature alarm. This instrument automatically cuts off the preheaters in the event of a temperature excursion. A thermocouple on the sodium boiler wall is similarly connected. The millivolt signal from the flowmeter, in addition to the other read-out methods mentioned above, can be read out on a Wheelco

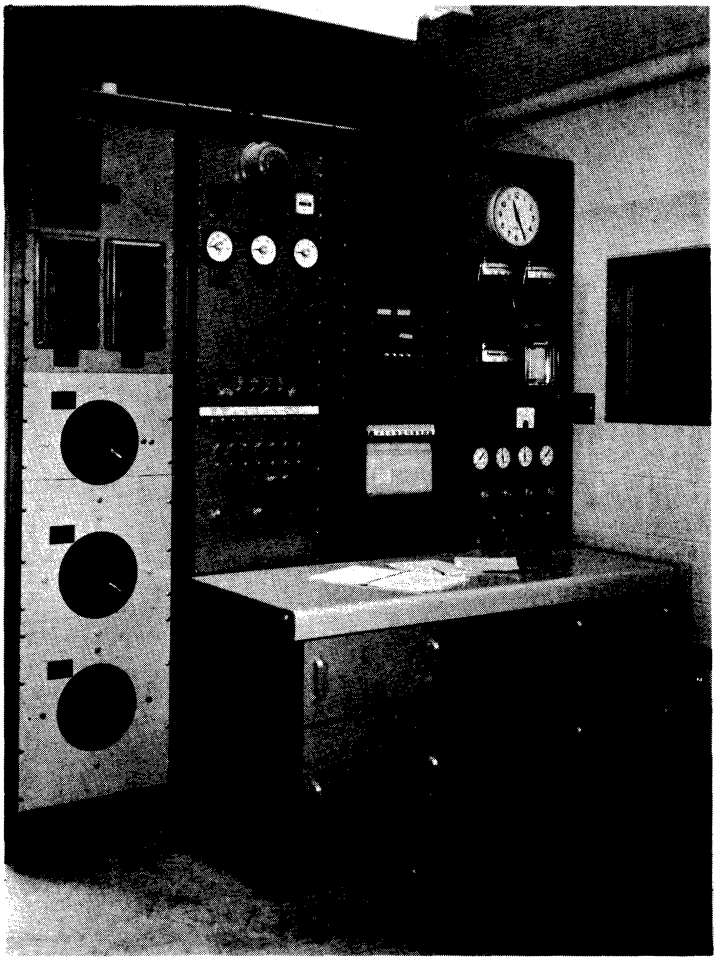

Figure 5. Potassium Boiling Heat Transfer Test Loop, Control Panel

"Limitrol" equipped with a low-signal alarm. In the event of a low flow rate the power to the pump, preheaters, and sodium boiler is cut off. A thermocouple measuring the exit air temperature from the condenser is connected to a Wheelco temperature indicator equipped with a high temperature alarm. The instrument automatically cuts off the power to the pump and preheaters in the event of a high exit air temperature. If a serious emergency should occur (such as a major leak accompanied by fire), use of a "scram" button will immediately drain the contents of both circuits to their respective supply tanks and cut off all electrical power to the loop.

Molten potassium and sodium at high temperatures when in contact with concrete will spall, giving off showers of burning drops. To prevent this added difficulty in the event of a major leak, the loop was housed in a sheet steel enclosure and on top of a steel pan. The pan not only prevents spalling but also aids in the disposal of residues after such an emergency.

Synopses offering advice on safety and handling procedures to observe when working with sodium and potassium are available (43, 60).

2. Temperature Measurement

Because the accurate measurement of certain temperatures is very important to the two-phase flow study, a discussion of the temperature measurement facilities is given.

There are seven main thermocouples which are platinum/platinum plus 10 per cent rhodium: TC25 through TC31, indicated in Figure 1. Temperatures measured by these thermocouples are essential for establishing heat balance and thus for the determination of two-phase mixture quality. The thermocouples were calibrated against a secondary standard which had been previously calibrated by the National Bureau of Standards. All the Pt/PtRh thermocouples are well type. In experimental runs, millivolt signals from these

thermocouples were read on a Leeds and Northrup type K-2 potentiometer, and the temperatures recorded to within 0.1°F with the aid of the calibration charts. For loop shakedown and hot trapping operations where less accuracy was required, the signals from the seven Pt/PtRh thermocouples were traced on the strip chart of a Taylor Transcope Recorder. Six of these thermocouples are Thermoelectric Model CEI-18-P10 Ceramo Type; thermocouple TC28 is a Thermoelectric Model CEI-116-P10 Ceramo Type.

The remaining thermocouples are chromel-alumel. With the exception of the flowmeter thermocouple (TS15), these thermocouples function solely for monitoring loop operation. They are read out on a Brown 12-point recorder used in conjunction with a 48-point stepping switch. Some of these thermocouples are in instream wells. The remaining ones are in surface wells except for the flowmeter thermocouple which is exposed. All the instream, surface, and preheater chromel-alumel thermocouples are Thermoelectric Model CEI-18-CT Ceramo Type.

Standardized thermocouple lead wire connects all thermocouples to the read-out instruments; all thermocouples are electrically insulated from the loop. Selected important thermocouples are designated by number in Figure 1. Table I summarizes these thermocouples, stating their kind and location.

That thermocouples in high-temperature environments tend to age, with accompanied calibration change, is a well-known circumstance. Throughout loop operations this condition was watched for, especially in the Pt/PtRh thermocouples. Near the end of the two-phase experiments, some of the Pt/PtRh thermocouple locations were interchanged during a steady-state run. The temperatures agreed within 1°F. Upon completion of two-phase flow experiments, some all-liquid pressure drop runs were made. The flows were expected to be isothermal since there was no power input. The emf signals from thermocouples TC26, TC29, TC30 and TC31 all agreed within 6 microvolts. These results indicate that the all-important heat balance thermocouples had not aged.

TABLE I

SUMMARY OF IMPORTANT THERMOCOUPLES

Thermocouple Number *	Type**	Location
TS 1, 2, 3	C-A	On inlet pipes to preheaters
TS 4, 5, 6	C-A	Preheater: on surface of exterior wall
TS 7	C-A	Sodium boiler
TC 10	C-A	Condenser inlet
TC 11	C-A	Condenser outlet
TC 12	C-A	Middle of hot well
TC 13	C-A	Subcooler inlet
TC 14	C-A	Subcooler outlet
TS 15 +	C-A	Flowmeter
TC 16	C-A	Primary supply tank
TC 18	C-A	Sodium boiler inlet
TC 20	C-A	Secondary supply tank
TC 25 +	Pt/PtRh	Preheater inlet flow divider
TC 26 +	Pt/PtRh	Funnel neck
TC 27	Pt/PtRh	Sodium condensing section
TC 28	Pt/PtRh	Heat transfer section head (not in stream)
TC 29	Pt/PtRh	Heat transfer section outlet
TC 30 +	Pt/PtRh	Pressure drop section inlet
TC 31 +	Pt/PtRh	Pressure drop section outlet
TC 33	C-A	Condenser exit air stream
TS 54	C-A	Hot trap

* TC denotes instream well-type thermocouple
TS denotes surface-type thermocouple

** C-A denotes chromel-alumel thermocouple
Pt/PtRh denotes platinum/platinum plus 10 per cent rhodium thermocouple

\+ Denotes thermocouples of primary importance in the two-phase flow study

3. Two-Phase Pressure Drop Measurement

The pressure drop measurement section, an integral part of the test loop, is a seamless tube of Haynes-25 alloy 5/8-inch OD by 0.495-inch ID, indicated in Figure 1. The section is oriented horizontally, its level being the highest of all loop components. The differential pressure taps are 1/4-inch schedule 40, 4-inch long, Haynes-25 pipe nipples welded vertically onto the bottom of the tube. They are spaced 36 inches apart.

Two-phase flows are generated in the three parallel 3-inch ID vertical preheaters. The three streams merge into a 0.476-inch ID tube and flow proceeds vertically upward through the heat transfer test section. Just downstream of the heat transfer section, the two phase mixture is turned by an elbow into a 10-inch (20 tube diameters) horizontal calming section from which it enters the pressure drop measurement section. The calming section is merely a portion of the pressure drop tube, extending upstream from the first pressure tap.

Pressure drop is measured with a Taylor Transaire Volumetric D-P Transmitter. Pressure transmitting diaphragm assemblies of 316-stainless steel are transition-welded to the Haynes-25 pressure taps. These 5-ply diaphragms lie in a horizontal plane and are 5 1/8 inches in diameter. At time of installation, the volume above the diaphragm was empty. This volume was filled with potassium upon startup of loop operations. Trace heaters lie alongside the pressure taps and upper portion of the diaphragm housings, the purpose of which is to keep the potassium in contact with the diaphragms liquid at all times. The upper diaphragm housings and pressure taps are insulated with Johns-Manville Cerafelt and Banrock insulation materials. The insulated assembly is shown in Figure 3.

Attached to the lower side of the diaphragm housings are flexible stainless steel capillary hoses. These hoses from the pressure transmitting

diaphragms are attached to opposite faces of a single diaphragm which is a component of the transmitter. The capillary hoses and lower portions of transmitting diaphragm housings are filled with sodium-potassium eutectic alloy. This alloy is liquid at room temperatures, and these static legs thus do not require trace heating.

The differential transmitter is horizontally mounted at floor level. Because a pressure drop occurs in the flow test section, the transmitter's single diaphragm receives unequal signals from the two static legs and thus is deflected. Such deflection, being proportional to the pressure drop, causes a deflection on a lever assembly. The differential pressure transmitter, which is a pneumatic force balance system, translates the lever deflection into a proportional air signal at the loop control panel.

Differential pressure was recorded on the strip chart of a Taylor Transcope Recorder. Chart speed was 1 inch per hour. Values were read as per cent of either 100, 300 or 600 inches of water. Taylor Differential Transmitters are usually permanently set at the factory to a single full scale range between 100 and 600 inches of water. However, to add flexibility to the experiments, Taylor Instrument Company in this case provided three calibrated notches on the force beam, allowing the choices in range mentioned above.

The pressure drop measurements made by this system are accurate to within 1 per cent of full scale. In the range of flow parameters encountered only the 100 and 300 inch ranges were used, giving maximum errors of about 0.05 and 0.1 psi, respectively. Further details on the instruments are given in bulletins issued by the Taylor Instrument Company (81, 82, 84).

Fluid temperatures at the inlet to the calming section and about 13 inches from the downstream pressure tap are measured with thermocouples TC30 and TC31, described previously. These well type thermocouples were located away from the ends of the pressure drop section in order to minimize their effect

on flow patterns in the test section. The temperatures at the pressure taps were estimated from the thermocouple readings by means of the experimental pressure gradient, assuming thermodynamic equilibrium existed (see Appendix C).

In treatment of data to obtain qualities in the flowing two-phase mixtures the power supplied to the preheaters is an important experimental measurement. Total preheater power was read to within 0.1 KW on a General Electric AC Kilowatt meter having a 0-30 KW range. The maximum power attained in the preheaters was 20.3 KW for one run. Several runs were made at 19 KW. A Superior Electric Company Powerstat variable transformer regulated the power input to the preheaters. The limitation in power input below the design value of 30 KW was caused by premature failure of four heating elements.

The liquid metal flow rate is measured by the MSAR magnetic flowmeter, described previously. The calibration curve supplied with the flowmeter was checked and found accurate. Appendix B provides a discussion of the calibration and accuracy of the flowmeter. Flowmeter signals were read to within 0.02 millivolt on a Brown potentiometer.

4. Void Fraction Measurement

The theoretical basis of the gamma ray attenuation method for measuring void fractions is given in Appendix I. Radiation attenuation has been used by many workers to obtain void fraction data in flowing two-phase systems. The technique, in general, is reliable for mixture qualities (mass fraction vapor) up to about 0.20. Appendix F illustrates this limitation. Basically, the method measures either the mean or local mixture density of the two-phase fluid, depending on whether a traversing or single-shot procedure is employed. Because appropriate gamma ray absorption coefficients are usually lacking, density values are not directly obtained. The usual procedure is to indirectly obtain the void fraction by interpolation between

detector signals read for all-liquid and all-vapor flows.

The type of interpolation valid for certain two-phase flows can be derived theoretically, and it is pointed out in Appendix I that the resulting expressions depend on the spatial orientation of the fluid phases with respect to the gamma-ray beam. The actual data processing methods will be given in Chapter V.

In determining void fractions by the radiation attenuation method, the most obvious necessities in addition to a flow test section are a suitable radiation source and detection system. Maurer (58) furnishes an extensive review of components used by various investigators. Shields for the source and detector must also be used, the designs of which vary widely, and many different types of electronic equipment have been used in detection systems.

Void fraction measurements were made at approximately the mid-point of the pressure drop section in the potassium test loop. Temperatures of the void fraction measurements were taken as the average between inlet and outlet thermocouples. This section will discuss specifications for the source, detection equipment, and shields.

A schematic diagram of the measuring system is given in Figure 6. Figure 7 provides a layout of the apparatus and indicates the types of shields specified for source and detector.

Source: The gamma-ray source used was Tm-170 (Thulium). The decay scheme for this nuclide is given in Figure 8 (22, 89). The relative occurrences of the two beta particles are 76 per cent and 24 per cent for the higher and lower energy betas, respectively.

A typical energy spectrum exhibited by Tm-170 is given in Figure 9 (58). The exact spectrum of gammas and X-rays will vary with sample size and cladding thickness. The peaks in the spectrum are due to an excited state of Yb-170.

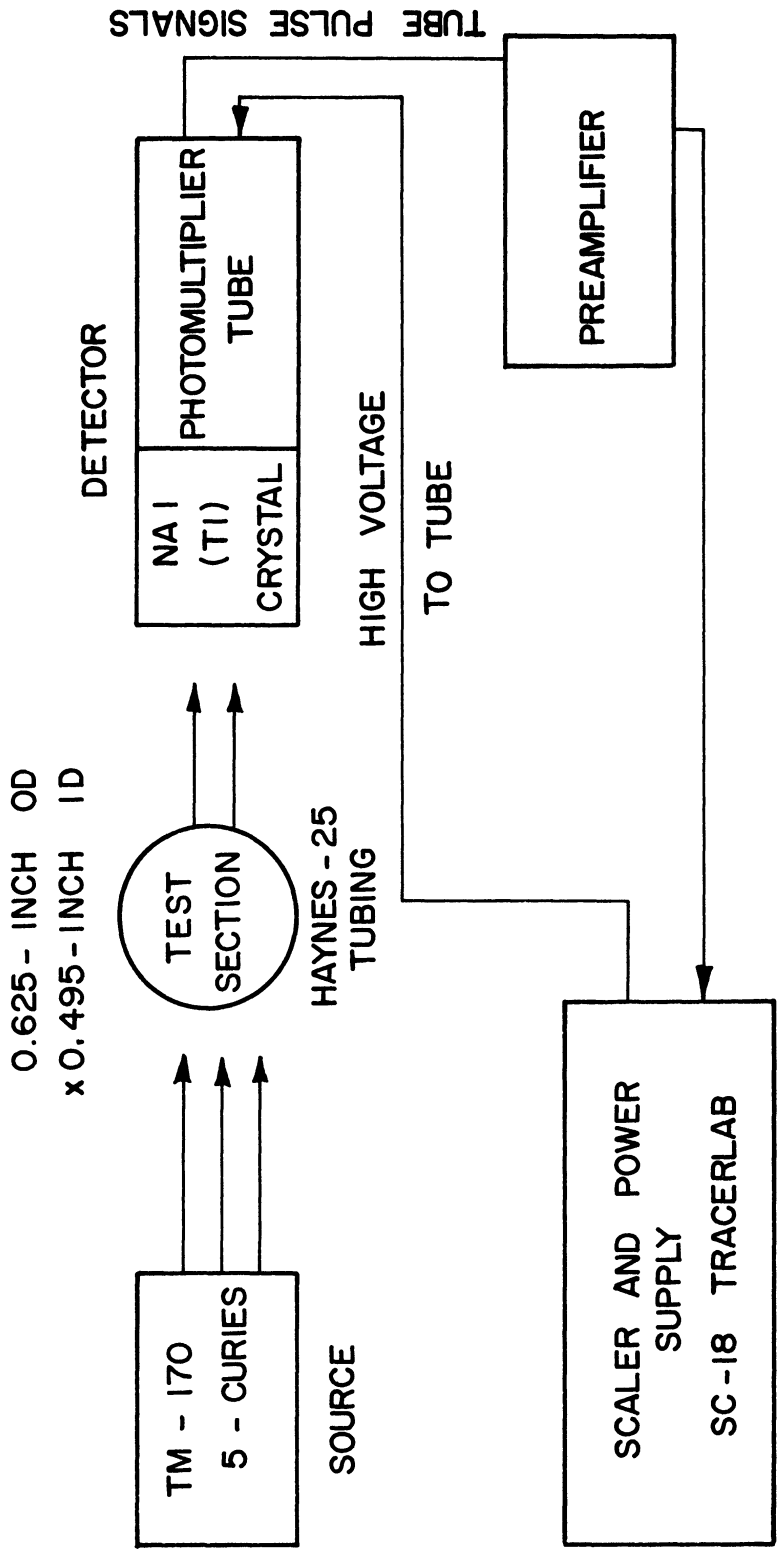

Figure 6. Schematic Diagram of Void Fraction Measuring System

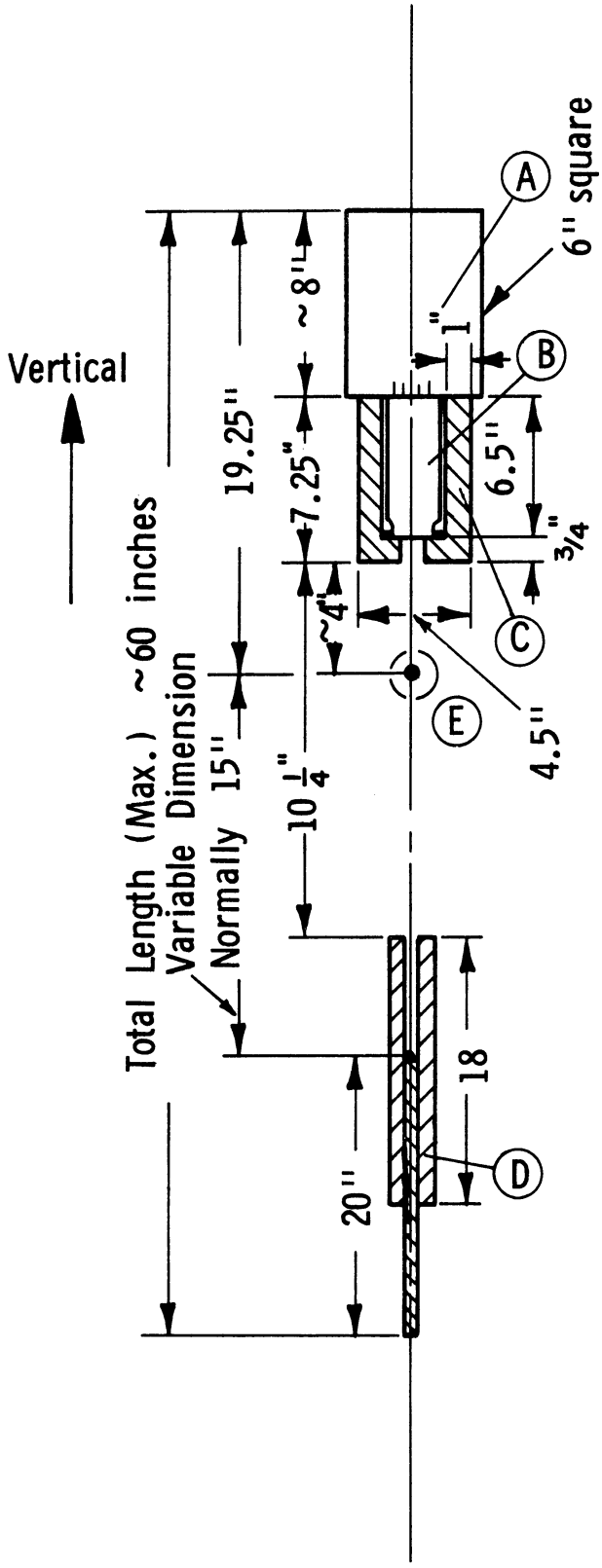

Key

A Preamplifier

B Harshaw Integral Line Scintillation Crystal & Photo-multiplier Tube, Type 6S4/E

C Steel Shield for Phototube, ~23 lbs.

D Source Shielding & Positioning Components ~21 lbs. Rod threaded to take source.

E Haynes 25 Tube 0.495-in. ID with 0.0625-in. wall

Figure 7. Layout of Void Fraction Measuring Apparatus

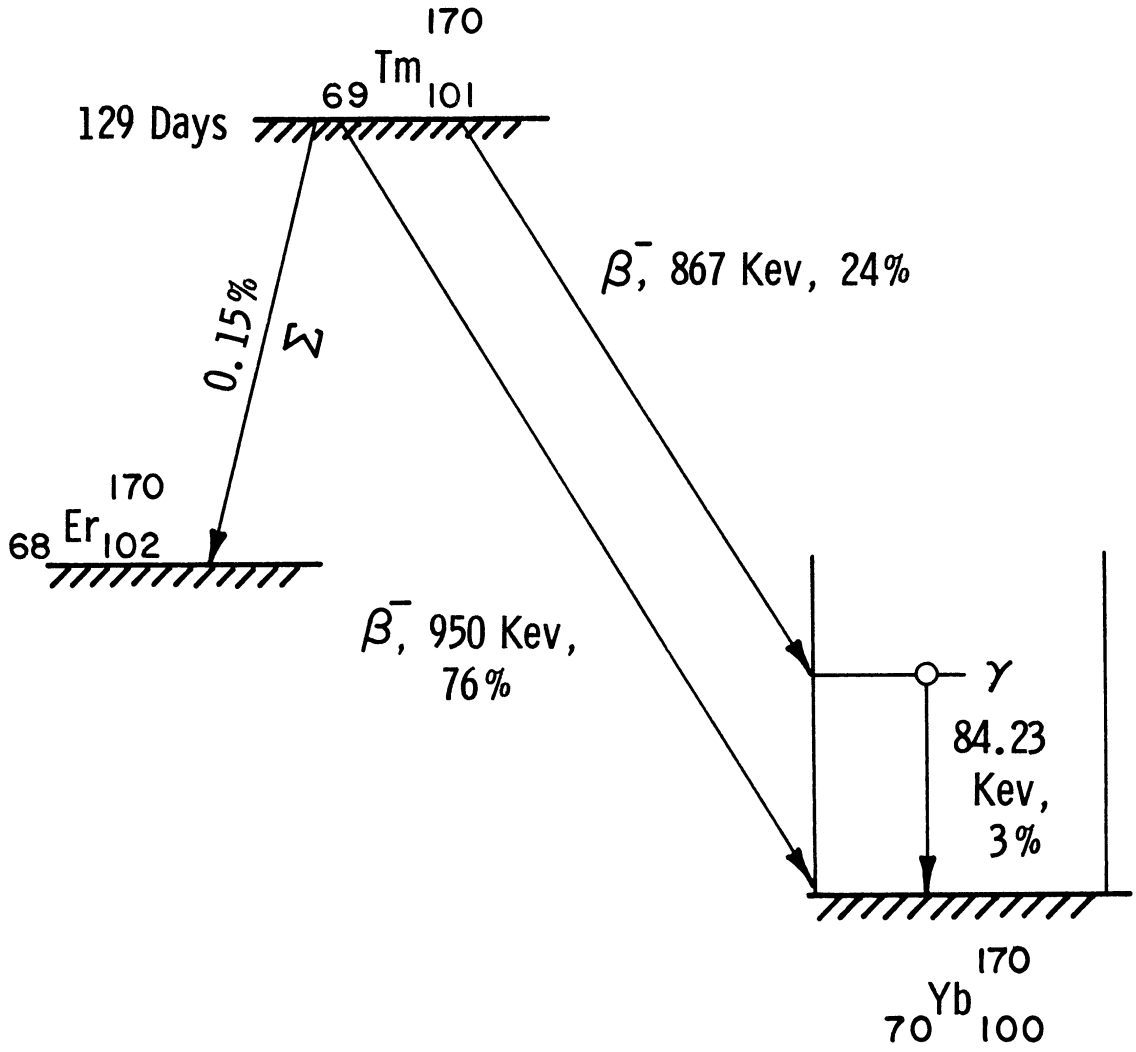

Legend:

Percent abundance is based on total Tm - 170 disintegrations.

Σ indicates orbital electron capture.

β^- indicates beta particle emission.

γ indicates gamma ray emission.

Figure 8. Radioactive Decay Scheme of Tm-170

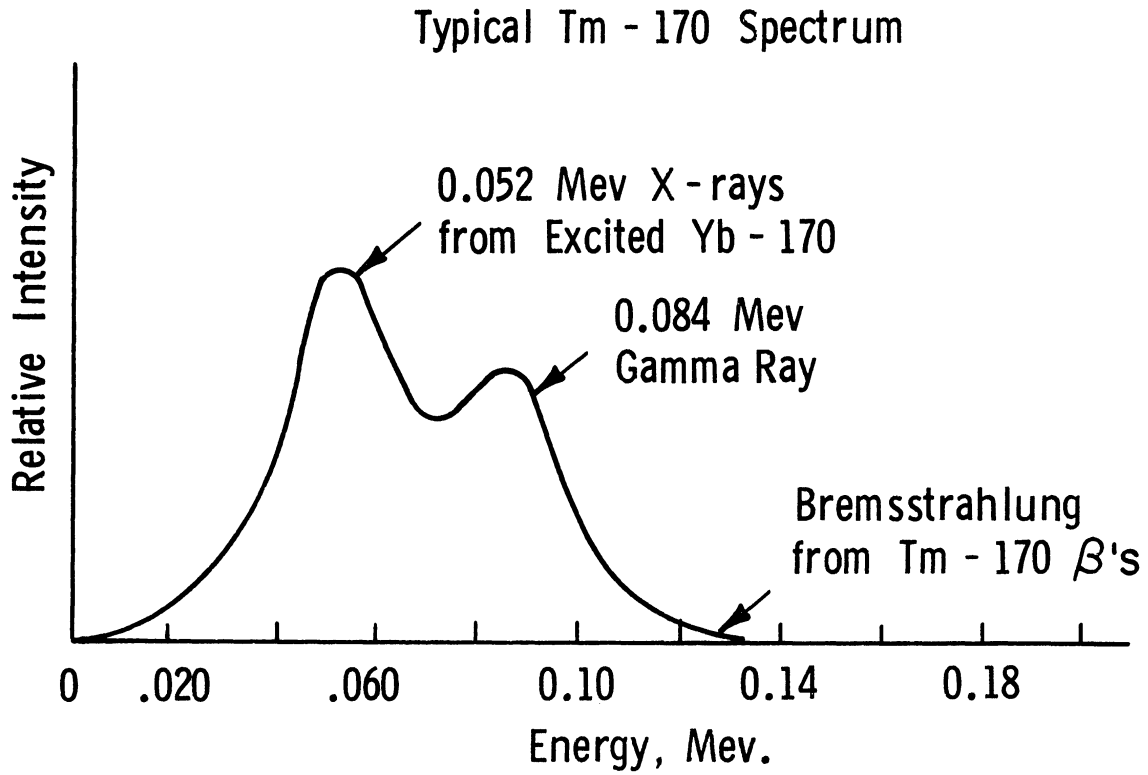

Figure 9. Typical Electromagnetic Energy Spectrum of Tm-170

The most intense photon is a 0.053 Mev K X-ray which occurs from 5 per cent of the total Tm-170 disintegrations. The less intense peak is due to a 0.084 Mev unconverted gamma-ray, which occurs 5 per cent of the time. The excited Yb-170 also emits a 0.008 Mev L X-ray and a 0.002 Mev M X-ray. Although these two X-rays occur from 16 per cent of the total Tm-170 disintegrations, they are so weak that their transmission by the source capsule is negligible.

The equations developed in Appendix I are based on a monoenergetic beam. Fortunately, the 0.053 Mev K X-ray is almost completely absorbed by the pipe wall, permitting the detector to see an essentially monoenergetic beam. The useful photon for these experiments is the 0.084 Mev gamma-ray. Figure 9 indicates the presence of Bremsstrahlung radiation caused by interactions of some of the Tm-170 beta particles with the encapsulation material.

Myers (61) discussed in detail the reasons for choosing Tm-170 as the gamma-ray source. It was necessary to obtain an isotope with a sufficiently long half-life to insure essentially constant source strength during any one experimental run. The 127-day half-life of Tm-170 meets this requirement, although it is short when considering experimental operations over several months. In long range use, however, corrections can be made for the decay. In addition to half-life considerations, the photon energy and approximation to monoenergeticity were examined. The density ratio of the potassium vapor-liquid system is in about the same range as for the air-water system. This fact suggested choosing a low energy gamma emitter which would allow detection of small changes in mixture density. However, if a photon too low in energy were chosen, the constant attenuation due to the channel wall would lower the emergent intensity below detection level and also damp out sensitivity. Myers' predictions (61) showed that for photon energies lower than about 60 Kev the tube wall attenuation would require using an unreasonably large source. On the other hand, for energies greater than 100 Kev the

sensitivity in the potassium experiments would suffer. These considerations, together with others discussed by Myers (61), led to the choice of Tm-170, which has a photon in the desirable energy range. For safety reasons, a beta decay source was preferred over an alpha decay type.

A nominal 10-curie Tm-170 source was purchased from Atomic Energy of Canada Limited (Ottawa). Preliminary calculations indicated that this strength was higher than necessary and could even lead to scaler overloading. However, the supplier offered Tm-170 radiography sources at 230 dollars for any strength up to 10 curies. Since experimental difficulties and delays were anticipated, it seemed wise to obtain the highest possible activity per unit cost. Excess strength was handled through collimation and shielding.

The source supplied by Atomic Energy of Canada had a strength of 9.8 curies on April 13, 1963. At the time of the potassium void fraction runs (August 22 through August 30, 1963) the source strength was about 4.7 curies.

The source is composed of metallic thulium and is encapsulated in stainless steel. Figure 10 provides an isometric view of the capsule and gives its main dimensions.

Detection Equipment: The schematic diagram of Figure 6 indicates the counting equipment which was employed. Scintillation detection was chosen over Geiger-Müller or proportional detection because of negligible dead time correction and high intrinsic counting efficiency.

The detector unit is an "Integral Line Assembly" produced by the Harshaw Chemical Company. It consists of a 1 1/2-inch diameter by 1-inch thick, thallium activated, sodium iodide crystal coupled optically to a 2-inch photomultiplier tube. The assembly includes an external magnetic shield to minimize the effects of the various electric and magnetic fields present near the potassium test loop. The assembly obtained has a pulse height resolution of

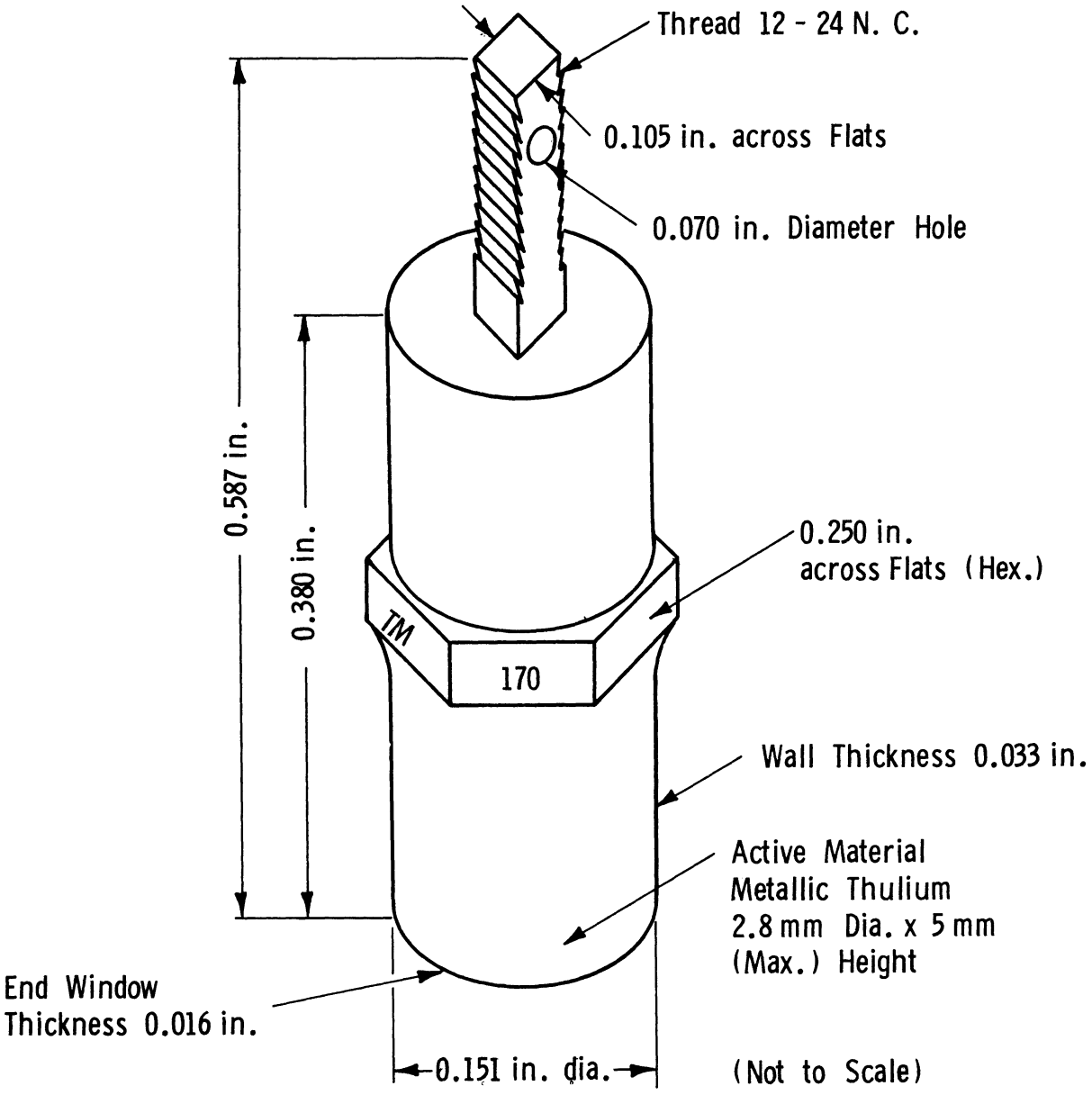

Figure 10. Tm-170 Gamma-Ray Source

8.3 per cent at 661 Kev photon energy. The Harshaw literature (32) furnishes dimensions of these assemblies.

Physically, the detection of gamma radiation by the scheme in Figure 6 is as follows. When a photon impinges on the NaI(Tl) crystal, the interaction in the crystal yields a flash of light. This light flash is picked up by the photomultiplier tube which converts it to a low level current pulse. This pulse must be amplified before it can traverse a cable and furnish a signal to the scaler. The preamplifier provides the necessary amplification which has a high degree of linearity. The scaler has a discriminator which may be set to accept voltage pulses from the preamplifier only when the signal is above a minimum value. The discrimination is necessary to eliminate effects due to amplifier and phototube noise. In the potassium experiments, the discriminator was set at 0.25 volt. For every current pulse accepted by the discriminator, a count is registered by the scaler. Obviously, some photon interactions in the NaI(Tl) crystal are so weak that the amplified pulse is rejected by the discriminator. Thus, not every gamma photon striking the crystal produces a count.

The preamplifier was specially built to electronically match the scaler. The scaler is a Tracerlab SC-18 Superscaler. This scaler has a built-in high voltage power supply which is used to drive the phototube. The Tracerlab manual (77) gives complete instructions for operation and maintenance of this instrument. Table II summarizes the important features of this scaler.

Prior to flow experiments, the detection system was tested in background counting and also against a small Co-57 source. The main objective of the test was to locate the proper high voltage level to use in driving the photomultiplier tube. The results of this test are given in Figure 11, which shows the characteristic plateaus in the count rate versus tube voltage curves. It was desired to use a tube voltage such that the experimental counting would be

TABLE II

IMPORTANT FEATURES OF THE TRACERLAB

SC-18 SUPERSCALER

(a) A built-in mechanical register, preceded by an electronic scale of 1000 which provides for automatic "pre-set count" operation.

(b) An odometer type timer which permits automatic "pre-set time" operation.

(c) A high voltage power supply for driving the photomultiplier tube, continuously variable from 300 to 3000 v.; electronically regulated so that 1 per cent change in line voltage yields 0.2 v. output change; ripple and noise level limited to about 200 m.v.

(d) Resolving time of 5 microseconds. This implies count rates of up to 120,000 cpm with less than 1 per cent coincidence loss.

(e) Input sensitivity (discrimination) adjustable from 0.20 to 0.35 v.

(f) Electronic scaling system counts 1000 before pulsing the mechanical register.

(g) Can totalize up to 9,999,999 counts.

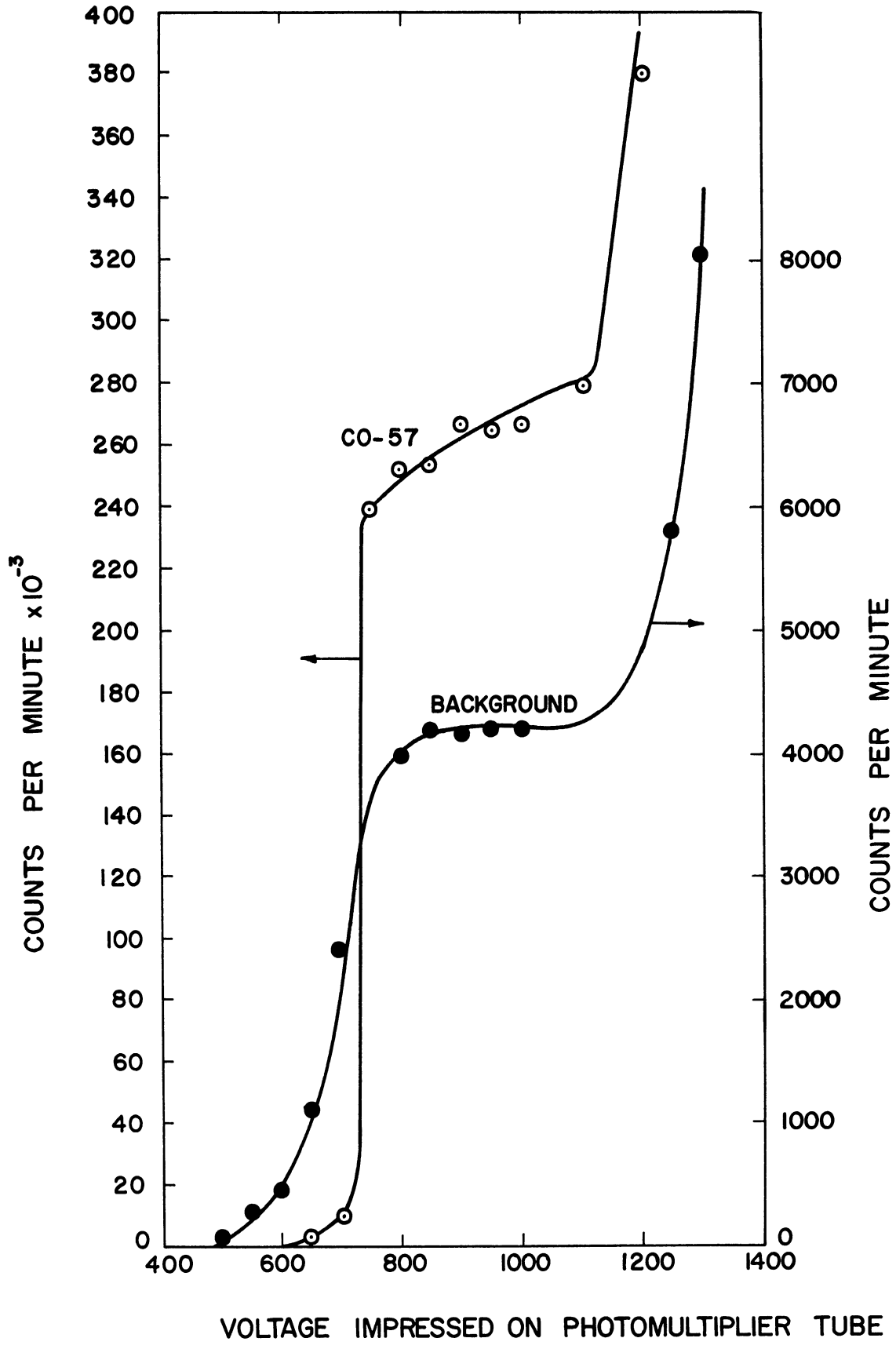

Figure 11. Count Rate As A Function of Voltage Impressed on Photomultiplier Tube

on these plateaus. The count rate level at the plateau varies with the intensity of the detected radiation.

The results in Figure 11 indicate that a driving potential of 950 volts should allow operation on the count rate plateau, and this voltage was used in the potassium measurements.

Before concluding this discussion of the detection equipment, mention should be made of its efficiency. The resolving time of the photomultiplier tube is about 0.25 microsecond (32). Inorganic scintillation crystals such as NaI(Tl), due to their high density, have a high stopping power and consequently a greater counting efficiency for gamma rays than do gaseous detectors. The alkali halides--particularly NaI(Tl)--have the added advantage of high light output, transparency, and suitable refractive index. The high atomic number of inorganic scintillators aids in photon conversion.

The theoretical absorption coefficients of NaI(Tl) for gamma rays having energies ranging over three orders of magnitude are available (32). Using these coefficients, the theoretical efficiencies of crystals of various thicknesses can be obtained as a function of gamma energy. These theoretical or "intrinsic" efficiencies depend on source-to-crystal distance. They do not account for absorption by the crystal container or for the fact that only a fraction of the total interactions in the crystal are counted. (This latter factor depends on the scaler's discriminator setting.) Price (69) presents intrinsic efficiencies for 1 1/2-inch diameter by 1-inch thick NaI(Tl) crystals. For the source-to-detector distances suggested in Figure 7 and for the low energy radiation employed, the theoretical detection efficiency approaches unity. Although actual detection efficiencies cannot be this high, one can confidently assume that they were greater than 0.50 and perhaps as high as 0.80.

Shields and Collimator: In the interest of personnel protection it was necessary to shield the Tm-170 source. The shielding employed was such that

the narrow working beam impinged unhindered on the flow channel but radiation in all other directions was substantially reduced. The detector was also shielded in order to minimize the effect of background radiation on the count rate.

The source has an end output of 4.5 mr/hr at 1 meter per curie. This strength includes Bremsstrahlung radiation. Figure 7 shows the shields for both source and detector and indicates the method of varying the source-to-detector distance by adjusting the location of source inside the shield by means of the positioning rod. Figure 12 gives details of the shield designs. Both shields are made from seamless mechanical steel tubing.

The source shield was designed assuming that all the radiation is of 0.084 Mev energy, which was believed to allow considerable safety factor. Moreover, the design was based on a 10-curie strength. Even though these design precautions were taken, it was found that the steel tube did not stop the gamma rays as effectively as planned, and a 1/2-inch thickness of lead sheet was fastened around the steel tube during the experiments. Even before the lead was added, however, the dose rate in the loop control room was well within the acceptable safe limit.

The output end of the source shield was tapped to accommodate a standard 3/4-in bolt from which the collimator was fabricated, as shown in Figure 13. The collimator was interchanged with a solid shut-off plug for background determinations. Unscattered background radiation--i.e., photons penetrating the 1 1/2-inch long bolt piece--was negligible, according to the design calculations. The background radiation observed is attributed to scattering of beam photons. It is seen from Figure 13 that the collimated gamma beam was about 1/32-inch in diameter.

The source and detector shields are accurately aligned on a common frame. The latter shield has 1-inch thick walls for reduction of background effects.

As shown in Figure 12, the face plate on the detector shield is removable to allow ease in changing the size of the window in front of the scintillation crystal.

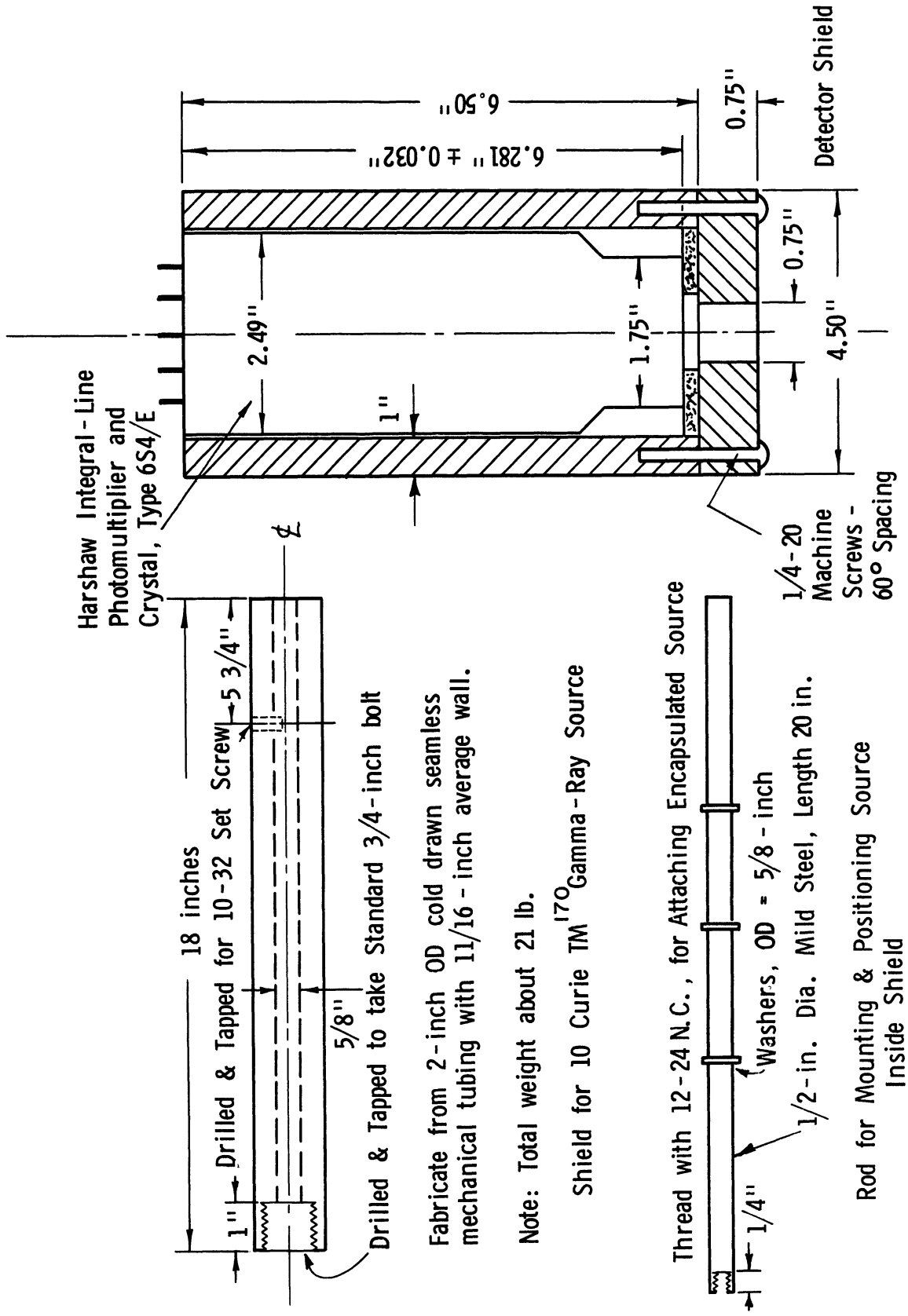

Figure 12. Source and Detector Shields

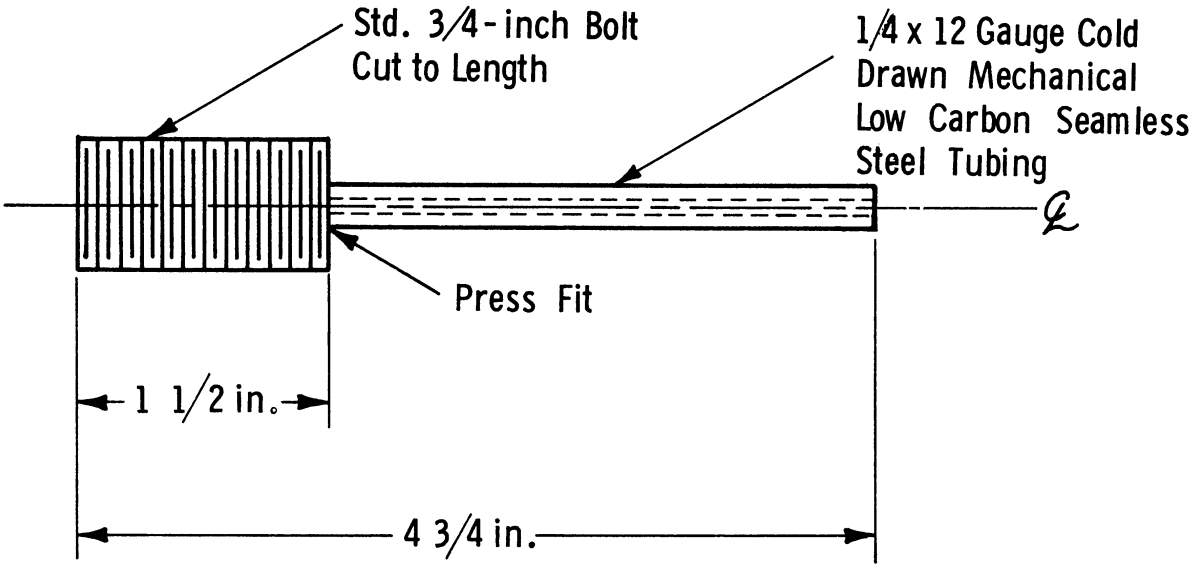

Notes:

1. 1/4 x 12 Gauge Tubing: 0.109 - inch Wall
   by 0.032 - inch ID

2. Cut second std. 3/4 - inch bolt to 1 1/2 - inch length. To be used as plug in background counting.

Figure 13. Gamma-Ray Beam Collimator

IV. EXPERIMENTAL PROCEDURES

1. Two-Phase Pressure Drop Study

When making the two-phase flow experimental determinations, the potassium test loop was continuously operated for several days at a time. Such extended operating periods were necessary because 6 to 8 hours are required in startup to bring the loop into pseudo-steady state two-phase flow. The overall response of the loop to a change in preheat power input or pumping rate is somewhat slow. When such a change is made, temperatures throughout the primary circuit are disturbed and slowly change to new steady-state values. The strongest thermal damping force in the system is the hot well. Here, the large volume of liquid is slow to assume its new temperature after a change is made in operating conditions. Even such an obscure variable as ambient temperature has been observed to affect loop operating characteristics through its influence on heat losses. In addition to process reasons, extended operating periods were desirable to minimize thermal cycling of the loop.

Pressure drop data were obtained for flow rates ranging from 108 to 752 lb/hr and for preheater power settings ranging from 6.0 to 19 KW (as mentioned previously, one point was obtained at 20.3 KW). Readings were made at 30- or 60-minute intervals when the loop was operating in essentially steady state. The loop was considered to be in such condition when, following a control change, temperatures throughout the system varied less than about 10°F between adjacent observations. The steadyness of readings from thermocouples TC25, TC26, TC30, and TC31 was particularly noted.

For most operating conditions several sets of data were obtained. Readings from all chromel-alumel thermocouples were entered hourly on the loop log sheet. These 40-odd temperatures, except for the flowmeter reading, are not vital to the two-phase flow results. However, their history was important to the analysis of loop performance as well as the establishing of whether steady-state conditions existed. The following list summarizes the readings essential for each pressure drop data point:

a) Temperatures indicated by thermocouples TC25, TC26, TC30 and TC31.

b) Flowmeter temperature indicated by thermocouple TS15.

c) Flowmeter signal in millivolts.

d) Power input to preheaters.

e) Time and date of the above readings marked on the pressure drop chart.

The temperatures mentioned in item (a) above are essential in calculating qualities. The millivolt signals read on the K-2 potentiometer were recorded as well as the temperatures derived from them. In addition, the signal from TC29 was also noted. The K-2 potentiometer was frequently standardized--at least every two hours. At the time of these readings the average pressure drop was recorded as per cent of full scale on the strip chart. However, all pressure drop values reported were derived from subsequent careful study of the strip chart.

The differential pressure transmitter was zeroed frequently. Although the zero of the instrument exhibited a drift, the zero was checked often enough--about once a day--so that there is negligible error in the data due to this zero drift. Checking the transmitter zero consisted in shutting down the flow, in which condition no pressure drop would exist. The zero reading on the chart was noted and sometimes adjusted at the transmitter. The pressure drop section is inclined about 3 degrees from the horizontal,

allowing it to drain when flow is stopped. At the time of such temporary flow cessation it was necessary to reduce the preheater power to prevent unstable pool boiling in the preheaters. After such temporary shutdown, two to three hours was necessary to return the loop to pseudo steady operation.

Prior to running two-phase flow experiments, a series of all-liquid flow data were taken to determine heat losses from the preheaters, heat transfer section, and pressure drop section. The method of determining and correlating heat losses is described in Appendix D. The preheater and heat transfer section losses were found to be independent of mass flow rate, but pressure drop section losses displayed a parametric dependence on flow rate. When necessary in processing of the two-phase flow data, pressure drop section losses were obtained by interpolation between flow rates run in the heat loss determinations. A knowledge of heat losses is essential for determination of quality in the two-phase flow runs (see Appendix C).

After completion of the two-phase flow runs, three all-liquid pressure drop values were obtained in order to check the single-phase friction factor--Reynolds number relationship used in data processing.

2. Void Fraction Study

Void fraction data were obtained over about the same range of total flow rates as were the pressure drop data--131 to 749 lb/hr.

Detector counts were recorded for three-minute time intervals. Choice of a three-minute counting time was based on consideration of statistical error and coincidence loss. Statistical error arises from the random nature of the gamma emission process. It can be shown that the standard deviation in counting is usually equal to the square root of the number of counts recorded (69). It follows that the larger the number of counts read, the smaller the percentage the standard deviation is of the total. Hence, the probable

error in counting is reduced as the number of counts is increased. Of course, an appreciable reduction in statistical error may result in prohibitively long counting times.

Although the statistical error is diminished by increasing the counting rate, some of the advantage is lost by inaccuracies introduced by coincidence loss in the counting system. Normally, the coincidence loss of a system is determined by that component which has the greatest dead time (i.e., the time interval immediately following a pulse during which no succeeding pulse will be counted). In this case, the scaler is the limiting component since it has a resolving time of 5 microseconds (77) as compared with about 0.25 microsecond for the scintillation detector (32). Although coincidence loss can be measured and subsequent data corrected for it, the following relation is valid for small corrections (77).

$$N = \frac{r}{1-r\tau} \qquad (3)$$

where N = true count rate

r = observed count rate

τ = dead time

The fraction of the true counting rate which is lost is equal to $r\tau$.

Preliminary experiments showed that three-minute counting periods would lead to counts in the neighborhood of 10^6. For a million counts the standard deviation amounts to only 0.1 per cent, while the observed count rate produces a coincidence loss of 2.8 per cent. These same preliminary experiments established that an 18.25-inch source-to-detector distance would be suitable (i.e., ten inches of positioning rod protruding from the source shield). This distance was maintained in all two-phase determinations. It was thus established that, for the source and geometry specified, a three-minute counting interval struck a good balance between statistical accuracy and coincidence loss.

The counts obtained in the two-phase experiments ranged from 600,000 to 1,500,000. The experimental procedure involved taking a series of three counts with the collimator in place. Then the collimator was replaced with the shut-off plug and another series of three counts taken. These latter counts measured background radiation striking the crystal. Deduction of the average corrected background count from the average corrected collimated count led to a count rate attributed primarily to the collimated beam (about 1/32-inch in diameter). Usually six separate counts were recorded per data point, but occasionally seven or more counts were read if values seemed to drift. The approximately twenty minutes it took to make the gamma-ray attenuation readings usually fell within the time interval necessary for recording other data from the loop.

A chromel-alumel thermocouple was attached to the outer surface of the detector shield, but no attempt was made to control the detector temperature. The upper safe temperature limit for the photomultiplier tube is about 165°F. Sometimes the detector temperature approached this level, but it was always possible to cool the tube by use of a large exhaust fan located in the loop room. In fact, rough control of the detector temperature was possible with the fan. The photomultiplier tube temperature was recorded at each data run and ranged from 128 to 160°F.

The shield assembly was supported by and clamped to the framework of the loop housing. It was found that the pressure drop section moved only a negligible amount from thermal expansions. The source was aligned with the center of the flow tube by means of the collimator. Insulation was stripped off a segment of the test section and a 1/32-inch welding rod inserted upward through the source shield and collimator and pushed up to the channel. The shield assembly position was adjusted until the welding rod rested on the center of the tube. To allow for slight bend in the welding rod, it was rotated about its axis, letting the free end describe a circle. When this

small circle centered on the pipe center, alignment was considered satisfactory. The alignment was checked several times during the course of the experiments, using this procedure.

Early measurements showed that too much background was scattering through the bolt portion of the collimator. To overcome this, a circular piece of lead was fitted over the end of the 1/4-inch collimator tube. A steel cap 1/2-inch thick was also placed over the collimator end to reduce the beam intensity somewhat.

The theory section in Appendix I points out the necessity of obtaining single-phase calibration count rates. All-liquid values were obtained for an average flow temperature of 500°F; the all vapor count was taken as an empty channel reading at 551°F. These calibrations are included in the data tables of Appendix H. The temperature correcting equations were used in data reduction.

As mentioned previously, the detection system was operated with 950 volts impressed on the photomultiplier tube.

The following list summarizes the readings essential for each void fraction data point:

a) Temperatures indicated by thermocouples TC25, TC26, TC30 and TC31.

b) Flowmeter temperature indicated by thermocouple TS15.

c) Flowmeter signal in millivolts.

d) Power to preheaters.

e) Three-minute gamma-ray counts from collimated beam (at least three counts).

f) Three-minute gamma-ray background counts (at least three counts).

g) Detector temperature (not essential in data processing).

V. EXPERIMENTAL RESULTS

1. Two-Phase Pressure Drop Results

A typical section of the Taylor chart showing pressure drop and flowmeter traces is given in Figure 14. The section shown is for a flowmeter output of about 4 millivolts and 18.5 KW preheater power. The pressure drop here was recorded in the 0-300 inches of water range, with the transmitter zero at 30 per cent of full scale. The mean pressure drop at 3:00 p.m. is 2.38 psi; this value, together with other loop data, furnished data point 74.3 given in Appendix G.

For most of the data reported, the pressure drop fluctuated regularly about a mean value, as is illustrated in Figure 14. This mean value is reported as the value of the pressure drop. The pressure drop fluctuations were accompanied by oscillations in the flow rate, also recorded on the Taylor chart during most of the experimental operation. The potassium loop thus exhibited instabilities, a situation commonly found in such two-phase test loops. The data reported in this study were obtained for steadiest possible flow conditions--i.e., at conditions of zero or minimum flow rate fluctuations.

The differential pressure fluctuations were greatest at high preheater power levels and low pumping rates. Superheating of the liquid is believed to be the explanation for this trend. At low flow rates the liquid moves into the preheater with little disturbance and the high power level causes it to superheat as it "crawls" upward. More or less periodically a sudden nucleation occurs, producing a large volume of vapor which pushes a liquid slug up through the heat transfer section and through the pressure drop section.

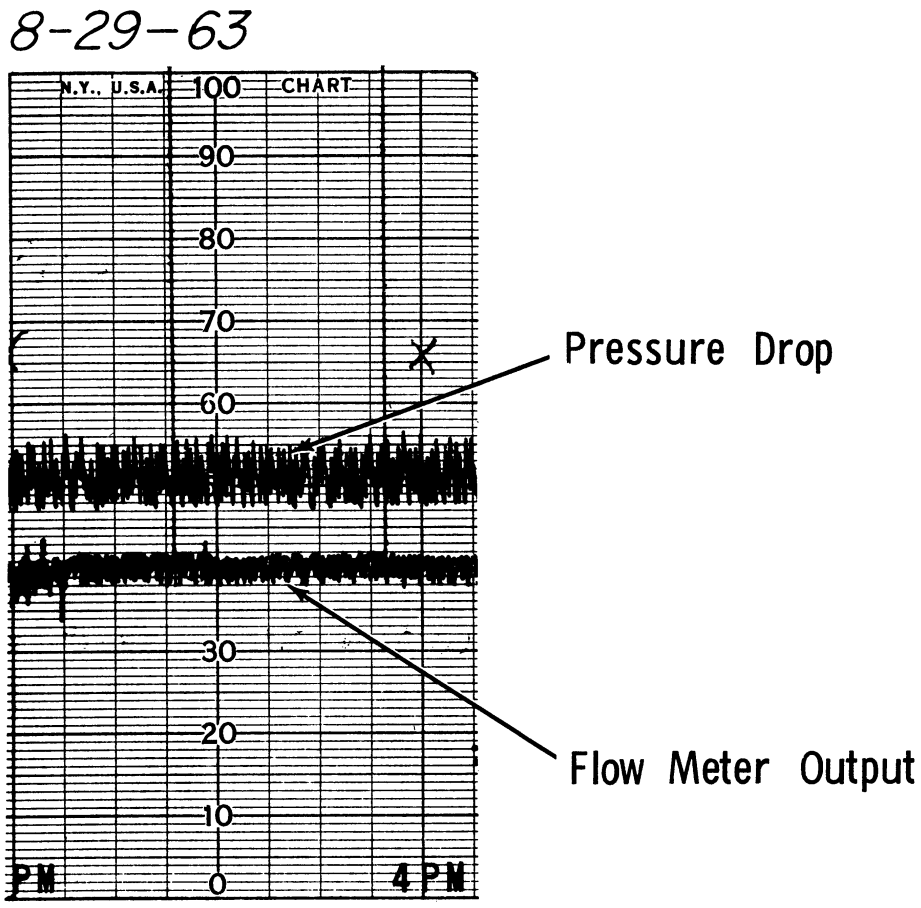

Preheat Power	18.5 KW (Full)
Pressure Drop Scale	0-300 in. of Water
	zero = 30%
Flow Meter Scale	0-10 Millivolts

Figure 14. Typical Section of Taylor Transcope Recorder Chart, Showing Pressure Drop and Flowmeter Traces

This surge is evidenced by a fluctuation in the pressure drop and flow meter traces, the latter being due to the momentary flow reversal caused by the sudden generation of vapor. At lower power settings the magnitude of the liquid superheat is diminished; an increase in flow provides disturbance for more frequent nucleation. Thus, as was experienced, lower power levels and/or higher pumping rates produced smoother operation.

After completion of two-phase runs, three all-liquid pressure drop values were obtained. These values are presented in Table G-I of Appendix G. In comparing the two-phase data with the Lockhart-Martinelli correlation (53), it was necessary to use single-phase friction factors. The three all-liquid data points were used to verify the expression from which smooth-tube friction factors were calculated. As mentioned in Chapter III, the single-phase runs also afforded a check as to whether the Pt/PtRh thermocouples had aged. The fact that only three points were taken over a narrow flow rate range is due to the test section's inclination of 3 degrees. At lower all-liquid flow rates the tube does not flow full. That the tube was flowing full for the three points in Table G-I was verified by a calculation in which shear loss was balanced against gravity head, using the hydraulic radius concept.

All data were processed using the IBM-7090 electronic data processing system. Physical and thermal properties necessary in data processing were estimated for the sodium-potassium mixture by the methods discussed in Appendix A.

The experimental two-phase pressure drop data and associated experimental quantities are given in Table G-II of Appendix G. A total of 226 pressure drop values are reported. The table includes flow rates, quality values, temperatures, and correlating parameters. The latter results will be discussed in the next chapter. Pressure drop values are compared with values obtained as the difference in vapor pressure at inlet and outlet temperature.

--i.e., experimental data are checked to determine whether thermodynamic equilibrium existed. This aspect will also be examined in a later chapter.

Table III summarizes the overall ranges of important experimental quantities. From comparison of temperatures in this table with the loop design specifications in Chapter III it is seen that data were not obtained over the entire design temperature range.

TABLE III

RANGES OF EXPERIMENTAL QUANTITIES OBTAINED IN TWO-PHASE PRESSURE DROP STUDY

Test Section Length, feet	3.0		
Test Section ID, inches	0.495		
Pressure Drop, psi	0.054	-	3.10
Mass Flow Rate, lb/hr	108	-	752
Mass Velocity, lb/hr/ft^2	8050	-	56,100
Inlet Pressure, psia	0.54	-	15.8
Inlet Temperature, °F	923	-	1428
Outlet Temperature, °F	862	-	1419
Inlet Quality	0.0004	-	0.3788
Average Quality	0.0065	-	0.3784
Quality change across section	- 0.0051	-	0.0312

It was impossible to achieve temperatures higher than the upper limits given in the table due to excessive heat losses in the condenser, subcooler, and return lines to the pump. To attain fluid temperature substantially higher than 1400°F requires that the pump deliver fluid at 1400°F. The heavy heat losses reduced the preheater inlet temperature such that the maximum level attained was 1030°F. The condenser and subcooler proved to be overdesigned

(the air blower not being necessary usually), and, in an effort to achieve higher operating temperatures, these heat exchangers were stuffed with Johns-Manville Banrock insulating material. This modification extended pressure drop section inlet temperatures to 1428°F.

Temperatures at the inlet and exit to the pressure drop section were not measured directly; thermocouples TC30 and TC31 were located 10 inches upstream and 13 inches downstream from the section, respectively. The thermocouples were located away from the section to minimize disturbances in flow pattern inside the test section as might be caused by the thermocouple wells. Temperatures at the inlet and exit (listed as T1 and T2 in Table G-II) were estimated from the experimental pressure gradients, assuming thermodynamic equilibrium existed. The exact procedure in calculating these temperatures is given in Appendix C. The accuracy of the temperatures thus calculated is also considered in this appendix, and it is shown that the maximum error in T1 or T2 depends on the temperature level of the measurements. The error is most serious at low temperature--below 1000°F. Since 72 per cent of all readings on TC30 and TC31 were greater than 1100°F, it follows that the bulk of the experimental results represent cases where T1 and T2 maximum errors are very small (less than 2°F).

The flow rates given in Table G-II were calculated from the flowmeter millivolt signal, using the procedure outlined in Appendix B. This appendix also considers the maximum error possible in measured flow rate. Maximum uncertainty in flow rate is about 2.8 per cent at the lowest flow rate, decreasing to about 1 per cent at highest flow rates.

The inlet and outlet qualities listed in the results table were calculated from the First Law of thermodynamics, using an open system analysis as outlined in Appendix C. The accuracy of the calculated qualities is considered in detail in Appendix E. The probable error in x_1 or x_2 was found

to depend primarily on preheater power level and total flow rate, since the values of these operating variables essentially set temperature levels throughout the loop. The results of the error analysis in Appendix E indicate that 81 per cent of the data occurred for conditions where qualities are known within 10 per cent; 46 per cent of the data represent conditions where qualities are known within 5 per cent.

In addition to quality and total flow rate, it was found that average test section pressure is of primary influence on two-phase pressure drop. The absolute pressure gauge at the outlet of the heat transfer section, mentioned in Chapter III, did not function satisfactorily throughout the two-phase flow runs. In the early runs the pressures indicated by the gauge compared favorably with equilibrium pressures corresponding to readings from TC29. Soon, however, the calibration changed and was not re-established. Both the zero and span of the pneumatic transmitter behaved erratically. Pressure levels in the pressure drop section are taken as equilibrium vapor pressures. Table G-II gives absolute pressures at the test section inlet.

2. Void Fraction Results

Void fraction values were measured by the gamma-ray attenuation method at approximately the mid point of the pressure drop section. Appendix I presents a detailed discussion of the theoretical basis for measuring void fraction by this technique. To summarize briefly, the gamma-ray beam from the Tm-170 source was passed upward through the flow channel, and the intensity of the transmitted beam was obtained as a count rate by the scintillation detection system. The raw count rate was corrected for background and coincidence loss.

It is shown in Appendix I that void fraction can be obtained, without knowledge of gamma-ray mass absorption coefficients, with reference to

attenuation measurements for all-liquid and all-vapor flows. Moreover, if a broad gamma-ray beam is employed, the equation relating void fraction to the two-phase and single-phase attenuation measurements depends strongly on the spatial orientation of the fluid phases with respect to the radiation beam. In Chapter VII the matter of flow regime is discussed. When all the experimental flow conditions were examined with regard to the regime prediction methods of Baker (3) and Ros (75), most predictions suggested that the two-phase flows were either annular or dispersed. Since a narrow gamma-ray beam was employed, the physical situation in annular flow is approximately one in which fluid layers are oriented perpendicularly to the gamma-ray beam (see Figure I-2a). The dispersed flows behave essentially homogeneously. These physical considerations led to the use of the following equation (given as Equation (I-11) in Appendix I) for calculation of void fraction results.

$$\alpha = \frac{\ell n\ N/N_\ell}{\ell n\ N_g/N_\ell} \qquad (4)$$

where α = void fraction

N = average corrected count rate obtained for two-phase flow

N_ℓ = average corrected count rate obtained for all-liquid flow

N_g = average corrected count rate obtained for all-vapor flow

Correct utilization of Equation (4) requires that all the N's be observed at the same flow temperature. It is inconvenient to obtain N_ℓ and N_g values corresponding to all two-phase flow conditions, but Appendix I demonstrates how the N_ℓ and N_g values, each taken at a single temperature, can be corrected to all other temperatures encountered.

The single-phase gamma-ray attenuation measurements are given in Table H-I of Appendix H. The average temperatures are the arithmetic mean between inlet and outlet values. For the all-liquid determination inlet and outlet temperatures were 505 and 495°F, respectively; for the all-vapor readings

inlet and outlet temperatures were 557 and 545°F, respectively. In order to obtain N_ℓ and N_g values, the average count rates in Table H-I were corrected for coincidence loss (see Chapter IV) and the background readings subtracted from the collimated beam readings. Since it influences the count rate, the detector temperature is also tabulated. The N_ℓ and N_g values were adjusted to the two-phase flow temperatures by the methods of Appendix I.

The experimental void fraction results are given in Table H-II of Appendix H. A total of 17 values are reported. The quality value given is the arithmetic mean between inlet and outlet qualities to the pressure drop section, approximating the value at the position of the attenuation readings. The temperatures are again the arithmetic mean between inlet and outlet to the pressure drop section. Several calculations were made by an iterative procedure, using the frictional pressure drop results of this study, in order to estimate the pressure and temperature profiles along the pressure drop section. Thermodynamic equilibrium and a linear variation of quality were assumed. These calculations showed that the accelerative contributions to the pressure drop were negligible compared to friction losses, and that the temperature at the middle of the test section was within about 10°F of the arithmetic mean between inlet and outlet temperatures. Table H-II lists the average uncorrected count rates obtained. The average corrected count rate N was evaluated by subtracting the background from the collimated beam readings, after each reading was corrected for coincidence loss. The photomultiplier tube temperature is given. Except for one run, Code 55.4, the detector temperature between collimated and background counting differed by no more than 2°F.

It was mentioned in the Introduction that the mean velocities of the two phases in vapor-liquid flow, based on the cross sectional area occupied by each phase, are usually not equal. The ratio of mean vapor velocity to

mean liquid velocity is therefore greater than unity in most two-phase flows. From a consideration of mass balance this velocity slip ratio is given by

$$S = \frac{V_g}{V_\ell} = \left(\frac{x}{1-x}\right)\left(\frac{1-\alpha}{\alpha}\right)\left(\frac{\rho_\ell}{\rho_g}\right) \qquad (5)$$

where

S = velocity slip ratio

V_g = vapor average velocity

V_ℓ = liquid average velocity

x = quality

α = void fraction

ρ_ℓ = liquid density

ρ_g = vapor density

Table H-II also includes a quantity X_{tt}. This is the void fraction correlating parameter and will be discussed in the next chapter.

Table IV summarizes the range of experimental quantities obtained in the void fraction study. Although the table shows that void fractions were obtained over the same flow rate range as were the pressure drop data, comparison with Table H-II shows that the distribution of flow rates is narrow. Nine values occurred for flows between 200 and 300 lb/hr, and four values occurred for flows between 300 and 400 lb/hr.

The accuracy of the void fraction results is considered in Appendix F. The theoretical standard deviation in void fraction, based upon the known standard deviation in the count rate data, is obtained as a function of void fraction. For sixteen of the experimental points the standard deviation in void fraction ranges from 4 to 19 per cent of the void fraction value. One point, code 72.4, exhibits a standard deviation which is 73 per cent of the void fraction. Appendix F also discusses the limitation of the gamma-ray attenuation method to qualities below about 0.20.

TABLE IV

RANGES OF EXPERIMENTAL QUANTITIES
OBTAINED IN VOID FRACTION STUDY

Void Fraction	0.153	-	0.860
Mass Flow Rate, lb/hr	131	-	749
Quality	0.0172	-	0.1647
Temperature, °F	879	-	1320
Velocity Slip Ratio, V_g/V_ℓ	53	-	1150
Photomultiplier Tube Temperature, °F	128	-	160

VI. CORRELATION OF DATA

1. Two-Phase Pressure Drop Correlation for Potassium

In operation of the potassium loop, pressure drop data were obtained over a wide range of preheater power settings while keeping the flow rate essentially constant. In this way, the two-phase pressure drop was obtained as a function of average quality in the pressure drop section, with total flow rate maintained as a parameter. In such operation, minor variations in flow rate occurred due to changes in temperature throughout the system, whenever the preheater power setting was changed. Such operation at first led to plots of pressure drop as a function of average quality in the test section. Since total flow rate was a parameter, several experimental lines were derived corresponding to the several constant flowmeter signals maintained during loop operation. Further examination of the data, however, revealed that the pressure drop was also influenced by the absolute pressure level in the pressure drop section. For any given flow rate and quality, the pressure drop varied inversely with system pressure. This inverse variation had been anticipated, since the correlation of Martinelli and Nelson (55) for pressure drop during forced-circulation boiling of water had displayed this trend.

It thus became evident that the primary variables influencing the experimental two-phase potassium pressure drops were the following:

(a) Total mass flow rate
(b) Average quality in the pressure drop section
(c) Pressure level in the pressure drop section

The inlet pressure to the test section is a measure of the pressure level. It was pointed out in Chapter V that the inlet pressure is taken as the vapor pressure corresponding to the inlet temperature. Values of inlet pressure are included in Table G-II.

In considering these results for potassium, it was noted that one other prominent variable, tube inside diameter, had not been investigated. If it had been possible to use smooth tubes of different internal diameters, a body of data would have been produced which should allow a general correlation of data for the horizontal two-phase pressure drop of potassium in smooth tubes. The preliminary treatment of the data had suggested that the potassium data might best be correlated using some type of two-phase friction factor. The methods of Kosterin and Huntington (41) were tried, but no correlation of the data was obtained. An attempt at correlating the data using the two-phase friction factor and Reynolds number forms of Bertuzzi, Tek, and Poettmann (13) also gave no satisfactory correlation.

After these unsuccessful attempts at correlating the pressure drop data, it was decided to derive suitable correlating parameters using dimensional analysis. The following quantities were chosen as being of primary influence in this study:

Dependent variable:

Two-phase pressure gradient	$\Delta P/\Delta L$	psi/ft

Independent variables:

Total mass velocity	G	$lbm/hr/ft^2$
Average quality	x	(mass fraction vapor)
Pipe inside diameter	D	ft
Vapor density	ρ_g	lbm/ft^3

The effect of system pressure level is accounted for by the vapor density, since this quantity is most heavily influenced by pressure. The pipe inside diameter, while not a variable in this study, is included since it would be varied in a general study of two-phase potassium flow. Any generalized dimensional analysis of vapor-liquid flow in pipes, such as that performed by Ros (75), would also include liquid density, viscosity of both phases,

and surface tension. These quantities did not vary widely over the range of temperatures encountered in this study and thus were not included in the dimensional analysis. Application of the Pi-theorem (76) to the above variables yielded a two-phase friction factor as a function of quality.

$$f = \varphi(x) \tag{6}$$

where

$$f = \frac{\rho_g D (\Delta P/\Delta L) g_c}{G^2} \tag{7}$$

This friction factor has the same basic form as used by several other investigators. Huntington's factor, f'_g, was based upon the flow rate of gas only, but used vapor density (41). Kosterin's factor, f_m, was based on total flow rate but utilized a mean mixture density, based on the volumetric ratio of gas and liquid entering the system. The f' of Bertuzzi, Tek, and Poettmann (13) was based on a mean mixture density derived from the gas-to-liquid mass flow ratio. These latter two friction factors included a density which is physically correct in the limit as flows become all-vapor or all-liquid, but in both cases slip is ignored. It turns out that the two mean densities used are equivalent, differing only in the point of view used in their derivation --i.e., whether they are derived from mass or volume balance.

Figure 15 presents a plot of the two-phase pressure drop data according to the relationship suggested by Equation (6). All the data are included in this correlation. The least-squares line through the data is given by

$$\ell n\, f = -4.2839 + 1.5395\, \ell n\, x \tag{8}$$

which may be transformed to

$$f = 0.01379\, x^{1.5395} \tag{9}$$

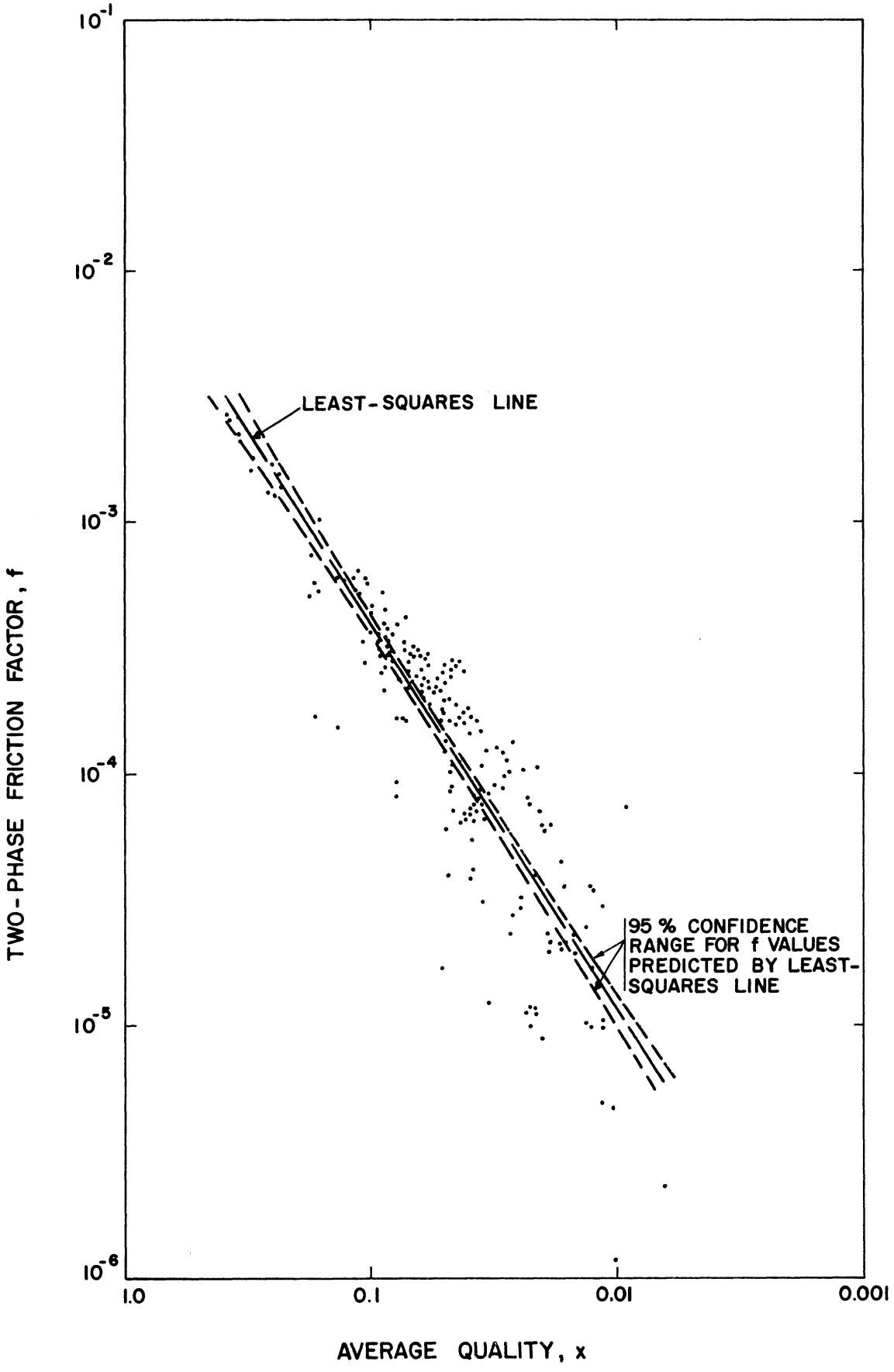

Figure 15. Two-Phase Frictional Pressure Gradient Correlation for Potassium

In presenting a correlation of data in terms of a best line through the points, such as the least-squares line given above, one must consider whether the form of the equation reasonably represents the data. In this case one could ask whether the data are adequately represented by a straight line on log-log paper. Sometimes an investigator has a firm theoretical basis to aid in the form of presenting experimental data. Frequently, as is the case here, the firm theoretical basis is lacking. Fortunately, however, statistical techniques can be used to establish the significance of a correlation (86). The linear correlation coefficient allows evaluation of the significance of a linear correlation to be done rather simply. This coefficient ranges from zero for no correlation, to unity for a perfect correlation. The coefficient is a measure of the portion of the sum of the squares of deviation of the dependent variable from its mean that is removed by the correlation. Volk (86) points out that the use of the correlation coefficient is really a statistical hypothesis test. One hypothesizes that no relation exists between the variables (zero correlation coefficient). Tabulations are available of the maximum values of the correlation coefficient that can be expected by chance, for the amount of data involved, if there were no correlation. The investigator independently calculates the correlation coefficient for the least squares line through his data. If, at a selected probability level, the calculated coefficient exceeds the tabulated maximum value, then the no-correlation hypothesis is rejected with only the selected probability of being wrong.

The concepts outlined above were used to establish the significance of the linear log-log correlation in Figure 15. The probability level selected was 0.001. For 226 points, the maximum value of the correlation coefficient that can exist for a no-correlation situation is less than 0.321 (26). The calculated coefficient from the data and least-squares line is 0.896, a value greatly exceeding the theoretical value. From the statistical viewpoint, then,

the correlation of Equation (8) is highly significant--i.e., there is less than a 0.1 per cent chance of being wrong in correlating the data in the form given by Equation (8) or Equation (9).

Figure 15 also indicates the 95 per cent confidence range for average f values predicted by the correlation. This confidence band is based upon the determination of the variance of any average value of f given by the correlation. The interpretation of this confidence range is that at any given quality, there is only a 5 per cent chance that the corresponding true mean f value lies outside the band shown. This again is a statistical concept which is quite useful in examining the worth of a correlation. That the potassium two-phase pressure gradient correlation exhibits a narrow 95 per cent confidence range is most helpful in comparison with other correlations and data of other investigations (see Chapter VII). The procedure used to establish the confidence range in Figure 15 is outlined (with regard to the void fraction results) in the first two paragraphs of Appendix F. Volk (86) shows that the confidence range of any single estimated value of the dependent variable is wider than that of an average estimated value.

Before ending this presentation of the pressure gradient correlation, it should be emphasized that the result is valid only for potassium flows where acceleration contributions to the pressure gradient are negligible compared to frictional losses. This matter is carefully considered in the next chapter, along with several other aspects of the experimental results. The potassium results of Figure 15 are general in that all major influencing variables are included (admittedly, the pipe ID was not a variable in this study). In the next chapter these results will be compared with corresponding values predicted by prominent two-phase flow correlations and also with pressure drop data reported for flows of other two-phase systems.

2. Metallic Void Fraction Correlation

Historically, several methods have been derived for correlating void fraction (or liquid fraction) data. The most famous and widely employed method is that proposed by Lockhart and Martinelli (53). It will be recalled from Chapter II that the frictional pressure drop correlation of these authors resulted in four curves depending on the flow type--i.e., one curve for each possible combination of turbulent and viscous behavior that would be displayed by the two separate phases if they were passed through the pipe at their individual flow rates. Lockhart and Martinelli found that for all practical purposes a single correlation of their liquid fraction data was obtained, with no apparent dependence upon flow type. Data from later studies, when correlated in the same manner, did show dependence on flow type. Liquid fraction data in annular flow of air-water mixtures, reported by Hewitt, King, and Lovegrove (35), resulted in two distinct curves, corresponding to viscous liquid-turbulent gas (vt) and turbulent liquid-turbulent-gas (tt) flow types. The vt data agreed quite well with the Lockhart-Martinelli correlation curve, but the tt data fell substantially lower. The mercury-nitrogen data of Kiraly and Koestel, as reported by Baroczy (9), also showed distinct curves for the vt and tt flow types; all these liquid fraction data fell substantially lower than the Lockhart-Martinelli correlation. In the mercury-nitrogen study the data encompassed a variety of flow patterns. The Lockhart-Martinelli correlation was based on data which included many commonly observed flow patterns, and the fact that it agrees with some of the annular flow data of Hewitt, et al. indicates that the prediction of liquid fraction is possible without definite knowledge of flow pattern.

Other techniques of void fraction correlation have been presented, although they are less frequently utilized in presenting new data. The extensive dimensional analysis of Ros (75), mentioned in Chapter II, led to a

method of predicting liquid fraction. Depending on whether one has low, intermediate, or high gas throughput, the prediction method involves as many as four dimensionless correlation parameters, which are functions of Ros' dimensionless groups. Such a technique can only be used effectively when one has a very large number of data points. The Ros correlation is based on vertical flow of two-phase oil reservoir fluids, the properties of which are distinctly different from those of metallic systems.

Bankoff (8) in his analytical treatment produced a particularly simple expression for prediction of void fraction

$$\alpha = \frac{K}{1 + \rho_g/\rho_\ell \left(\frac{1-x}{x}\right)} \qquad (10)$$

The major difficulty in using this equation is the necessity to specify the flow parameter K. Bankoff's work with steam-water data showed that for this system K is a function of pressure.

$$K = 0.71 - 0.0001\ P \qquad (11)$$

where P = pressure, psia. This pressure function for K makes it possible to predict steam-water void fractions quite accurately from Equation (10). Hughmark (39) realized that Bankoff's K equation would not lead to successful predictions for air-liquid systems, and he developed a K correlation for such systems. The use of Hughmark's K correlation allows Equation (10) to be used effectively. A major difficulty in Hughmark's correlation is that void fraction calculations must be done by trial and error. This difficulty arises because K is correlated against a parameter which itself must be evaluated using the void fraction. The parameter is a power function of a two-phase Reynolds number, a two-phase Froude number, and the no-slip liquid fraction. The Froude number is based on a no-slip velocity, but the Reynolds number is arbitrarily defined using a mixture viscosity weighted by void fraction. This latter feature produces the computational difficulty.

Considering liquid metal void fraction results Baroczy's preliminary correlation (9), purportedly applicable to metallic systems, is a modification of the Lockhart-Martinelli approach. The correlation is based only on two-component flow data, since single-component metallic data were unavailable at the time of its proposal. It will be shown in Chapter VII that the Baroczy correlation does not adequately predict single-component metallic void fractions, although this failure does not necessarily invalidate the method of correlation. The method of presenting metallic void fraction data as described in Kutateladze's summary (48) was also used by Smith, Tang, and Walker (78) in presenting mercury void fraction results. Void fraction was plotted against the ratio of superficial vapor velocity to total liquid velocity, taking an all-liquid Froude number as a parameter. The mercury data of Smith, et al. were favorably correlated in this manner; the data displayed scatter but not significantly more than the Russian work at other Froude numbers with which the results were compared. When the work of Smith, et al. was extended to flows of potassium-mercury amalgams, the data could not be satisfactorily correlated in the same manner (80). However, a satisfactory correlation of the Lockhart-Martinelli type was obtained.

The purpose of the discussion thus far has been to show that a variety of methods have been used to present void fraction data. The basic methods of correlation discussed above may be summarized as follows:

(a) Method of Lockhart and Martinelli(53)

(b) Method of Ros (75)

(c) Method of Hughmark (39) based on the Bankoff model (8)

(d) Baroczy's modification of Lockhart-Martinelli method (9)

(e) Method introduced by Russian workers (48)

Of these methods, item (a) above has been most frequently used.

In the first examination of the void fraction data from this study, it was found that ten points occurred for all-liquid Froude numbers between 1.05 and 1.15; small groups of points also represented other Froude number ranges. This situation prompted an attempt at correlating the data by the Russian method (6). The resulting plot showed widely scattered points with no discernible parametric effect of Froude number. This type of correlation was therefore abandoned.

The potassium data were next plotted in the manner of Lockhart and Martinelli (53). In this type of correlation, void fraction (or liquid fraction) is plotted as a function of the variable X which is defined as

$$X = \left[\frac{(\Delta P/\Delta L)_\ell}{(\Delta P/\Delta L)_g}\right]^{1/2} \tag{12}$$

where

$(\Delta P/\Delta L)_\ell$ (or g) = pressure gradient that would occur if the liquid (or vapor) were passed through the tube at its own flow rate.

For flows in which the liquid and vapor each exhibit Reynolds numbers in the turbulent range (Re > 2000)--i.e., for the tt flow type--X may be approximated as (53).

$$X_{tt} = \left(\frac{1-x}{x}\right)^{0.9}\left(\frac{\rho_g}{\rho_\ell}\right)^{0.5}\left(\frac{\mu_\ell}{\mu_g}\right)^{0.1} \tag{13}$$

For flows in which the liquid flow is viscous (Re < 1000) and the vapor flow turbulent--i.e., for the vt flow type--X may be approximated as (53).

$$X_{vt} = \left[\frac{C_\ell}{C_g}\,\frac{\rho_g}{\rho_\ell}\,\frac{\mu_\ell}{\mu_g}\left(\frac{1-x}{x}\right)\right]^{0.5} \cdot Re_g^{-0.4} \tag{14}$$

where Re_g = vapor-phase Reynolds number based on pipe diameter, xGD/μ_g

C_ℓ = constant in expression for Fanning friction factor for the liquid (16 for viscous flow).

C_g = constant in expression for Fanning friction factor for the vapor (0.046 for turbulent flow).

Since the potassium data were all of the tt flow type, void fraction was plotted against X_{tt}. The resulting graph, while showing a substantial amount of scatter, indicated a definite correlation existed.

Even though the potassium void fraction data were few in number, the resulting Lockhart-Martinelli plot showed considerable difference compared with data from air-water flows and also with the correlation curve of Lockhart and Martinelli. However, the potassium data did appear to lie on about the same curve as the mercury and potassium-mercury amalgam data of Smith, et al. (80). In addition, Noyes' four reported points for sodium (64) also fell in the same region. The favorable comparison of the potassium data with these other metallic data led to a general liquid fraction correlation for single-component metallic systems--Figure 16.

The mercury and potassium-mercury data were scaled from Figure 9 of reference (80). Almost all these data occurred for vt type flows. The four sodium points, scaled from Figure 11 of reference (64), were listed as occurring for tt type flows. These scaled liquid fraction values from literature sources are listed in Table V.

The least-squares line for all metallic data, indicated in Figure 16, is given by

$$\log (1-\alpha) = - 0.2414 + 0.3421 \log X \qquad (15)$$

from which the void fraction, α, may be expressed explicitly as

$$\alpha = 1 - 0.5735\, X^{0.3421} \qquad (16)$$

The significance of the log-log linear fit given by Equation (15) was examined in terms of the linear correlation coefficient. At the 0.001 probability level for a 41-point fit, the maximum value of the correlation coefficient that can

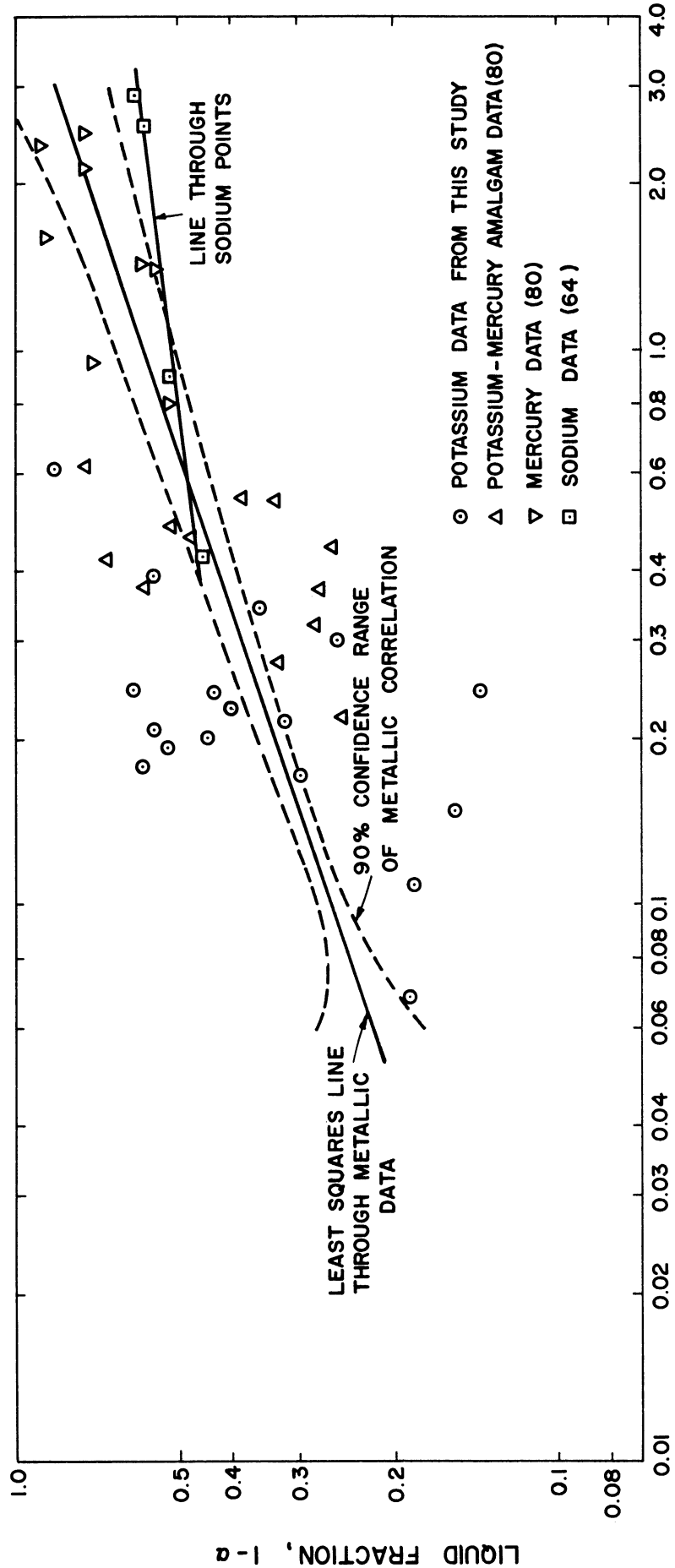

Figure 16. General Correlation of Liquid Fraction Data for Single-Component Metallic Systems

exist for no correlation is 0.496 (26). The calculated correlation coefficient for the leat-squares fit is 0.640. Since the calculated value exceeds the maximum no-correlation value, the correlation of Equation (15) is highly significant. Figure 16 also shows the 90 per cent confidence range for mean liquid fraction values predicted by the correlation. The technique for establishing this confidence range is described in Appendix F; the interpretation of confidence range was given in the preceding section on pressure drop correlation.

The correlation curve for liquid fraction in single-component metallic flows, as in the original Lockhart-Martinelli work (53), does not distinguish between flow types. The scatter in the data precludes making such a distinction. The data used in developing the correlation of Figure 16 are all the single-component metallic data reported in this country.

TABLE V

SINGLE-COMPONENT METALLIC LIQUID FRACTION
DATA FROM OTHER INVESTIGATIONS

A. Mercury Data (80)

Liquid Fraction (1-α)	X_{vt}
0.57	0.80
0.72	0.94
0.88	1.60
0.58	1.42
0.55	1.40
0.75	2.15
0.90	2.35
0.75	2.50

B. Data for Potassium-Mercury Amalgams Containing 44.5 and 14.7% Potassium by Weight (80)

Liquid Fraction (1-α)	X_{vt}
0.25	0.220
0.325	0.275
0.28	0.320
0.275	0.370
0.26	0.44
0.33	0.54
0.38	0.54
0.475	0.46
0.515	0.48
0.58	0.375
0.675	0.42
0.73	0.61

C. Sodium Data (64)

Liquid Fraction (1-α)	X_{tt}
0.60	2.90
0.58	2.55
0.54	0.896
0.45	0.426

VII. DISCUSSION OF RESULTS

1. Fluid Properties

It was stated in the Introduction that, due to a leak in the loop's heat transfer section, the two-phase pressure drop and void fraction data were obtained for flows of a sodium-potassium mixture containing 8 weight per cent sodium. The composition of this mixture was determined by flame photometry on two separate samples taken from the loop via the sampling valve indicated in Figure 1. One sample was drawn when the two-phase runs were about half complete, the other at the termination of operation. These samples analyzed 8.2 and 8.3 weight per cent sodium; the nominal composition was thus 8 per cent sodium.

The fact that the experimental results are for a binary mixture poses the following question: how closely do the results approximate the behavior exhibited by two-phase flows of pure potassium? While this question cannot be answered indisputably in the absence of pure-potassium data, it is possible to estimate differences from the pure metal.

Accurate estimates of the properties of the binary mixture were made using the procedures outlined in Appendix A. The methods employed were primarily those recommended by the Liquid Metals Handbook (43). A comparison was made between properties of pure potassium and the sodium-potassium mixture over the temperature range 900-1400°F. The average deviations between systems for several properties are given in Table VI. The vapor pressure lowering leads to lower vapor density values for the metallic mixture, since vapor densities were computed using the ideal gas law. The viscosities and

TABLE VI

AVERAGE PER CENT DEVIATION IN PROPERTIES BETWEEN PURE POTASSIUM AND MIXTURE CONTAINING 8 WEIGHT PER CENT SODIUM OVER THE TEMPERATURE RANGE 900-1400°F

Property	Average deviation of mixture from pure potassium
Liquid Density	1.6 per cent higher
Vapor Density *	4.0 per cent lower
Liquid Viscosity	1.0 per cent higher
Vapor Viscosity	0.3 per cent higher
Liquid Heat Capacity	5.1 per cent higher
Vapor Pressure **	11.3 per cent lower
Heat of Vaporization ***	3.6 per cent higher

* Ideal Gas Law assumed

** Raoult's Law assumed

*** Based on equilibrium vapor composition--i.e., for partial vaporization

densities, properties normally of greatest influence on fluid dynamics, do not show extensive deviations. Likewise, the heat of vaporization and liquid heat capacity, thermal properties of importance in quality calculations, do not differ greatly between pure potassium and the mixture.

Because these deviations are not serious, it would seem that the experimental results of this study probably correspond closely to the two-phase flow behavior of pure potassium. Certainly, no significant degree of generality is lost from the metallic void fraction correlation by presenting data for the sodium-potassium mixture, since most of the data plotted display more scatter than can be attributed to uncertainty in physical properties.

With regard to the pressure drop results, the shift in potassium properties due to the addition of 8 per cent sodium must be examined in terms of both the two-phase friction factor and quality, since both quantities are calculated using properties in Table VI. Considering first the friction factor

$$f = \frac{\rho_g \, D \, (\Delta P/\Delta L) \, g_c}{G^2} \tag{7}$$

the effect of the 1.6 per cent liquid density deviation on the total mass velocity, G, is negligible. The effect of property deviations on the pressure gradient, $\Delta P/\Delta L$, cannot be stated and is assumed negligible since the viscosity and density changes are small. The effect of vapor density deviation on f can be easily determined using the notion of a differential of a function of several variables.

$$\Delta f = \frac{\partial f}{\partial \rho_g} \Delta \rho_g \tag{17}$$

In reality the total deviation in f includes terms with respect to G and $\Delta P/\Delta L$, but, as mentioned above, these effects are ignored. From the defining equation for f,

$$\Delta f = \frac{D \, (\Delta P/\Delta L) \, g_c}{G^2} \Delta \rho_g = \frac{f}{\rho_g} \Delta \rho_g \tag{18}$$

But referring to Table VI the mean deviation in ρ_g is given by

$$\Delta\rho_g = + 0.04\ \rho_g$$

so that

$$\Delta f = + 0.04\ f \tag{19}$$

Equation (19) shows that two-phase friction factors for pure potassium may be about 1.04 of those determined experimentally for the 8 per cent sodium mixture (pure potassium values are higher because of higher vapor densities). When the correlation line in Figure 15 is displaced vertically upward by a factor of 1.04, the new line still lies within the 95 per cent confidence band of the experimental correlation. Thus, as far as calculated values of the two-phase friction factor are concerned, the effect of 8 per cent sodium in potassium appears to be negligible.

The evaluation of the pressure drop correlation in terms of fluid composition is not complete, however, without examination of the influence of property deviations on quality values. As shown in Appendix C, the inlet qualities to the pressure drop section are calculated from

$$x_1 = \frac{1}{\lambda_1}\left[\frac{Q_1 - Q_2 - Q_3}{\dot{m}} - Cp_\ell\ (T_1 - TC25)\right] \tag{20}$$

where

x_1 = quality at inlet to pressure drop section

λ_1 = heat of vaporization at temperature of test section inlet, Btu/lb

Q_1 = heat input to preheaters, Btu/hr

Q_2 = heat loss from preheaters, Btu/hr (see Appendix D)

Q_3 = heat loss from heat transfer section, Btu/hr (see Appendix D)

$\dot{m}$ = total flow rate (see Appendix B)

T_1 = temperature at inlet of pressure drop section, °F (estimated from reading of thermocouple TC30 by the method given in Appendix C).

TC25 = temperature at preheater inlet as given by thermocouple TC25, °F

Cp_ℓ = mean heat capacity of liquid over the temperature range T_1 to TC25, Btu/lb/°F

Again, the effect of liquid density deviation on the flow rate, $\dot{m}$, may be considered negligible. Changes in quality then must arise from deviations in heat of vaporization and liquid heat capacity. The property deviation in x_1 then may be obtained from

$$(\Delta x_1)_{prop} = \frac{\partial x_1}{\partial \lambda_1} \Delta \lambda_1 + \frac{\partial x_1}{\partial Cp_\ell} \Delta Cp_\ell \qquad (21)$$

After insertion of Equation (20) one obtains

$$(\Delta x_1)_{prop} = \frac{- x_1}{\lambda_1} \Delta \lambda_1 - \frac{T_1 - TC25}{\lambda_1} \Delta Cp_\ell \qquad (22)$$

The x_1 values on the right side of Equation(22) are quality values calculated for the 8 per cent sodium mixture. For the purpose of this discussion, the following constant values may be taken for λ_1 and Cp_ℓ.

$$\lambda_1 = 900 \text{ Btu/lb}$$
$$Cp_\ell = 0.2 \text{ Btu/lb/°F}$$

Then from Table VI

$$\Delta \lambda_1 = - (0.036)(900)$$
$$\Delta Cp_\ell = - (0.051)(0.2)$$

The negative signs indicate that values for pure potassium are lower. Insertion of these values in Equation (22) yields

$$(\Delta x_1)_{prop} = + 0.036\, x_1 + 1.13 \times 10^{-5} (T_1 - TC25) \qquad (23)$$

Equation (23) shows that at the same flow conditions calculated qualities for pure potassium will be higher than for the 8 per cent mixture. The use of Equation (23) in examining property effects on x_1 is not as simple as it first appears, since the x_1 term includes the flow rate as well as heat input and loss terms. Thus, the shift in quality is dependent upon loop operating

conditions as well as upon the deviations given in Table VI. Equation (22) is somewhat similar to Equation (E-4) in Appendix E, which is used to establish experimental uncertainty in quality values. It is mentioned in Appendix E that values of T_1, TC25, and other temperatures throughout the system are set primarily by two loop operating variables: preheater power, Q_1, and flow rate. Since the heat loss terms in Equation (20) are set by thermocouple TC26, the preheat power and flow rate also establish quality values in Equation (23). A study of the loop's operating history showed that at given flow rates and preheater power ratings the loop established particular mean temperature levels throughout (10). These mean temperature levels are given in Table E-I of Appendix E. Values from this table were used to calculate mean inlet qualities, Table E-II. The uncertainty in these qualities is the subject of the discussion in Appendix E. For the sake of this discussion, the mean qualities may be taken as exact, for it is desired to establish the deviation of the quality values from pure potassium behavior. It may be assumed with little error that T_1 = TC30. Values from Tables E-I and E-II were used in Equation (23) to establish the possible shift in quality due to property deviations. The results are plotted in Figure 17 as a function of the quality calculated for the 8 per cent mixture. The scatter of the points in Figure 17 arises because they are based on the mean operating history. This figure allows determination of the approximate quality shift in the pressure gradient correlation of Figure 15. This shift is indicated in Figure 18. The line diverges outside the 95 per cent confidence band for qualities below about 0.08. The effect appears to be serious at qualities below about 0.02, but even at this quality level the shift line lies within the overall scatter of the data. Even though the low quality end of the correlation appears to be translated toward higher qualities for flows of pure potassium, it would seem that pressure drop estimates for pure potassium should be made using the experimental line.

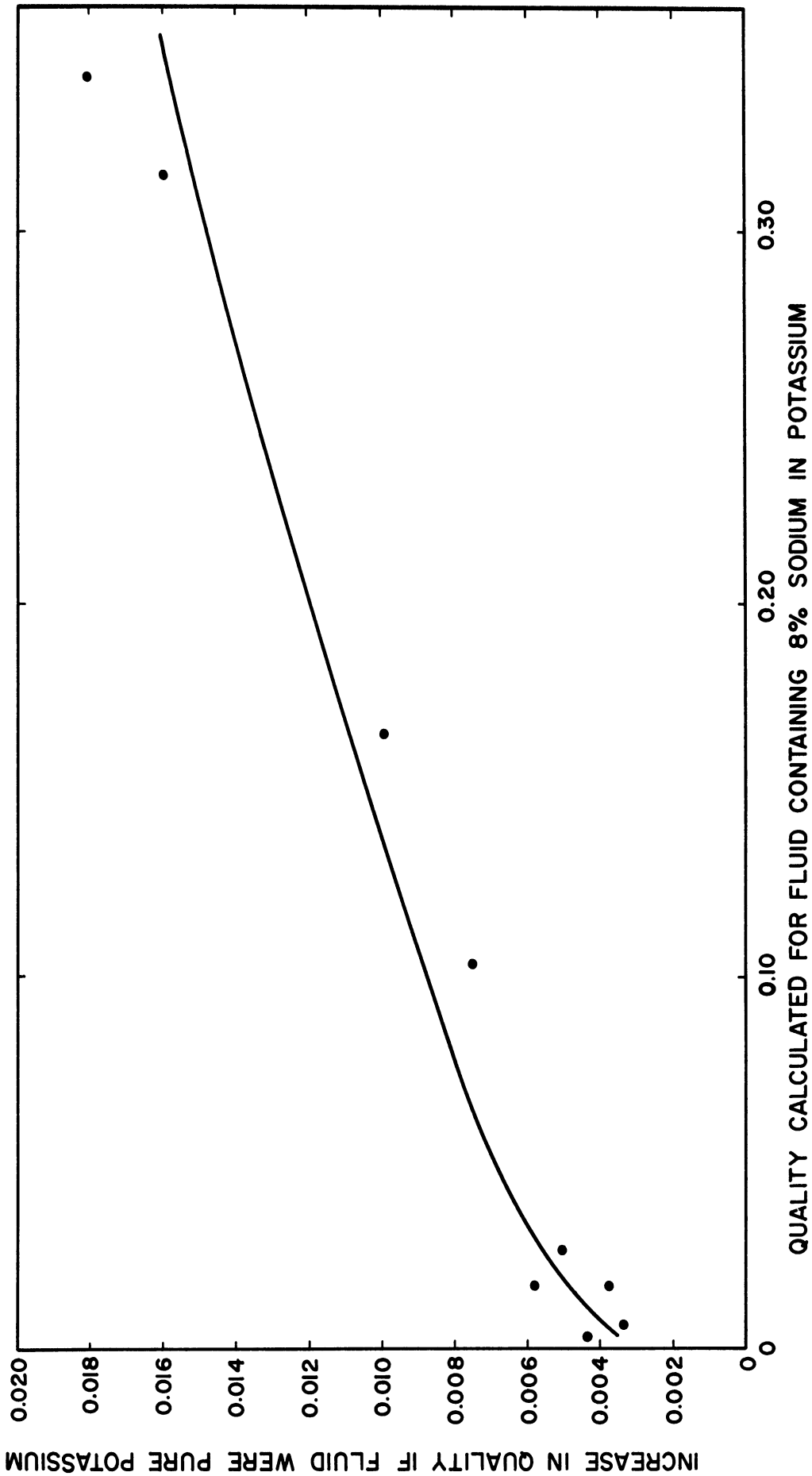

Figure 17. Increase in Quality Which Would Result if Fluid Were Pure Potassium

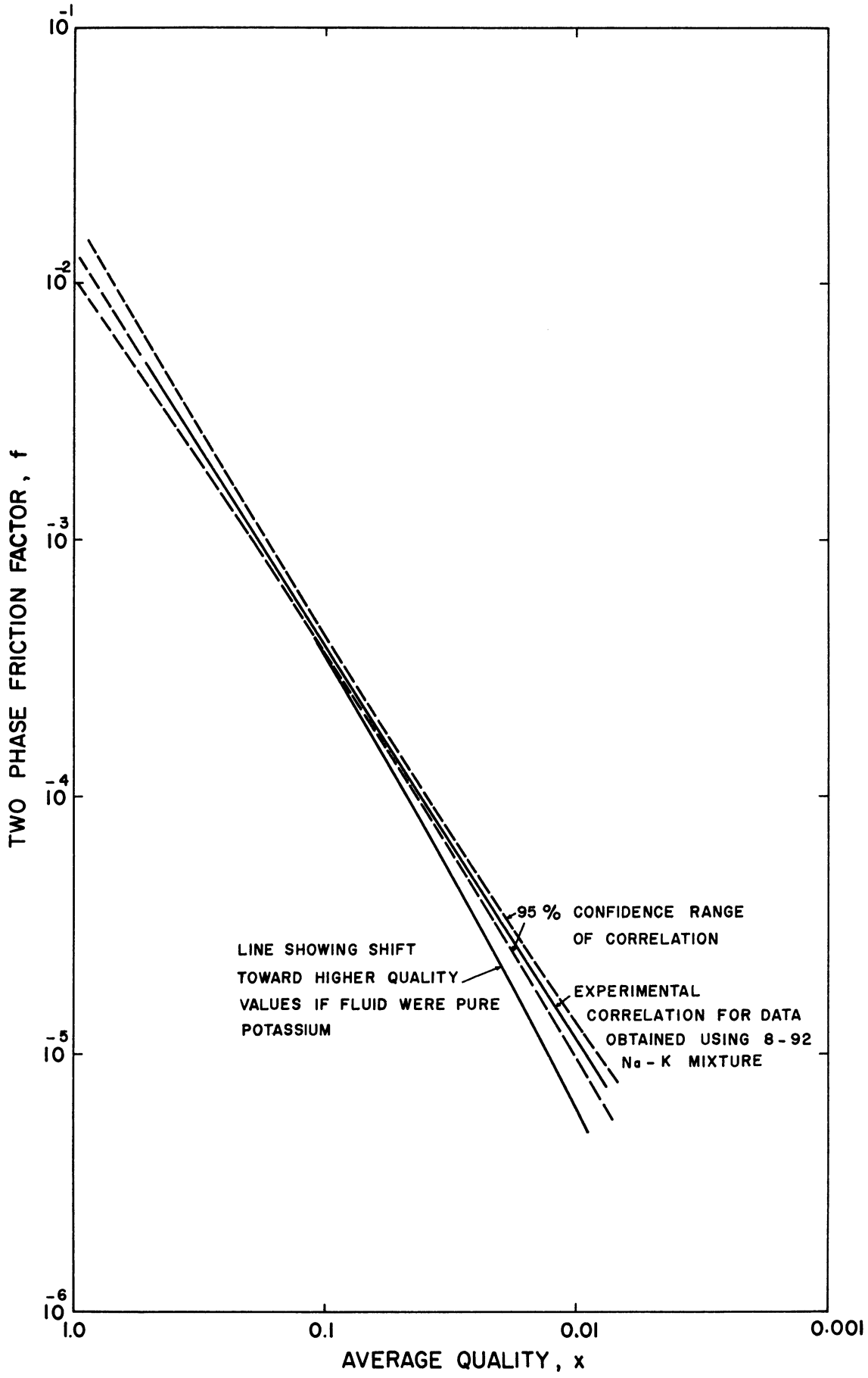

Figure 18. Two-Phase Pressure Gradient Correlation, Showing Estimated Location of Curve for Pure Potassium

This opinion is offered since the quality shift is still within the scatter of the data.

In summary, it is believed that the experimental results for the 8 per cent sodium mixture are good approximations to the two-phase flow behavior of pure potassium. The presence of 8 per cent sodium appears to have no appreciable effect on the two-phase friction factors. Due to changes in thermal properties, the presence of 8 per cent sodium tends to lower quality values slightly.

2. Flow Patterns

It was not possible in this study to investigate experimentally the flow patterns occurring in the two-phase potassium flows. The next sections of this chapter will show that the two-phase pressure gradient and void fraction results for potassium differ substantially from data for other fluid systems, notably the water-air and oil-natural gas systems. It is believed, even though confirming data are lacking, that the occurrence of various flow regimes is different for metallic fluids. This different occurrence of metallic flow patterns could be a primary factor in pressure drop and void fraction differences between metallic and nonmetallic fluid systems.

Gas-liquid flow patterns have been studied by a number of investigators. Recent literature surveys on this subject are available (7, 85). Few of the flow pattern studies reported have been concerned with single-component systems; the majority of the two-component studies has been for air-water flows at atmospheric pressure.

Gas-liquid flow patterns appear in a complex variety of forms, and visual observances have produced a wide variety of terminology. Vohr (85) points out, however, that observers seem to agree as to the basic types of flow patterns that occur, although they differ in classifying subdivisions of the basic patterns.

The basic horizontal flow patterns are (85):

(1) Bubble flow, in which gas bubbles are carried as a coarse suspension in the liquid;

(2) Plug flow, in which the gas bubbles coalesce to form long gas plugs;

(3) Stratified flow, in which the gas flows in a continuous stream above a smooth gas-liquid interface;

(4) Wavy flow, which is stratified flow with a wavy interface;

(5) Slug flow, in which periodic slugs of liquid that fill the duct cross section rapidly travel the length of the duct, leading to pulsating flow;

(6) Annular flow, in which the liquid flows in an annular film adjacent to the walls of the duct and the gas flows as a central core; the gas-liquid interface may be wavy, and the gas core may carry entrained liquid drops;

(7) Dispersed flow, in which the liquid is distributed as a spray or mist and is carried by the gas stream.

The occurrence of these regimes has usually been presented by mapping their regions of occurrence on a graph of gas flow rate plotted against liquid flow rate (the flow rates are usually expressed as mass flow rate, mass velocity, or superficial velocity). Such quantitative results for just the air-water system, show disagreement as to the bounds of the region for each flow pattern (85). Aside from variations in terminology used, this disagreement stems from difficulty in visually determining transitions between flow patterns, particularly since the transitions are by no means abrupt. In addition, the disagreement probably arises because factors other than gas and liquid flow rates also influence the occurrence of flow regimes. From visual observations of air-oil flows, Martinelli, et al. (54) offered a qualitative guide to the occurrence of the flow patterns listed above. Their results, in terms of the single-phase flow rates, are summarized in Table VII.

Only two authors have offered flow regime plots which attempt to include effects of varying fluid properties. The resulting flow regime maps basically

plot the gas throughput against that of the liquid, but the coordinates include physical property factors. Baker (3) mapped flow patterns using the coordinates G_g/λ and $G_\ell \lambda \psi / G_g$, where

G_g = superficial gas mass velocity, lb/hr/ft^2

G_ℓ = superficial liquid mass velocity, lb/hr/ft^2

and

$$\lambda = \left[\left(\frac{\rho_g}{0.075}\right)\left(\frac{\rho_\ell}{62.3}\right)\right]^{1/2} \tag{24}$$

$$\psi = \frac{73}{\sigma}\left[\mu_\ell \left(\frac{62.3}{\rho_\ell}\right)^2\right]^{1/3} \tag{25}$$

TABLE VII

QUALITATIVE OCCURRENCE OF TWO-PHASE FLOW PATTERNS AS OBSERVED BY MARTINELLI ET AL. (54)

Liquid Rate	Gas Rate	Flow Pattern
Very Low	Low and Medium	Stratified or Wavy
Very Low	High	Annular
Very Low	Very High	Dispersed
Low	Low	Plug, Stratified, or Wavy
Low	Medium	Plug, Stratified, or Wavy
Low	High	Annular
Low	Very High	Dispersed
Medium	Low	Bubble
Medium	Medium and High	Annular with Wavy Interface
High	Low, Medium, High	Froth

where $\rho_{\ell \text{ (or g)}}$ = liquid (or gas) density, lb/ft^3

μ_ℓ = liquid viscosity, centipoises

σ = surface tension, dynes/cm

These latter two parameters attempt to account for variations in physical properties. Unfortunately, the data available to Baker were essentially all for air-water flows, so that the range of physical properties used in development of his plot does not severely test the correlating parameters.

Ros (75) offered the other flow regime map which attempts to account for varying physical properties. The coordinates used were N and RN, where

$$N = V_{s\ell} \sqrt[4]{\frac{\rho_\ell}{g\sigma}} \tag{26}$$

$$R = \frac{V_{sg}}{V_{s\ell}} \tag{27}$$

$V_{s\ell}$ = superficial liquid velocity

V_{sg} = superficial gas velocity

Ros' correlation was developed from a very large number of data points for vertical flows of oil-air mixtures. The following variable ranges were covered:

$V_{s\ell}$	0	to	10.5	ft/sec
V_{sg}	0	to	328	ft/sec
D	1.26	to	5.6	inches
ρ_ℓ	48.7	to	62.4	lb/ft^3
σ	24.5	to	72.0	dynes/cm
μ_ℓ	2.42	to	6.38	lb/ft/hr

For the potassium flows, these same quantitaties covered the following ranges:

$V_{s\ell}$	0.3	to	3.5	ft/sec
V_{sg}	50	to	780	ft/sec
D	0.495			inch
ρ_ℓ	42.7	to	46.3	lb/ft^3
σ	69	to	85	dynes/cm
μ_ℓ	0.35	to	0.45	lb/ft/hr

The potassium V_{sg} values are higher because of lower vapor densities and lower tube diameter. Liquid viscosity is the only property which lies entirely outside Ros' range. The inclusion of surface tension in both the Baker and Ros correlations would seem to be correct, for this property would be expected to influence transitions of liquid-continuous flows to vapor-continuous or separated flows.

In an effort to establish the probable flow patterns for the potassium flows, the correlations of Baker (3) and Ros (75) were used to predict the regimes. The flow conditions corresponding to all pressure drop and void fraction points were employed. The distribution of predicted flow patterns is given in Table VIII. No accurate method was found for estimating the surface tension of the sodium-potassium mixture. The recent potassium surface tension data of Cooke (19) were used in the predictions.

The distribution of flow patterns predicted by the Baker method tends slightly toward the annular-dispersed transition. The Ros method points heavily toward dispersed flows for the potassium data. In retrospect the dispersed flow predictions do not seem physically accurate. The liquid fraction values, Table H-II, range from 0.1397 to 0.8472. Moreover, Figure 16 shows that only four values are less than 0.2. Thus, the liquid fraction data for the metallic systems are rather high. Bankoff (8) points out that bubble flow is usually observed in vertical flows when liquid fractions are

TABLE VIII

DISTRIBUTION OF PREDICTED POTASSIUM
TWO-PHASE FLOW PATTERNS

A. Flow Patterns Corresponding to Pressure Drop Data

Baker's Method (3):

Annular Flow	30% of Data *
Dispersed Flow	30% of Data
Annular-Dispersed Transition	40% of Data

Ros' Method (75):

Dispersed Flow	87% of Data
Dispersed-Froth Transition	5% of Data
Froth Flow	8% of Data

* % of Data refers to percentage of total pressure drop data predicted in indicated regime.

B. Flow Patterns Corresponding to Void Fraction Data

Baker's Method (3):

Annular Flow	None
Dispersed Flow	41% {55.4, 56.8, 56.9, 59.5, 68.9, 69.1, 72.4 **
Annular-Dispersed Transition	59% {51.12, 51.11, 60.11, 62.10, 63.3, 64.10, 64.11, 65.10, 67.12, 78.1

Ros' Method (75):

Dispersed flow predicted for all points

** Numbers inside bracket are Code numbers of data points predicted in indicated regime.

greater than 0.2. It certainly does not seem likely that dispersed flows would exist at the high liquid fractions observed in this study. The liquid superficial velocities were in the low range, while vapor superficial velocities ranged from low to high. Table VII suggests that plug, stratified or wavy flows may have existed for the lower qualities, while annular flow probably occurred at higher qualities. Since the void fraction data indicate the occurrence of high velocity slip ratios, it seems probable that flows were stratified or wavy at lower qualities and annular at higher qualities. The existence of bubble flows (which probably would occur in a vertical tube) is not probable, since gravitational asymmetry in these horizontal flows would tend to force liquid to the bottom of the tube, except at higher qualities.

The apparent failure of the Baker and Ros plots in predicting flow regimes for potassium may hinge on wettability considerations, since liquid metals probably have more affinity for metallic pipe walls than do water or oils. In any case, it appears that the occurrence of flow regimes for metallic systems is quite different from the few fluid systems studied previously. Another possible failure in the prediction methods is that they are based on two-component fluids. No methods are available for single-component systems. Perhaps the fact that the gas phase was noncondensable for the Baker and Ros data contributes to the failure of their method when applied to single component flows.

In summary, the flow regimes which occurred in the potassium flows are not exactly known and apparently cannot be satisfactorily predicted by two prominent methods in the literature (3, 75). The range of liquid fractions, total fluid throughputs, and qualities suggests that the flow regimes were probably stratified or wavy at lower qualities and annular at the higher qualities. The occurrence of dispersed flows, in view of the high liquid fractions encountered, seems improbable.

3. Two-Phase Pressure Drop Study

3.1 All-Liquid Pressure Drop Measurements.

It was stated in Chapter V that three pressure drop readings were obtained for all-liquid flows. Because of the slight inclination of the pressure drop section, the tube in all-liquid flows does not flow full except for high throughputs. For this reason only three all-liquid points were obtained over a very narrow flow rate range. The use of single-phase friction factors is necessary in comparing the potassium data with values predicted by the Lockhart-Martinelli correlation(53). The three all-liquid data points were therefore important for checking the validity of the equation used to calculate single-phase friction factors.

Knudsen and Katz (46) suggest the following equation for smooth-tube friction factors

$$f_{sp} = 0.0056 + 0.500\ Re^{-0.32} \qquad (28)$$

where f_{sp} denotes the Moody friction factor for single-phase flow. This relationship is valid for Reynolds numbers from 3,000 to 3,000,000. Table G-I shows that the average deviation of the experimental friction factors from values calculated by Equation (28) is 7.7 per cent. This deviation is relatively small, and, because no range of liquid Reynolds numbers could be realized, Equation (28) was accepted as being sufficiently accurate.

3.2 Flow Characteristics.

The flow patterns that may have existed in the potassium flows have already been considered. Although the flow regimes cannot be exactly predicted, it is probable that flows were stratified, wavy, or annular, depending on the quality level.

Several other aspects of the two-phase flows deserve examination. The table of two-phase pressure drop data, Table G-II, includes a comparison of

the experimental pressure drops with values computed on the basis of thermodynamic equilibrium. The equilibrium pressure drops were obtained by subtracting the outlet vapor pressure from that at the inlet; the temperatures at both locations were assumed to be known exactly. The comparison with equilibrium pressure drops was made by dividing the experimental values by the equilibrium values. These ratios are given in the column headed by the notation DP/EQDP. A study of this column is somewhat surprising, for only 30 per cent of the data display experimental-to-equilibrium pressure drop ratios between 0.8 and 1.2. Seven negative values appear; these occur because the estimated outlet temperature is higher than the inlet temperature (see Appendix C). Further study of the table shows that 20 per cent of the data have pressure drops greater than twice that predicted by equilibrium, and 14 per cent show ratios less than 0.5.

One might at first think something is wrong with single-component data that exhibit such departures from equilibrium. However, several authors have observed departures from equilibrium in their two-phase flow investigations. Notable examples are offered by investigators who studied flows of saturated liquids through nozzles and orifices (41). Pike (66), in a study of horizontal steam-water pipe flows, found that 15 of his 28 runs showed departure from equilibrium. Pike's apparatus allowed comparison between axial temperature and pressure profiles. Poppendiek (67) indicated that some of his two-phase mercury flows were not at equilibrium; Berenson and Killackey (12) found that some of their boiling potassium flows did not appear to be at equilibrium.

The assumption that thermodynamic equilibrium exists in a two-phase flow requires that the temperature be constant over the channel cross section. If, however, changes in temperature and pressure occur so rapidly along the tube that rates of heat and mass transfer become controlling, then temperature

gradients will occur in the liquid and vapor phases and departure from equilibrium must result. These remarks apply particularly to separated flows, such as annular or stratified flows, where high slip ratios can occur. Such conditions of radial temperature gradients are believed to characterize two-phase flows in nozzles and orifices. It thus seems possible that radial temperature gradients existed in many of the two-phase potassium flows. The departures from thermodynamic equilibrium probably do not seriously affect calculated quality values, since the liquid heat capacity and heat of vaporization are not strong functions of temperature.

Table G-II includes values of temperature and quality for both the inlet and outlet of the pressure drop section. Examination of the temperatures shows that about 60 per cent of the pressure drop data occurred under conditions where the temperature drop across the test section was greater than 15°F. Of these so-called "nonisothermal" points, about 60 per cent exhibited temperature drops between 30 and 60°F. The following list summarizes the distribution of temperature drop values:

ΔT, °F	No. of Data Points
> 100	2
80-90	5
70-80	6
60-70	23
30-60	84

In runs where significant temperature drops occurred across the test section, the quality often increased across the test section. This increase resulted because the sensible heat change of the fluid was greater than the heat loss from the pressure drop section. In some instances, however, the sensible heat change was less than the heat loss, and quality decreases occurred. In all cases where the quality decreased, the decrease was very slight. But in

many cases where an increase occurred, it was between 0.01 and 0.02, representing a significant percentage of the average quality in the test section. Such quality increases cause acceleration contributions to the pressure gradient.

In Chapter VI, it was emphasized that the potassium two-phase pressure gradient correlation was for frictional pressure losses. It is necessary to justify this statement, in view of the possible acceleration effect mentioned above. For any general flow system in which a change of phase is occurring, the differential pressure drop can be written as

$$-dP_{total} = -dP_{friction} - dP_{acceleration} - dP_{hydrostatic}$$

This relationship may be expressed quantitatively as

$$-dP = -dP_f + \bar{\rho} \frac{V dV}{g_c} + \left(\bar{\rho} \frac{g}{g_c} \sin\Theta\right) dL \qquad (29)$$

where $\bar{\rho}$ = local mean density of the two-phase mixture

$-dP_f$ = frictional pressure loss

V = local superficial mixture velocity

L = length along channel

Θ = angle of inclination of channel from horizontal

g_c = force-mass conversion constant

g = acceleration of gravity

For a two-phase mixture flowing with slip, the local mixture density is given in terms of the local void fraction and individual phase densities as (Appendix I)

$$\bar{\rho} = \alpha \rho_g + (1 - \alpha) \rho_\ell \qquad (30)$$

Since the flows under consideration here were horizontal, the hydrostatic term in Equation (29) drops out. The question that must now be answered is: what fraction of the total pressure drop is represented by the acceleration

component? The mean mixture velocity may be written in terms of the total mass velocity, G, and mean density as:

$$V = \frac{G}{\bar{\rho}} \tag{31}$$

Then the acceleration component of the total pressure drop becomes

$$-dP_a = \bar{\rho} \frac{VdV}{g_c}$$

$$-dP_a = -\frac{G^2}{g_c} \frac{d\rho}{\rho^2} \tag{32}$$

In order to establish the $-dP_f$ term, all the essentially isothermal potassium data (88 points in which the temperature drop was less than 15°F) were used to formulate a correlation for the two-phase friction factor. These data, because of the small temperature drops, displayed only very slight quality increases and hence were certain to represent almost purely frictional pressure drops. Use of these "isothermal" two-phase friction factors, together with Equation (32), reduces Equation (29) to

$$-dP = f_I\left(\frac{G^2}{g_c \rho_g D}\right) dL - \frac{G^2}{g_c} \frac{d\rho}{\rho^2} \tag{33}$$

where f_I denotes the isothermal two-phase friction factor, defined by Equation (7). Integration of Equation (33) between entrance and exit of the test section gives the overall pressure drop.

$$-\Delta P = \frac{G^2}{g_c D} \int_1^2 \frac{f_I}{\rho_g} dL - \frac{G^2}{g_c} \int_1^2 \frac{d\bar{\rho}}{\bar{\rho}^2} \tag{34}$$

Both f_I and $\bar{\rho}$ vary along the tube, due to the changes in temperature and quality. The unknown variation of f_I and $\bar{\rho}$ with axial position prevents analytical integration of Equation (34).

The integrations indicated in Equation (34) were performed numerically on the computer, under the following assumptions:

(a) Thermodynamic equilibrium existed at all points along the tube

(b) Flows were steady-state and fully developed

(c) The heat loss from the test section was distributed such that quality varied linearly from entrance to exit.

The experimentally known values of total flow rate, inlet and outlet quality, and inlet temperature were the only necessary input information for the computer program. Use of the metallic void fraction correlation, Equation (16), was the key to successful integration of Equation (34), since mixture densities could be readily calculated. The calculation procedure consisted in dividing the tube into a number of equal segments and stepwise calculating the pressure drop along the tube. The pressure at the outlet of any segment was iterated to a set tolerance before stepping ahead. At the end of the tube the total pressure drop was also tested against a set tolerance. If the overall tolerance was not met, the stepwise procedure was performed again using smaller length segments.

This procedure was used for many experimental flow conditions where the temperature drop was greater than 15°F. The calculated pressure drops agreed well with experimental values. The important result of these calculations, however, was that clear comparisons between the friction and acceleration components of pressure gradient could be made for a wide range of flow conditions. In all cases, the acceleration term was much smaller than the frictional component, always being less than 3 per cent of the overall pressure gradient. For most cases it was less than 1.5 per cent of the overall pressure gradient. While the frictional pressure gradients ranged from 0.016 to 1.03 psi/ft, the acceleration components ranged from 0 to 0.014 psi/ft. These results made it clear that the experimental potassium two-phase pressure drops were essentially frictional.

This conclusion was also obtained by a statistical approach. In addition to the correlation of essentially isothermal data, mentioned above, a correlation for the "nonisothermal" points was developed. Both these correlations were of the log-log type given in Figure 15, and both were fitted by the least-squares technique to equations of the form of Equation (8). When the two least-squares correlations were statistically tested by the t-test (86), no significant difference was found between the lines. The statistical interpretation, therefore, is that the so-called "isothermal" and "nonisothermal" sets of data are not different from each other, supporting the result found by analysis previously discussed.

Finally, it should be pointed out that low acceleration pressure gradients cannot be expected for boiling flows where the quality increase is very large. The computational approach outlined above may be used to estimate boiling pressure drops. The key to such calculations is the void fraction correlation and some measure of frictional characteristics, both of which are experimental results of this study. Hydrostatic terms can also be included.

3.3 Comparison with Other Correlations and Data.

In Figure 19 the potassium pressure gradient correlation is compared with values predicted using the frictional pressure drop correlations of Lockhart and Martinelli (53) and Bertuzzi, Tek, and Poettmann (13). Both these correlations were developed from air-liquid and natural gas-liquid data, covering fairly broad ranges of fluid properties, flow rates, and pipe diameters. As evidenced by Figure 19, both these correlations predict values for potassium which are appreciably high. Their predictions lie well above the 95 per cent confidence range of the potassium correlation. Indeed, they are beyond the overall scatter of the potassium data.

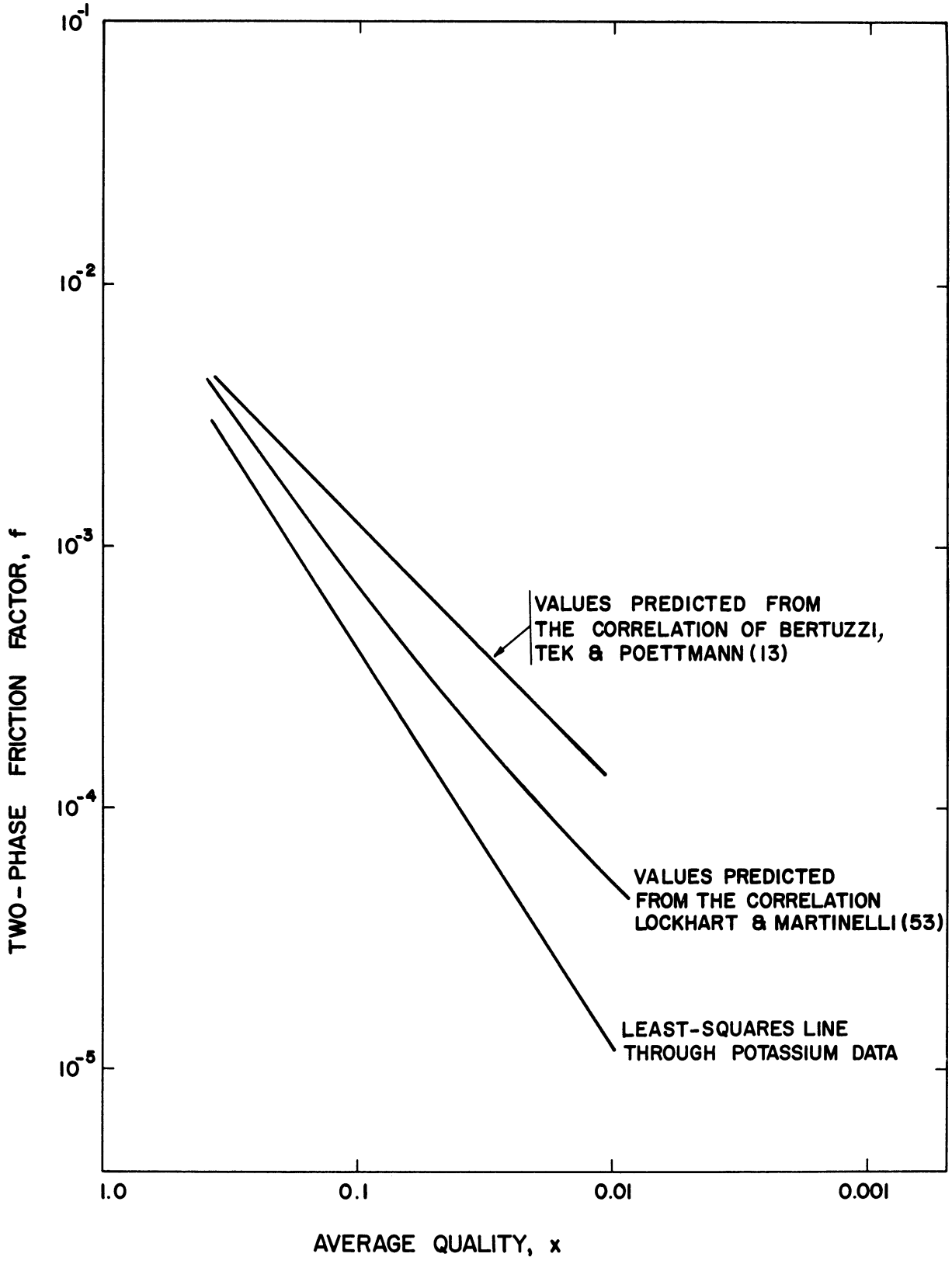

Figure 19. Comparison of Potassium Results with Values Predicted by Correlations of Lockhart and Martinelli (53) and Bertuzzi, Tek, and Poettmann (13)

In Figure 20 the potassium correlation is compared with values predicted by the Bankoff variable density single fluid model (8), which was quite successful in predicting behavior of steam-water flows. Bankoff's theory was briefly discussed in Chapter II, where it was pointed out that the derivations were for the bubble flow regime. A radial concentration of bubbles was imagined, with slip presumed negligible at any point, leading to analysis of a fluid with variable density. It was mentioned in Chapter VI that the primary difficulty in applying the Bankoff model is specification of the flow parameter K. As can be seen from Equation (10), K is a function of void fraction, quality, and temperature level. The void fraction data, Table H-II, were used to compute K values for potassium. As suggested by Bankoff's findings (8), the potassium K's were plotted against system pressure, taken as the vapor pressure corresponding to the average temperature in the test section. This plot, given in Figure 21, shows a rough correlation. Two lines appear to be present, but no clear parameter could be discovered. Thus, a least-squares line is given for the plot and is compared with Bankoff's line for steam-water data extrapolated into the low pressure range of the potassium experiments. Bankoff's equation for frictional pressure gradient, given in terms of the wall shear stress, is

$$\frac{\tau}{\tau_{sp}} = \left[1 - \alpha\,(1 - \rho_g/\rho_\ell)\right]^{3/4} \left[1 - x\,(1 - \rho_\ell/\rho_g)\right]^{7/4} \tag{35}$$

where τ = wall shear stress for two-phase flow

τ_{sp} = wall shear stress if flow were all-liquid at same total flow rate and temperature

The single-phase wall shear stress is determined from the well-known formula

$$\tau_{sp} = 1/2\, f_\ell\, \rho_\ell\, V_o^2 \tag{36}$$

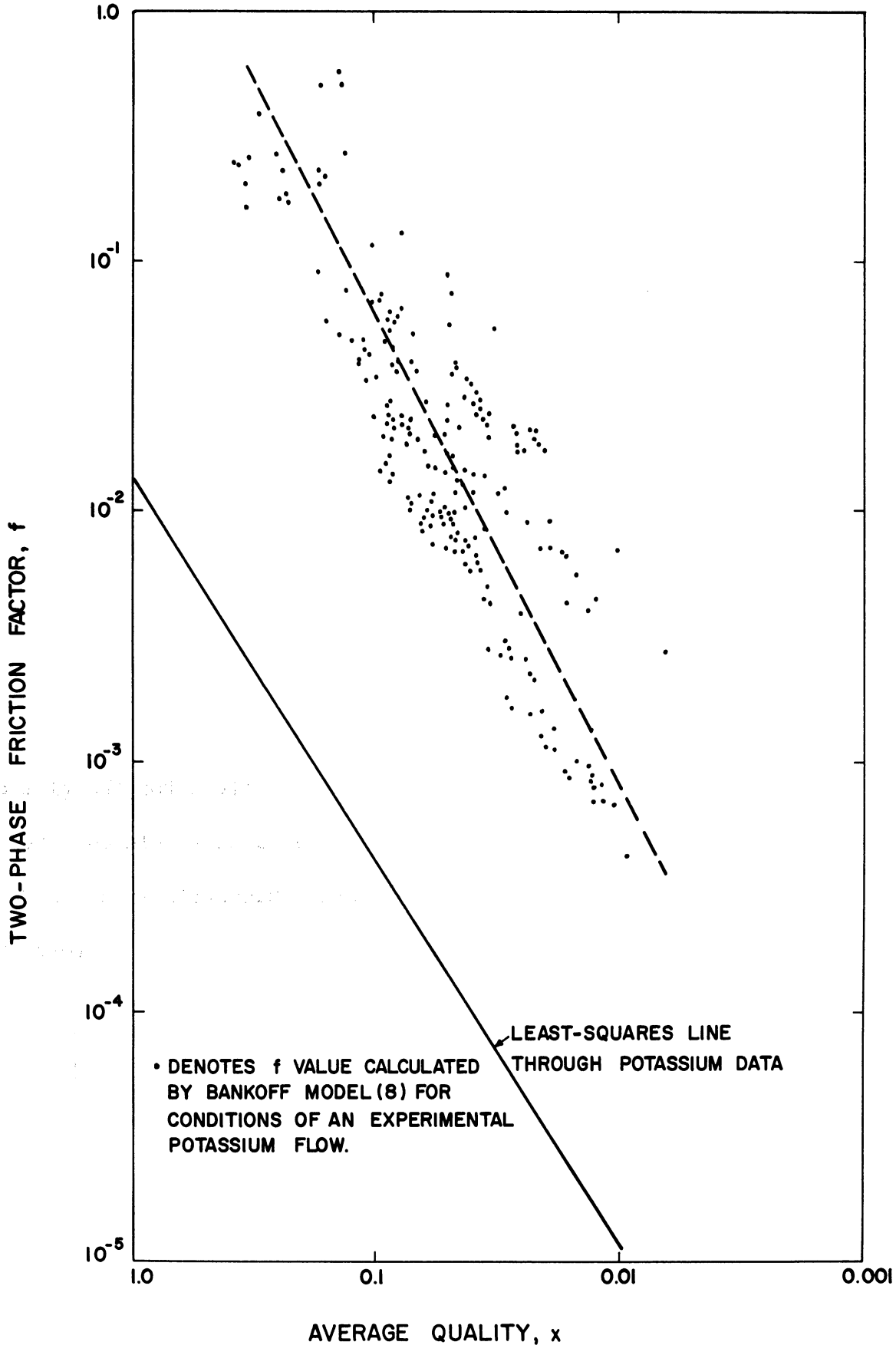

Figure 20. Comparison of Potassium Two-Phase Pressure Gradient Correlation with Values Predicted using Bankoff's (8) Model

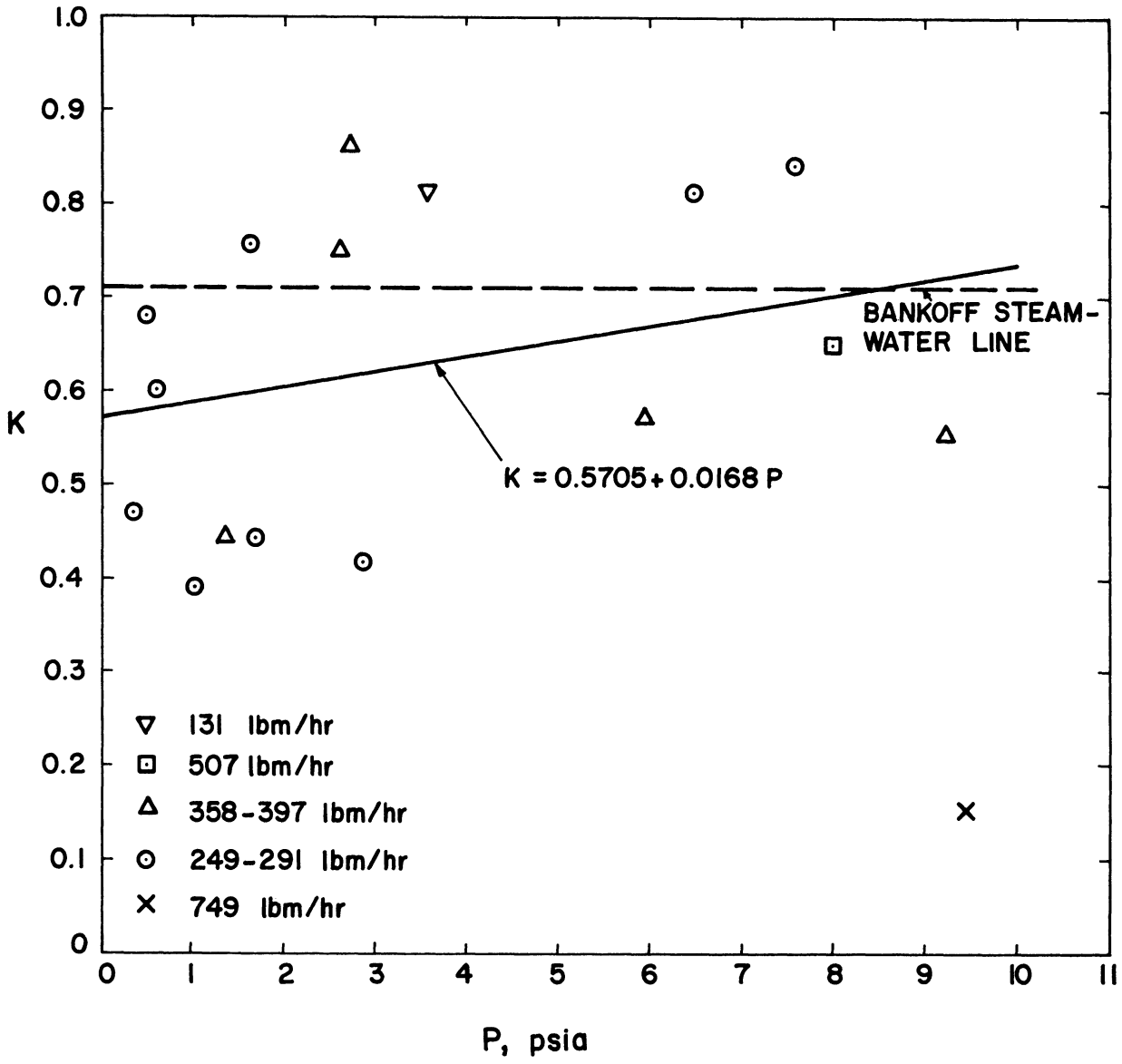

Figure 21. Values of Bankoff's K (8) for Potassium

where f_ℓ = friction factor for all-liquid flow

V_o = mean liquid velocity for all-liquid flow

The f_ℓ values are obtained from Equation (28). The pressure drop predictions made by applying the Bankoff theory to potassium flow conditions yielded the points given in Figure 20.

It is seen from Figure 20 that the Bankoff model predicts f values even higher than do the correlations used for comparison in Figure 19. Generally, the Bankoff predictions are a factor of 10^2 higher than the potassium data. The void fraction values in Equation (35) were obtained from Equation (10), using the potassium K values of Figure 21. Corresponding to all the experimental two-phase pressure gradient flow conditions, the K values ranged from 0.577 to 0.827. In contrast with values predicted by the correlations of Lockhart and Martinelli (53) and Bertuzzi, et al. (13) which lay essentially on curves, the Bankoff predictions show a great deal of scatter. The theory was also tried for experimental flow conditions using constant K values of 0.6, 0.7, 0.8, and 0.9. The predicted values showed about the same degree of scatter. The calculated values of f were a little lower at higher K values; at K = 0.9 the average Bankoff results were about half of those given in Figure 20 for the experimental K range.

Evidently there is some deficiency in the Bankoff model for making satisfactory pressure drop estimates for potassium, and probably also for other metallic fluids. Perhaps inaccuracy arises from the assumption that the ratio of mean two-phase viscosity to liquid viscosity is unity. The potassium void fraction data indicate high slip ratios, violating one of the primary assumptions of the theory. This suggests that perhaps the potassium flows, particularly at lower liquid flow rates, may have been stratified or plug.

In Figure 22 the potassium pressure drop data are presented on a Martinelli type of plot. The Martinelli parameters were defined in Equation (1), Chapter II. The comparisons in Figure 19 were made using the turbulent-turbulent correlation line, since all the potassium liquid and vapor Reynolds numbers were well into the turbulent range. Figure 22 also shows the air-water data of Richardson (74) for the tt type air-water flows in rectangular channels. Figure 22 shows that most of the potassium data lie between the tt and vv curves. It appears that the vt curve of reference (53) fits the potassium data quite well. Based on this finding, it is believed that two-phase pressure drops for other metallic fluids might be estimated using the Lockhart-Martinelli vt curve, which can be given as

$$\ell n \phi_{\ell_{vt}} = 1.247 - 0.488\ \ell nX + 0.0712\ (\ell nX)^2 - 0.0008\ (\ell nX)^3 - 0.0007\ (\ell nX)^4 \qquad (37)$$

In Figure 23 the potassium correlation is compared with data obtained from other fluid systems. The steam-water data of Isbin, Sher, and Eddy (42) were obtained in an 18 foot long, 0.872-inch ID vertical tube. These data were corrected for the hydrostatic head before plotting in Figure 23. Pike's steam-water data (66) were obtained in a 0.93-inch ID, 19.42-foot long horizontal test section. The data reported by Johnson and Abou-Sabe (44), Govier and Omer (28), and Reid, et al. (73) were all for air-water flows. Johnson and Abou-Sabe used a 15.7-foot long horizontal test section with a 0.87-inch ID. They reported data in isothermal and heated runs; data of both types are included in Figure 23. The data of Govier and Omer are for horizontal isothermal flows in a 1.026-inch ID by 30-foot long test section. Reid, et al. obtained isothermal, horizontal data in 4-inch and 6-inch commercial steel pipes, each measuring 56 feet between pressure taps. The data furnished by Tek (83) are for flows of oil and air or natural gas in pipes of various

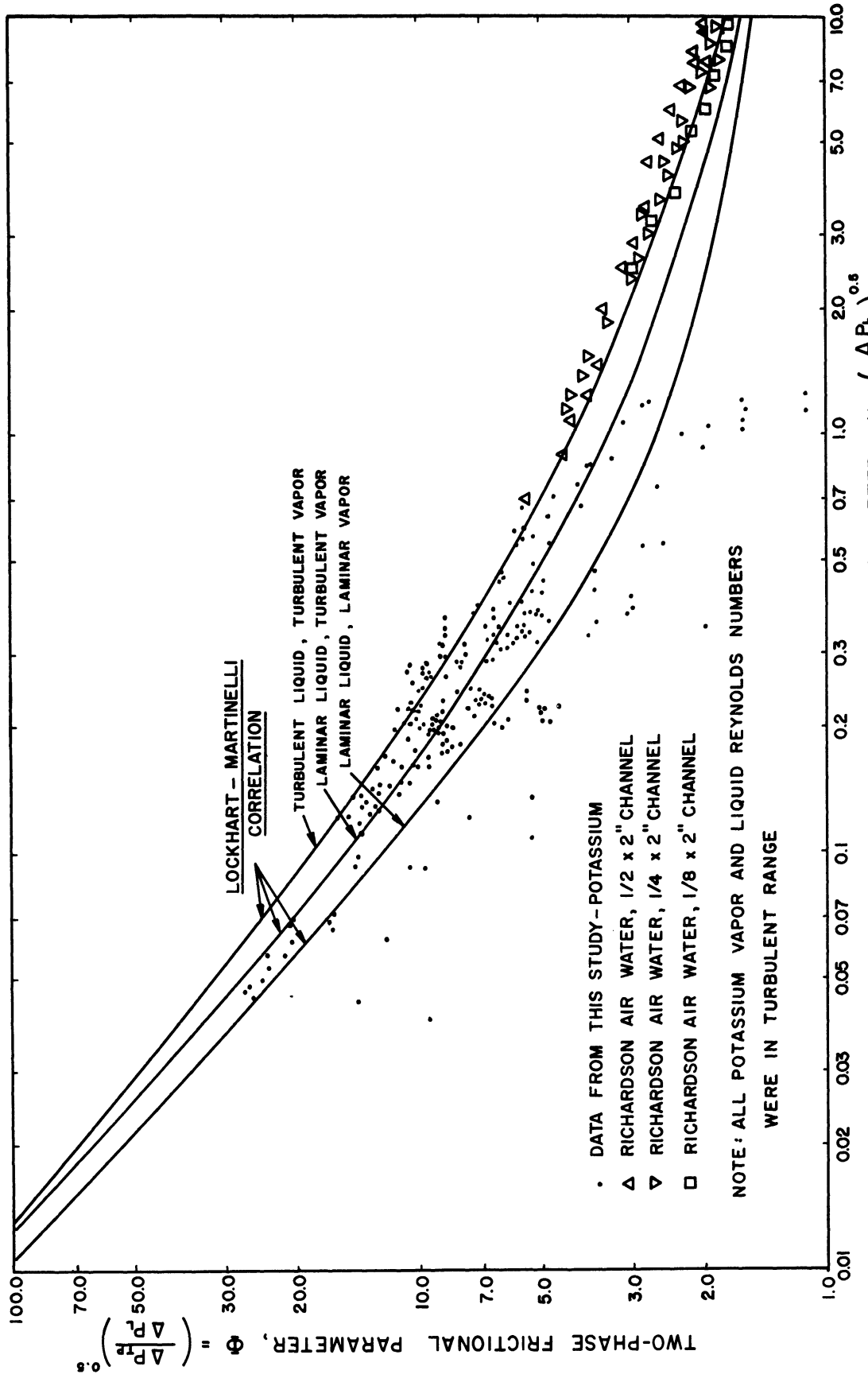

Figure 22. Martinelli Type Plot of Potassium Two-Phase Frictional Pressure Drop Data

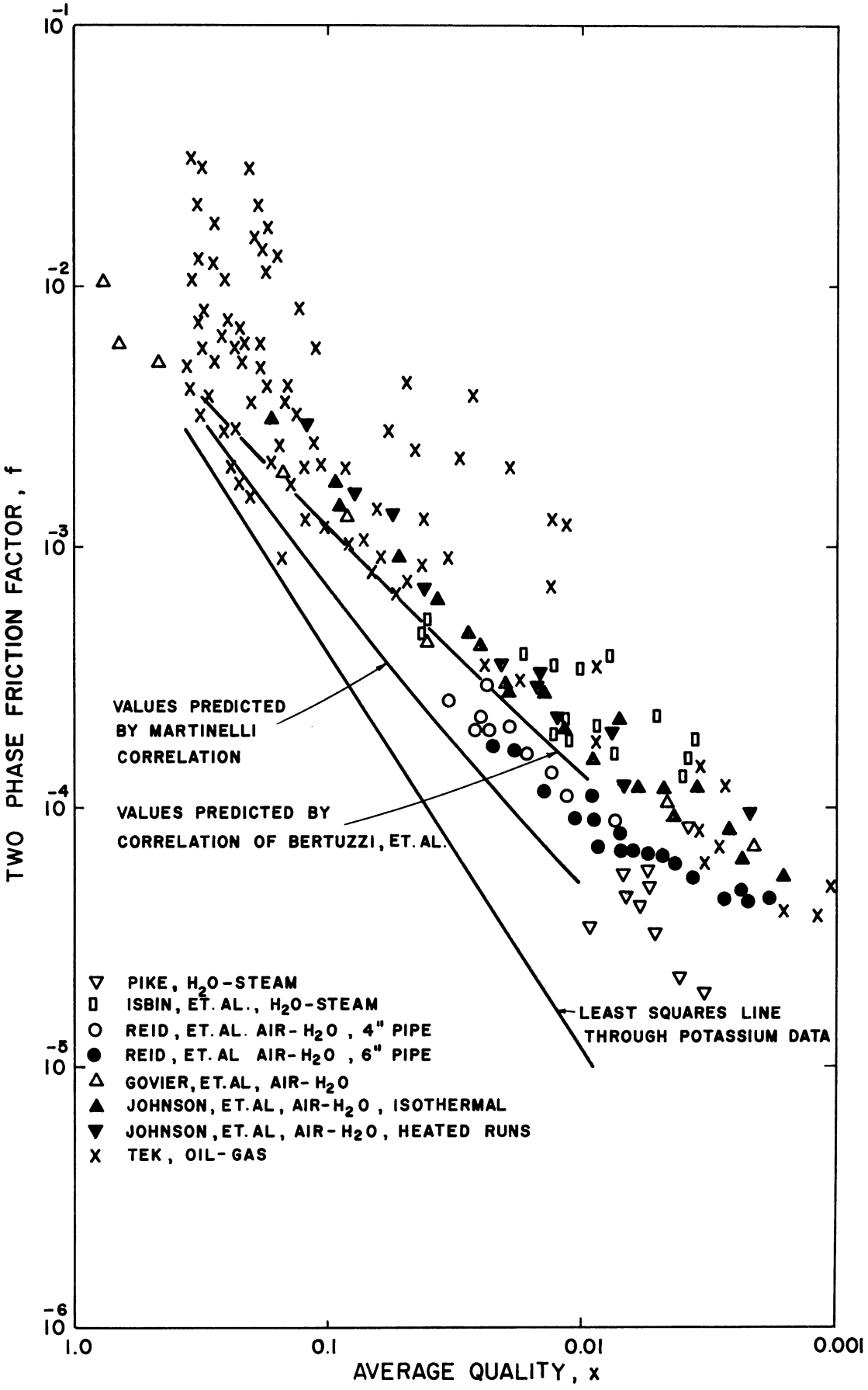

Figure 23. Comparison of Potassium Two-Phase Pressure Gradient Correlation with Data of Other Investigations

diameters. Figure 23 includes the curves corresponding to the correlations of Lockhart and Martinelli (53) and of Bertuzzi, Tek, and Poettmann (13).

The data shown in Figure 23 all fall substantially higher than the potassium results. Figure 20 indicated that this would be the case, since the correlations of references (53) and (13) are based on data of the type plotted in Figure 23.

It is highly desirable to compare the potassium results with data from other metallic experiments. Metallic pressure drop data have been obtained by a few investigators, but except for one case the data are not reported in a sufficiently clear manner for comparison with the results of this study. In most of these cases the flows were through boiling sections where substantial acceleration losses may be incurred. The void fraction correlation of this study, Figure 16, could be used to separate the friction and acceleration contributions, if enough experimental information was given by the authors.

Berenson and Killackey (12) have obtained data for potassium pressure drops through a horizontal boiler. The boiler tube was about 12.8 inches long, with a 0.180-inch ID. Flows were actually through a helical passage formed by insertion of a twisted ribbon into the boiler tube. Temperature profiles were obtained by application of the Lockhart-Martinelli correlation (53), a dubious procedure in view of the findings of Figure 19. Pressure drops were reported as ratios of experimental values to values predicted by the Martinelli correlation. The helical flow geometry together with the inexact data presentation preclude comparison with the results of this study.

Fisher (25) obtained data for boiling rubidium in a 0.28-inch ID, horizontal tube about 47 inches long. A Taylor differential pressure gauge was used. Data for 14 randomly selected runs (out of 67) were presented in a plot of calculated vs. measured pressure drop. The calculation procedure employed gave good agreement with the data, but the data are not otherwise presented in a manner suitable for comparison with this study.

Poppendiek, et al. (68) reported some results of boiling pressure drop for mercury in a 0.305-inch ID tube, approximately 14.8 inches long. Some flows were vertical and some horizontal; no accurate information was given concerning either system pressure level or fluid temperatures. A plot of pressure drop as a function of quality for mass flows of 65 lb/hr is given, but it is not clear whether the data are for horizontal or vertical flows, or possibly both with suitable corrections made in the vertical data. Whether the qualities are average, inlet, or outlet, is not stated.

Hoffman (36, 70) reports the results of studies of vertical boiling flows of potassium at Oak Ridge National Laboratory. The test section was 0.325-inch ID by approximately 80 inches long. Data are given in sufficient detail to allow comparison with the results of this study--i.e., hydrostatic and acceleration terms can be deducted. However, in addition to the boiler tube, an inlet mixing chamber, an exit end expansion section, and exit thermocouple wells were located between the pressure taps. Thus, the results include undetermined losses, rendering them unsuitable for comparison with this study. Calculated results for water-steam, excluding the undetermined losses, fell about a factor of 3 higher showing qualitative agreement with results of this study.

The only metallic data for which a valid comparison could be made with this study are the horizontal isothermal mercury-nitrogen flow data of Koestel (47). The experiments were performed in a 0.395-inch ID by 51.75 inches long Pyrex tube. Pressure gradient and liquid fraction data were obtained. The pressure gradient data are compared with the potassium correlation of this study in Figure 24. It is seen that the results from the two flow systems agree very favorably. This finding, when reviewed with regard to the differences shown in Figures 20 and 23, suggests that some fundamental difference exists between the pressure drop behavior for metallic flows and that for nonmetallic flows.

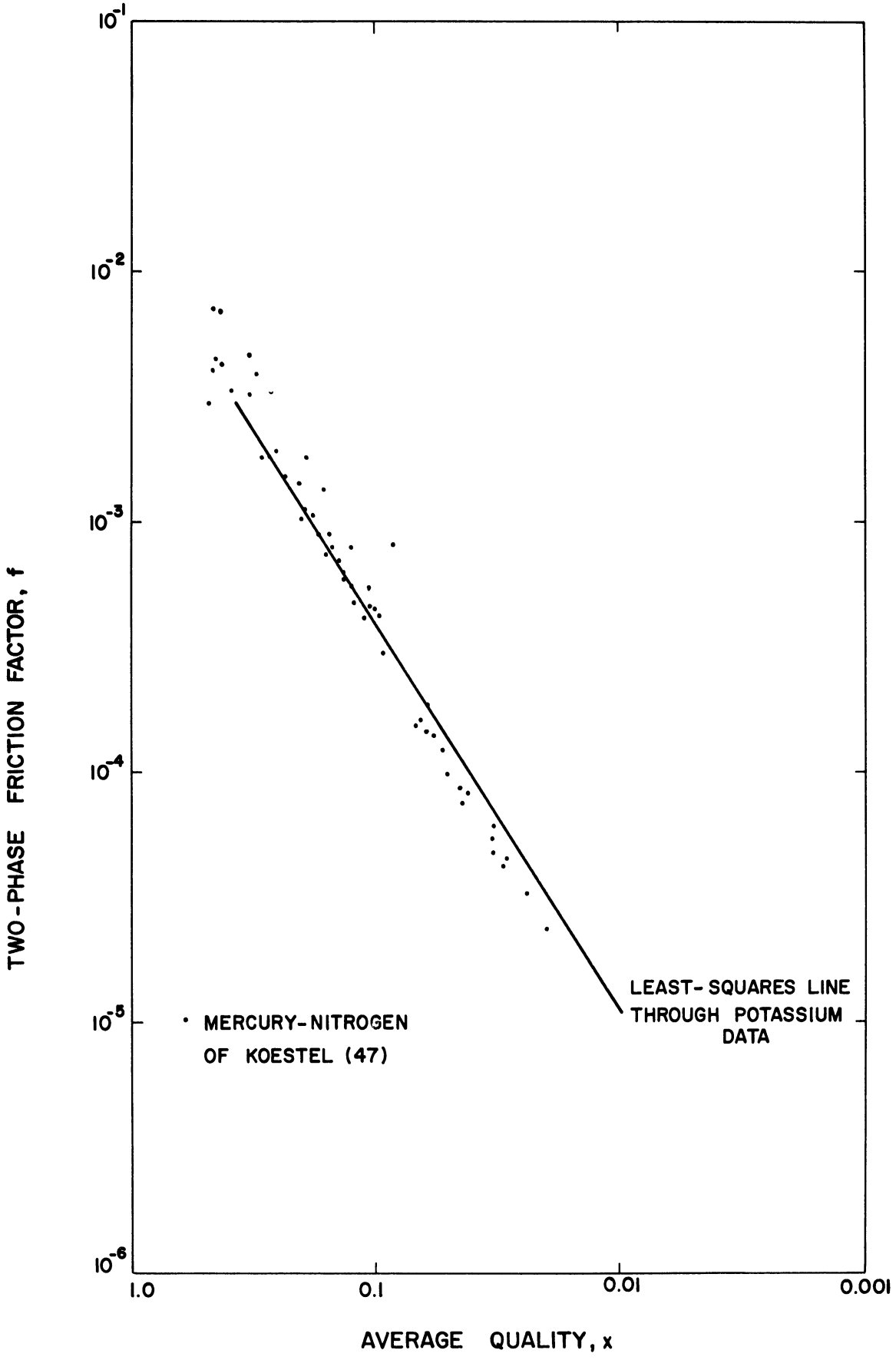

Figure 24. Comparison of Potassium Two-Phase Pressure Gradient Correlation with Mercury-Nitrogen Data of Koestel (47)

An effort was made to determine a parameter which separates the potassium data and the mercury-nitrogen data (47) from the data of other systems shown in Figure 23. Neither the gas-to-liquid viscosity ratio nor the density ratio proved to be the differentiating parameter. For example, the viscosity ratio ranges for various systems are given below:

Fluid System	μ_ℓ/μ_g	Temperature, °F
Potassium containing 8 per cent Na	7.53 to 11.36	1320 to 879
Water-steam	9.15 to 18.4	295 to 225
Water-air	13.15 to 64.0	200 to 60
Mercury-nitrogen	91.5	70

The fact that the μ_ℓ/μ_g values between potassium and the mercury-nitrogen system vary by about a factor of 10 is a failure at the outset. The density ratios similarly failed to display the parametric effect sought.

Of several other parameters tried, the liquid viscosity influence number of Ros (75) showed the most promise. This number is defined as

$$N_\ell = \mu_\ell \sqrt[4]{\frac{g}{\rho_\ell \sigma^3}} \qquad (38)$$

The ranges for this parameter are given below:

Fluid System	$N_\ell \times 10^4$	Temperature, °F
Potassium containing 8 per cent Na	3.52 to 3.12	879 to 1320
Mercury-nitrogen	3.7	60
Water-air	21.5 to 6.8	60 to 200
Water-steam	6.0 to 4.9	225 to 295

The metallic results for N_ℓ show very favorable agreement, but some inconsistencies exist between the other systems. Data from other fluids, such a

organic compounds where the surface tension is accurately known, would be helpful in carrying such parameter studies to a useful conclusion. The inclusion of surface tension in such a differentiating parameter seems particularly sound. It is believed that interfacial characteristics and wettability may be the principal variables which differentiate two-phase flow behavior between various fluid systems.

3.4 The Potassium Pressure Gradient Correlation in the All-Vapor Limit.

It is interesting to ascertain whether any correlation is physically significant, representing something more than mere empirical correspondence between variables. The potassium two-phase pressure gradient correlation of Figure 15 was developed from a dimensional analysis of the experimental variables considered to be of primary influence. Since the two-phase friction factor defined by Equation (7) is based on vapor density, it was decided to determine if the results would extrapolate to proper values in the all-vapor limit.

The friction factors of Equation (7) were all normalized against the single phase Moody friction factors corresponding to all-vapor flows at the same total flow rate and temperature. Equation (28) furnished these all-vapor Moody friction factors, f_g.

A plot of normalized two-phase friction factor is given as a function of quality in Figure 25. It appears that as quality approaches unity (all-vapor flow), the f/f_g values extrapolate to unity. This result is interesting and is believed to establish a firm physical basis for the method of correlation used. It is expected that a friction factor based on the liquid density would also show proper behavior in the all-liquid limit. Such a correlation was not derived, since ρ_g is a much more sensitive function of system pressure.

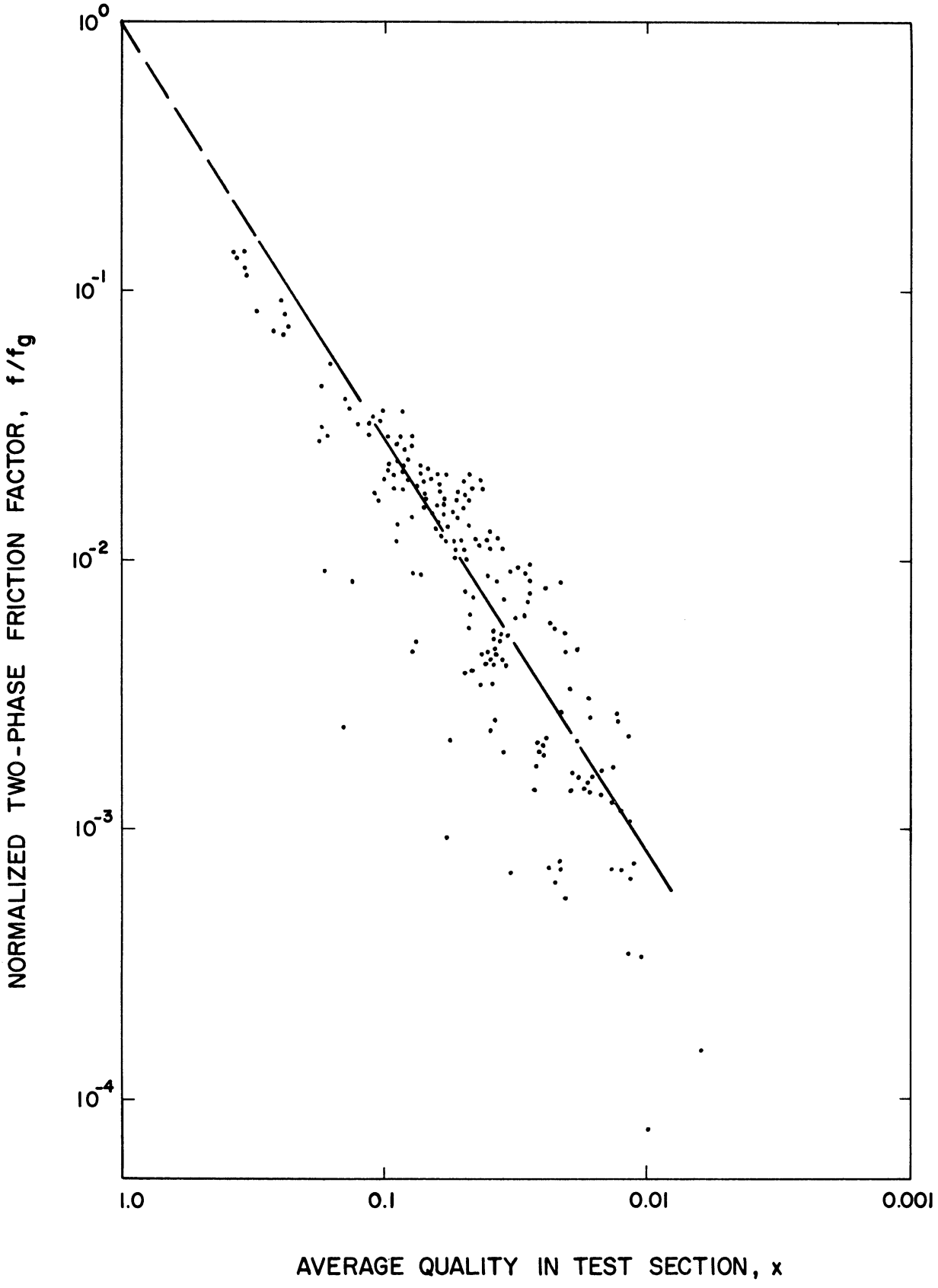

Figure 25. Normalized Two-Phase Friction Factor As a Function of Quality

4. Void Fraction Study

4.1 Flow Characteristics.

The remarks made under this heading for the two-phase pressure drop study are applicable to the void fraction study, since void fractions were measured during pressure drop runs. About 50 per cent of the void fraction data appear to be near thermodynamic equilibrium. The two-phase flows exhibited only frictional pressure losses.

As mentioned in Chapter V, the temperatures and qualities for the void fraction points are taken as the arithmetic mean between inlet and outlet values. These mean values are believed to give adequate description of conditions at the middle of the pressure drop section where the void fraction measurements were made.

The liquid fraction data for potassium are plotted in Figure 16, using X_{tt} values as approximations to the Martinelli X parameter. The X parameter was previously defined as

$$X = \left[\frac{(\Delta P/\Delta L)_\ell}{(\Delta P/\Delta L)_g}\right]^{0.5} \tag{12}$$

Equation (13) expressed the turbulent-turbulent approximation for X.

$$X_{tt} = \left(\frac{1 - x}{x}\right)^{0.9} \left(\frac{\rho_g}{\rho_\ell}\right)^{0.5} \left(\frac{\mu_\ell}{\mu_g}\right)^{0.1} \tag{13}$$

One might ask the following quation: how well do the X_{tt} values approximate X values calculated using Moody friction factors? Ten random points were surveyed, covering the overall flow rate and quality ranges. Percentage deviations of X_{tt} from Moody-based X values ranged from + 0.1 to + 10.9, with the average deviation equalling 6.5 per cent. The survey thus indicates that X_{tt} values are good approximations to X values calculated using single-phase friction factors.

4.2 Comparison with Other Correlations and Data.

The metallic liquid fraction correlation is compared with other correlations and data from other fluid systems in Figure 26. It is seen that all the comparative data and predictions fall substantially lower than the metallic data.

The correlation curve of Lockhart and Martinelli(53), previously discussed in Chapter VI, shows about the same trend as the metallic correlation line. The Lockhart-Martinelli curve was developed from water-air and oil-air data. The turbulent-turbulent water-air data of Richardson (74), for flows in horizontal rectangular channels, are shown. Richardson's data agree with the Lockhart-Martinelli curve, but the air-water tt flow data of Hewitt, King, and Lovegrove (35) fall somewhat lower than the correlation. The two most interesting comparisons are located in the lower part of Figure 26. It was mentioned in Chapter VI that Baroczy (9), using the mercury-nitrogen data of Koestel (47) and the water-air data of Hewitt, et al (35), developed a void fraction correlation which he believed could be generally applied for making metallic estimates. The Baroczy correlation was used to calculate liquid fractions corresponding to the actual potassium flow conditions. The calculated points, which show a substantial amount of scatter, are plotted in Figure 26. A mean line through the calculated points is indicated. It can be seen that Baroczy's correlation is even more deficient than the Lockhart-Martinelli correlation in predicting potassium liquid fractions.

Koestel's mercury-nitrogen data (47) are located near the Baroczy predictions in Figure 26. This situation would be anticipated, since Koestel's data were used by Baroczy in the development of his correlation. Two sets of points are indicated for Koestel's data. The dark squares were for vt type flows; the remaining points were for tt type flows.

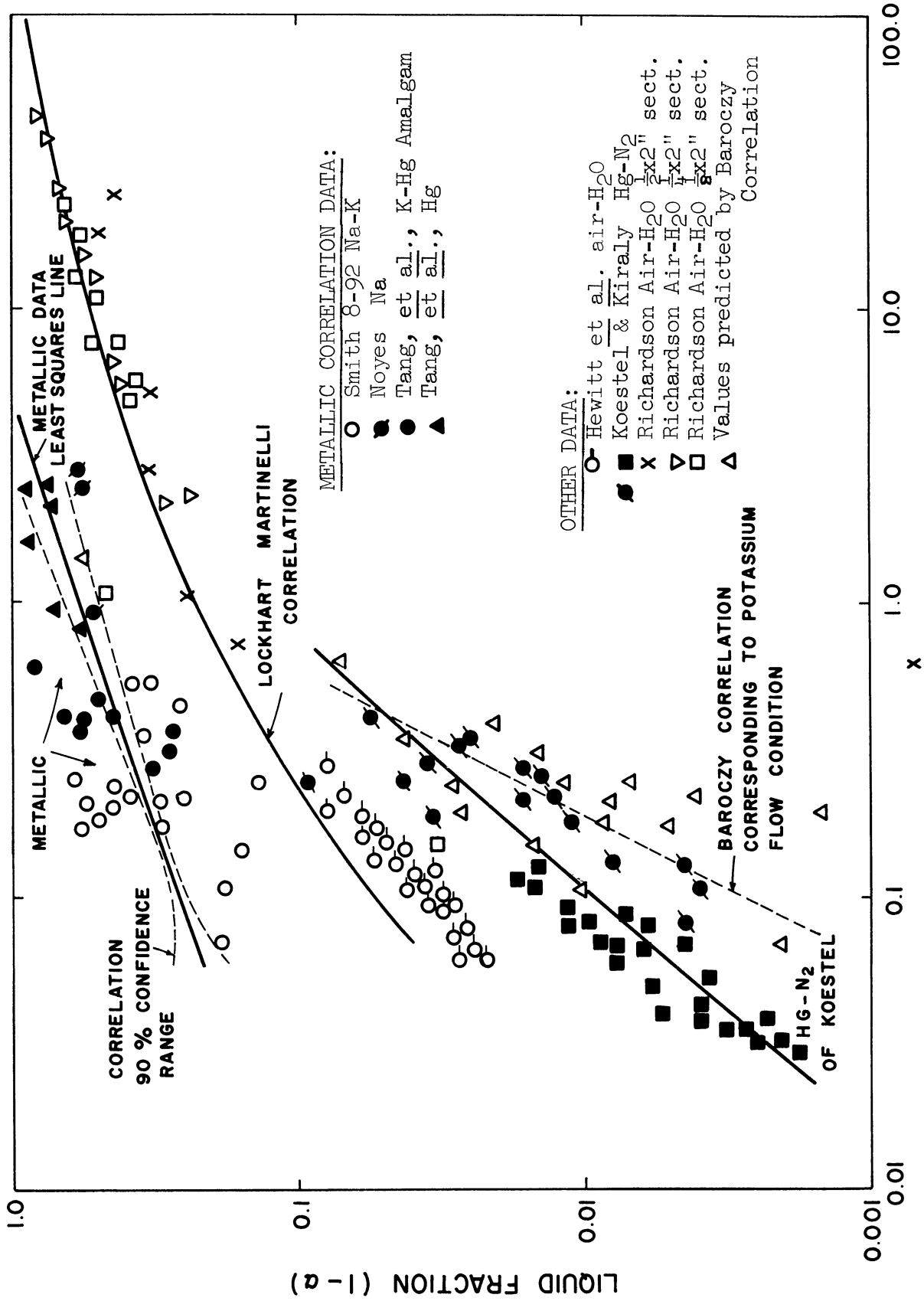

Figure 26. Metallic Liquid Fraction Correlation Compared with Other Data and Correlations.

The fact that Koestel's mercury-nitrogen data compare unfavorably with the metallic correlation is most interesting, since it was found that the mercury-nitrogen pressure gradient data compared favorably with the potassium correlation, as seen in Figure 24. One clear distinction may be drawn between Koestel's flows and the potassium flows. This is the liquid wettability with respect to the tube wall. Koestel's data were measured in a glass test section, which the mercury certainly would not wet. Liquid potassium, however, does wet Haynes-25 alloy. It would appear that while wettability may be a decisive factor in void fraction behavior, as suggested by Figure 26, it may be of only minor significance in two-phase frictional pressure gradient behavior. Another, but less decisive, factor in the wide divergence of Koestel's liquid fraction data is that his vapor phase was a noncondensable second component.

It is apparent from either Figure 16 or 26 that the potassium liquid fraction data show a wide degree of scatter. In comparison with the data of other investigations used to develop the general metallic correlation, it can be seen that the mercury and potassium-mercury amalgam data of Tang, et al. (80) show about the same degree of scatter. An interesting contrast is furnished by Noyes' four sodium point (64) which lie essentially on a straight line (Figure 16).

It is believed that some experimental modifications might have reduced the scatter in the potassium data. Table IV indicates that the photomultiplier tube temperature varied between 128 and 160°F. No attempt was made to control the photomultiplier tube temperature. It is known that the gain of a photomultiplier tube and the magnitude of the light flash emitted by a scintillator are influenced by temperature level (4, 45). The pulse height of NaI (Tl) crystals was found on the average to decrease 0.06 per cent per °C (4). Kinard (45) found that there are large differences in temperature

sensitivity between two photomultiplier tubes of the same type. Based on this evidence, it would seem advisable to control the temperature of the detector assembly. It is also believed that the data might have been improved by mounting a suitably dimensioned collimator on the face plate of the detector shield--i.e., on the emergent side of the flow channel.

4.3 The Metallic Liquid Fraction Correlation in the All-Vapor Limit.

As flows become all vapor, x = 1, the liquid fraction must vanish. According to the definition of the Martinelli parameter (Chapter VI)

$$X = \left[\frac{(\Delta P/\Delta L)_\ell}{(\Delta P/\Delta L)_g}\right]^{0.5} \qquad (12)$$

as flows become all vapor this quantity also vanishes. Therefore, the all-vapor criterion is that as X approaches zero, $(1 - \alpha)$ must also approach zero.

The log-log plot in Figure 16 does not clearly show whether the metallic correlation behaves properly in the all-vapor limit. The data and correlation curve of Figure 16 were plotted in Cartesian coordinates, Figure 27. This plot shows that, notwithstanding the scatter, the metallic correlation behaves correctly in the all-vapor limit.

4.4 Velocity Slip Ratios for Potassium.

The tabulated void fraction results for potassium, Table H-II, include calculated values of the velocity slip ratio, S. It was mentioned in Chapter V that the slip ratios are obtained from the void fraction data, using the following equation

$$S = \frac{V_g}{V_\ell} = \left(\frac{x}{1 - x}\right)\left(\frac{1 - \alpha}{\alpha}\right)\left(\frac{\rho_\ell}{\rho_g}\right) \qquad (5)$$

Table H-II shows that the slip ratios range from 53 to 1150. This wide range is a direct result of the scatter in the void fraction data. The arithmetic average slip ratio is 350.

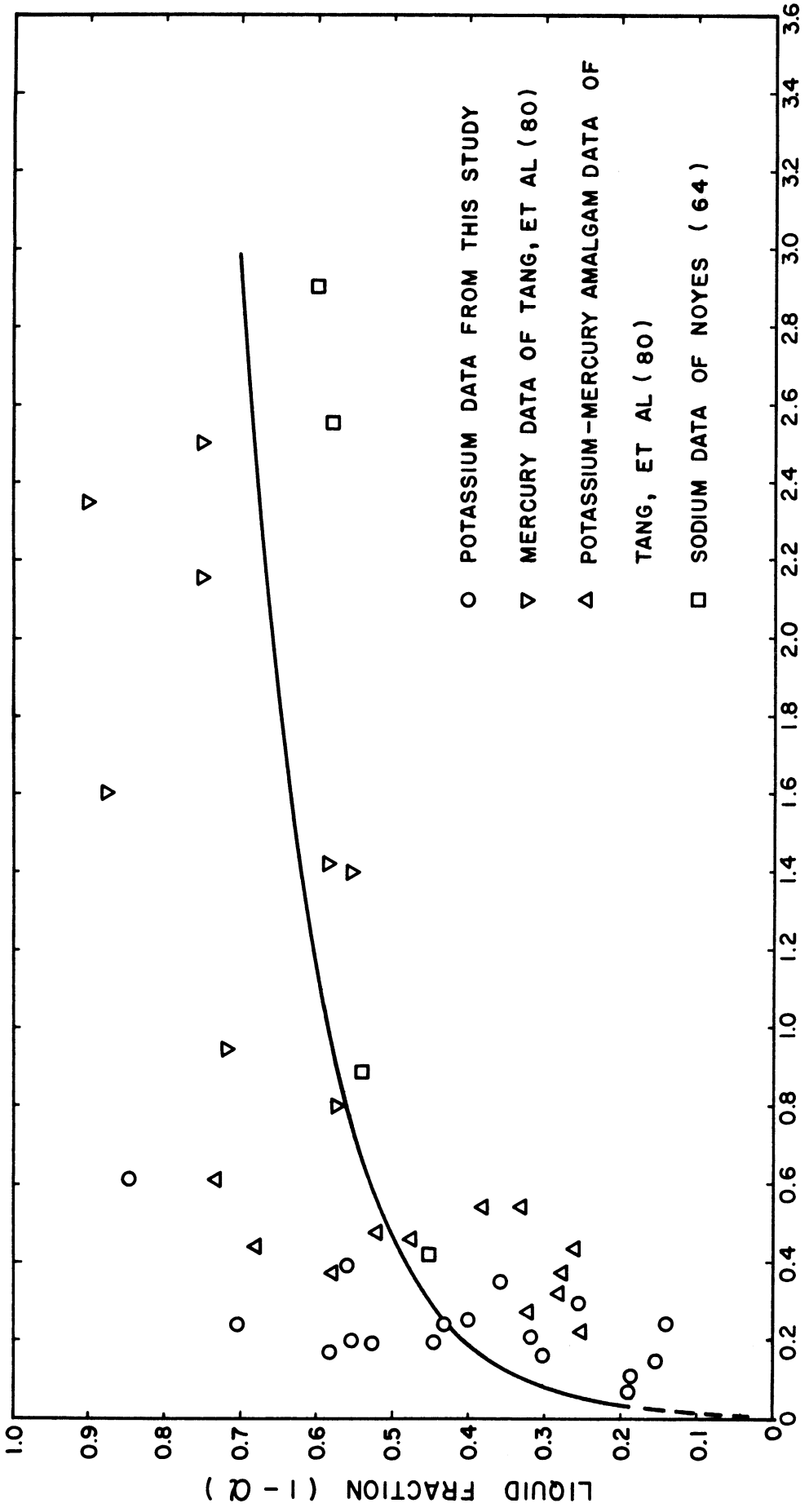

Figure 27. Metallic Liquid Fraction Correlation Plotted to Show All-Vapor Limit

Although the scatter in the void fraction data precludes precise knowledge of the potassium slip ratios, the results suggest that values are of the order of 10^2. These results are about a factor of 10^2 higher than the air-water slip ratios observed by Richardson (74) for flows in horizontal rectangular channels at atmospheric pressure. The overall ranges of quality and slip ratio obtained by Richardson were 0.00064 to 0.0517 and 0.56 to 8.41, respectively. The few fractional values reported by Richardson do not seem physically realistic.

That metallic slip ratios are appreciably higher than for such systems as air-water would be anticipated from Figure 26. Considering Equation (5), it is seen that higher metallic slip ratios arise from two effects. Generally, values of (ρ_ℓ/ρ_g) are higher in metallic systems. The metallic liquid fraction correlation in Figure 26 indicates that single-component metallic void fractions tend to be appreciably lower, leading to higher values for the factor $(1 - \alpha)/\alpha$.

The observation of high velocity slip ratios for potassium tends to substantiate the belief that the flow patterns were stratified-wavy or annular, depending on the quality range. Since the vapor flow area is unrestricted in these regimes, high slip ratios are quite feasible. Check calculations showed that mean vapor velocities were nowhere near the critical.

VIII. CONCLUSIONS

The experimental results of this study lead to the following conclusions:

1. Although the experiments were run with a fluid mixture of 8 weight per cent sodium in potassium, it is believed from comparison of the properties of this mixture with those of pure potassium that the two-phase flow correlations will yield reliable values for pure potassium.

2. Nearly 60 per cent of the two-phase flow data for potassium (with 8 per cent sodium) showed substantial departure from thermodynamic equilibrium, suggesting that metallic two-phase flows in general may tend to exhibit this effect.

3. The potassium two-phase flow patterns are not exactly known, and two prominent correlations (3, 75) appear to be unsatisfactory for predicting potassium flow regimes. From qualitative knowledge of the occurrence of horizontal flow patterns and the experimental ranges of liquid volume fraction, liquid flow rate, and vapor flow rate, it is probable that flows were stratified or wavy at lower qualities and annular at higher qualities.

4. The two-phase frictional pressure gradient data for potassium proved to be a function of total mass flow rate, quality, and system pressure. The potassium data may be correlated in terms of a two-phase friction factor, defined as

$$f \equiv \frac{\rho_g D (\Delta P/\Delta L) g_c}{G^2} \tag{8}$$

which is a function of quality. Experimentally the potassium friction factor--quality correlation is given as

$$f = 0.01379\, x^{1.5395} \qquad (9)$$

This correlation has high statistical significance and behaves correctly in the all-vapor limit, since f/f_g values extrapolate to unity when quality approaches unity. This type of correlation is suitable for the presentation of data from other two-phase fluid systems.

5. The well-known two-phase pressure drop correlations of Lockhart and Martinelli (53) and Bertuzzi, Tek, and Poettmann (13), when applied in the usual manner, predict potassium pressure gradients that are high by mean factors of 2.5 and 4, respectively. The Bankoff variable density single fluid model (8) predicts pressure gradients which are nearly a hundredfold high.

6. The potassium two-phase frictional pressure gradient results show remarkably good agreement with mercury-nitrogen data (47). These metallic data fall much lower than values reported for flows of water-air, oil-air, and water-steam systems. The parameters which cause such strong differences between metallic and nonmetallic two-phase pressure gradients have not been discovered. Surface tension and liquid viscosity may be two of the most decisive properties.

7. The potassium void fraction data, together with data for mercury (80), potassium-mercury amalgams (80), and sodium (64) have yielded a general liquid fraction correlation for single-component metallic systems. This correlation, of the Lockhart-Martinelli type, is given by

$$\alpha = 1 - 0.5735\, X^{0.3421} \qquad (16)$$

where

$$X = \left[\frac{(\Delta P/\Delta L)_\ell}{(\Delta P/\Delta L)_g}\right]^{0.5} \qquad (12)$$

This correlation has high statistical significance and behaves correctly in the all-vapor limit, since α approaches unity as X approaches zero.

8. Metallic void fractions are lower than those for water-steam and water-air systems. No other general correlation was found adequate in predicting metallic void fractions. The mercury-nitrogen data (47), which agreed very favorably with the potassium two-phase pressure gradients, show very large divergence with respect to void fractions. Since the mercury-nitrogen data were obtained from a glass test section, it appears that wettability may be of great effect on void fraction behavior.

9. Because they generally have higher values of (ρ_ℓ/ρ_g) and lower void fractions, metallic systems display much higher velocity slip ratios than nonmetallic systems. Although the scatter in the void fraction data precludes precise knowledge of slip ratios, the potassium values are certainly of the order of 10^2 (values between 1 and 10 have been observed for water-air flows at atmospheric pressure).

IX. RECOMMENDATIONS

In most experimental studies it is inevitable that new problems and questions arise out of the work performed. Some questions lead to whole new investigations; others lead to extensions and clarifications, often lengthy, of the previously "completed" work. Recognition of new problems arising out of a study is, in a sense, as important as the actual experimental results obtained. Based on the results of this study, the following recommendations for further work are offered:

1. It would be interesting to extend the two-phase pressure gradient data to very high qualities. The highest quality attained in this study was 0.378.

2. It would be interesting to investigate boiling potassium flows, or boiling flows of other metals. A very extensive study would include measurement of axial pressure, temperature, and void fraction profiles. Further knowledge of acceleration effects and departures from thermodynamic equilibrium would be especially sought.

3. An extension of the void fraction results would be valuable. Such extension would be especially fruitful if factors causing scatter in the data were determined and eliminated. Control of the gamma-ray detector temperature and addition of a suitable collimator on the detector side of the flow channel might help improve the data. A change to the radial traversing gamma-ray attenuation technique, while expensive, might lead to very useful experimental information.

4. An ultimate goal of two-phase flow research should be to determine the reasons why metallic two-phase fluids exhibit lower frictional pressure

gradients and void fractions than do the nonmetallic systems investigated to date. Eventually one would hope to define suitable quantitative parameters between various groups of data. The water-steam system is the only extensively studied nonmetallic single-component two-phase fluid. Further study of astutely chosen single-component nonmetallic systems could be of decided value in determining differentiating parameters. At the same time more metallic data are also needed.

5. Most serious theoretical attacks of two-phase flow problems demand knowledge of flow pattern. Two-phase pressure drop phenomena are certainly related to flow regimes, but, except for a few simple regimes, the flow pattern-pressure drop relationships are not clearly understood. No experimental information is known to exist concerning flow pattern occurrences for metallic fluids. Obtaining such data would represent a very significant technical contribution, the results of which might be of highest value in establishing why metallic two-phase fluids behave differently from nonmetallics. Metallic flow pattern study is recognized as a very difficult experimental problem. Radial gamma-ray traverses would be helpful. Use of an electrical resistivity probe, such as developed by Neal and Bankoff (63), or a probe with a small gamma-ray source at its tip might yield meaningful data. The use of probes in studying flow patterns in high temperature, corrosive environments would lead to serious secondary problems in sealing the opening through which the probe is inserted; at the same time the seal must permit variation of the probe's radial position.

6. Two-phase critical flow is a subject of great interest in atomic power technology. Accurate predictions of two-phase critical flow phenomena are valuable in evaluating nuclear reactor accidents and containment. Fauske (24) has developed a theory which satisfactorily describes steam-water critical flow phenomena. In view of current interest in using alkali metals as reactor coolants, it would be interesting to experimentally study metallic two-phase critical flows and to compare the results with Fauske's theory.

LITERATURE CITED

1. Anderson, G. H. and Mantzouranis, B. G. "Two-Phase (Gas-Liquid) Flow Phenomena--I Pressure Drop and Hold-Up for Two-Phase Flow in Vertical Tubes." Chem. Eng. Sci. Vol. 12, 109 (1960).

2. Armand, A. A., et al. "Investigation of the Resistance During the Movement of Steam-Water Mixtures in a Heated Boiler Pipe at High Pressures." United Kingdom Atomic Energy Authority, Report AERE-Lib/Trans-816 (1947).

3. Baker, O. "Simultaneous Flow of Oil and Gas." Oil and Gas J. Vol. 52, No. 14, 185 (1954).

4. Ball, W. P., Booth, R., and MacGregor, M. H. "Scintillation Temperature Coefficients." Bull. Amer. Phys. Soc. Series II, Vol. 1, No. 4, 185 (1956).

5. Balzhiser, R. E., et al. Fourth Quarterly Progress Report, Contract AF33(616)-8277, Item IIa, The University of Michigan (February 1963).

6. Balzhiser, R. E., et al. "Investigation of Liquid Metal Boiling Heat Transfer." United States Air Force Systems Command, Wright-Patterson Air Force Base, Ohio, Report RTD-TDR-63-4130 (November 1963).

7. Balzhiser, R. E., et al. "Literature Survey on Liquid Metal Boiling." United States Air Force Systems Command, Wright-Patterson Air Force Base, Ohio, Report ASD-TR-61-594, pp. 47-55 (December 1961).

8. Bankoff, S. G. "A Variable Density Single Fluid Model for Two-Phase Flow with Particular Reference to Steam-Water Flow." J. Heat Trans. Vol. 82, 265 (1960).

9. Baroczy, C. J. "Correlation of Liquid Fraction in Two-Phase Flow with Application to Liquid Metals." Atomics International, Div. of North American Aviation, Inc., Canoga Park, Calif. Report NAA-SR-8171 (April 1963).

10. Barry, R. E. The University of Michigan, Department of Chemical Engineering Liquid Metals Laboratory, Private Communication (1963).

11. Bennett, J. A. R. "Two-Phase Flow in Gas-Liquid Systems: A Literature Survey." United Kingdom Atomic Energy Authority, Report AERE-CERI-2497 (March 1958).

12. Berenson, P. J. and Killackey, J. J. "An Experimental Investigation of Forced-Convection Vaporization of Potassium." Presented at Third Annual High-Temperature Liquid Metal Heat Transfer Technology Conference, Oak Ridge National Laboratory, Sept. 4-6, 1963. Proceedings to be published.

13. Bertuzzi, A. F., Tek, M. R. and Poettmann, F. H. "Simultaneous Flow of Liquid and Gas Through Horizontal Pipe." J. Pet. Tech. Vol. 8, (Jan. 17, 1956).

14. Brown, R. A. S. and Govier, G. W. "High-Speed Photography in the Study of Two-Phase Flow." Can. J. Chem. Eng. Vol. 39, 159 (1961).

15. Brown, R. A. S., Sullivan, G. A. and Govier, G. W. "The Upward Vertical Flow of Air-Water Mixtures--III Effect of Gas Phase Density on Flow Pattern, Holdup, and Pressure Drop." Can. J. Chem. Eng. Vol. 38, 62 (1960).

16. Calvert, S. and Williams, B. "Upward Cocurrent Annular Flow of Air and Water in Smooth Tubes." AIChE J. Vol. 1, 78 (1955).

17. Chenoweth, J. M. and Martin, M. W. "Turbulent Two-Phase Flow." Petr. Ref. Vol. 34, No. 10, 151 (1955).

18. Chisolm, D. and Laird, A. D. K. "Two-Phase Flow in Rough Tubes." Trans. ASME. Vol. 80, 276 (1958).

19. Cooke, J. W. "Thermophysical Property Measurements of Alkali Liquid Metals." Presented at Third Annual High-Temperature Liquid Metal Heat Transfer Technology Conference, Oak Ridge National Laboratory, Sept. 4-6, 1963. Proceedings to be published.

20. Dukler, A. E. "Fluid Mechanics and Heat Transfer in Vertical Falling Film Systems." Presented at ASME-AIChE Third National Heat Transfer Conference, August, 1959.

21. Dwyer, O. E. and Romero, A. J. Review No. 67 in High-Temperature Liquid-Metal Technology Review, Brookhaven National Laboratory, Report BNL-825 (PR-4), Vol. 1, No. 4 (August 1963).

22. Dzhelepov, B. S. and Peker, L. K. Decay Schemes of Radioactive Nuclei. Pergamon Press, New York, 1961, pp. 497-499.

23. Egen, R. A., Dingee, D. A. and Chastain, J. W. "Vapor Formation and Behavior in Boiling Heat Transfer." Battelle Memorial Institute, Report BMI-1163 (Feb. 4, 1957).

24. Fauske, H. K. "Contribution to The Theory of Two-Phase, One-Component Critical Flow." Argonne National Laboratory, Report ANL-6633 (October 1962).

25. Fisher, C. R. "Heat Transfer and Pressure Drop Characteristics for Boiling Rubidium in Forced Convection." Presented at Third Annual High-Temperature Liquid Metal Heat Transfer Technology Conference, Oak Ridge National Laboratory, Sept. 4-6, 1963. Proceedings to be published.

26. Fisher, R. A. and Yates, F. Statistical Tables for Biological, Agricultural, and Medical Research. Oliver and Boyd, London, 1953. Table VI.

27. Goldmann, K. "Selected Parameters for Two-Phase Flow of Sodium." Presented at Third Annual High-Temperature Liquid Metal Heat Transfer Technology Conference, Oak Ridge National Laboratory, Sept. 4-6, 1963. Proceedings to be published.

28. Govier, G. W. and Omer, M. M. "The Horizontal Pipeline Flow of Air-Water Mixtures." Can. J. Chem. Eng. Vol. 40, 93 (1962).

29. Govier, G. W., Radford, B. A. and Dunn, J. S. C. "The Upwards Vertical Flow of Air-Water Mixtures." Can. J. Chem. Eng. Vol. 35, 59 (1957).

30. Govier, G. W. and Short, W. L. "The Upward Vertical Flow of Air-Water Mixtures--III Effect of Tubing Diameter on Flow Pattern, Holdup, and Pressure Drop." Can. J. Chem. Eng. Vol. 36, 195 (1958).

31. Gresham, W. A., Foster, P. A. and Kyle, R. J. "Review of the Literature on Two-Phase (Gas-Liquid) Fluid Flow in Pipes," United States Air Force, WADC Report No. 55-422, Part I (June 1955).

32. "Harshaw Scintillation Phosphors." Harshaw Chemical Company, Cleveland, Ohio, pp. 43 (1962).

33. Heineman, J. B., Marchaterre, J. F. and Mehta, S. "Electromagnetic Flowmeters for Void Fraction Measurements in Two-Phase Metal Flow." Rev. Sci. Insts. Vol. 34, 399 (1963).

34. Hewitt, G. F. "Analysis of Annular Two-Phase Flow: Application of the Dukler Analysis to Vertical Upward Flow in A Tube." United Kingdon Atomic Energy Authority, Report AERE-R-3680 (January 1961).

35. Hewitt, G. F., King, I. and Lovegrove, P. C. "Holdup and Pressure Drop Measurements in the Two-Phase Annular Flow of Air-Water Mixtures." Brit. Chem. Eng. Vol. 8, 311 (1963).

36. Hoffman, H. W. "Recent Experimental Results in ORNL Studies with Boiling Potassium." Presented at Third Annual High-Temperature Liquid Metal Heat Transfer Technology Conference, Oak Ridge National Laboratory, Sept. 4-6, 1963. Proceedings to be published.

37. Hoogendoorn, C. J. "Gas-Liquid Flow in Horizontal Pipes." Chem. Eng. Sci. Vol. 9, 205 (1959).

38. Hooker, H. H. and Popper, G. F. "A Gamma-Ray Attenuation Method for Void Fraction Determinations in Experimental Boiling Heat Transfer Test Facilities." Argonne National Laboratory, Report ANL-5766 (Nov. 1958).

39. Hughmark, G. A. "Holdup in Gas-Liquid Flow." Chem. Eng. Prog. Vol. 58, 62 (April 1962).

40. Hughmark, G. A. and Pressburg, B. S. "Holdup and Pressure Drop with Gas-Liquid Flow in a Vertical Pipe." AIChE J. Vol. 7, 677 (1961).

41. Isbin, H. S., Moen, R. H. and Mosher, D. R. "Two-Phase Pressure Drops." United States Atomic Energy Commission, Report AECU-2994 (November 1954).

42. Isbin, H. S., Sher, N. C. and Eddy, K. C. "Void Fractions in Two-Phase Steam-Water Flow." AIChE J. Vol. 3, 136 (1957).

43. Jackson, C. B., Editor. Liquid Metals Handbook, Na-NaK Supplement. Atomic Energy Commission and Bureau of Ships, Third Edition, 1955, pp. 32-45.

44. Johnson, H. A. and Abou-Sabe, A. H. "Heat Transfer and Pressure Drop for Turbulent Flow of Air-Water Mixtures in a Horizontal Pipe." ASME Trans. Vol. 74, 977 (1952).

45. Kinard, F. E. "Temperature Dependence of Photomultiplier Gain." Nucleonics. Vol. 15, 92 (April 4, 1957).

46. Knudsen, J. G. and Katz, D. L. Fluid Dynamics and Heat Transfer. McGraw-Hill, New York, 1958.

47. Koestel, A. Thompson-Ramo-Wooldridge, Inc., Cleveland, Ohio. Tabulated data which had been previously published in TRW Report ER-4104 (June 1960). Private communication, January 1964.

48. Kutateladze, S. S., Editor. "Liquid Metal Heat Transfer Media." Atomnaia Energiia, Suppl. No. 2, Moscow (1958), Translated by Consultants Bureau, Inc., New York, 1959.

49. Levy, S. "Prediction of Two-Phase Pressure Drop and Density Distribution from Mixing Length Theory." J. Heat Trans. Vol. 85, 137 (1963).

50. Levy, S. "Steam Slip--Theoretical Prediction from Momentum Model." J. Heat Trans. Vol. 82, 113 (1960).

51. Levy, S. "Theory of Pressure Drop and Heat Transfer for Annular Steady State Two-Phase Two-Component Flow." Second Midwestern Conference on Fluid Mechanics, Ohio State University Engineering Experiment Station. Bulletin 149, pp. 337-348, September 1952.

52. Linning, D. L. "The Adiabatic Flow of Evaporating Fluids in Pipes of Uniform Bore." Inst. Mech. Engrs. London, Proceedings (B), IB, 64 (1952).

53. Lockhart, R. W. and Martinelli, R. C. "Proposed Correlation of Data for Isothermal Two-Phase, Two-Component Flow in Pipes." Chem. Eng. Prog. Vol. 45, 39 (1949).

54. Martinelli, R. C., Boelter, L. M. K., Taylor, T. H. M., Thomsen, E. G. and Morrin, E. H. "Isothermal Pressure Drop for Two-Phase, Two-Component Flow in a Horizontal Pipe." Trans. ASME. Vol. 66, 139 (1944).

55. Martinelli, R. C. and Nelson, D. B. "Prediction of Pressure Drop During Forced-Circulation Boiling of Water." Trans. ASME. Vol. 70, 695 (1948).

56. Martinelli, R. C., Putnam, J. A. and Lockhart, R. W. "Two-Phase, Two-Component Flow in the Viscous Region." Trans. AIChE. Vol. 42, 681 (1946).

57. Masnovi, R. "Literature Survey of Two-Phase Fluid Flow." United States Air Force, Report WAPD-TH-360 (1958).

58. Maurer, G. W. "The Measurement of the Densities of Flowing Fluids by Radioactivity Methods." M.S. Thesis, University of Pittsburgh (1959).

59. Mickley, H. S., Sherwood, T. K. and Reed, C. E. Applied Mathematics in Chemical Engineering, 2nd Edition. McGraw-Hill, New York, 1957, pp. 53-59.

60. MSA Research Corporation. "Operating Manual for University of Michigan Boiling Liquid Metal Test Loop." MSAR 63-24, Callery, Pa. (Feb. 4, 1963).

61. Myers, W. A. "A Method for Determining the Void Fraction of Two-Phase Potassium." Final Report for Course CME-690, University of Michigan, Department of Chemical and Metallurgical Engineering, Ann Arbor (May 1963).

62. Neal, L. G. "Local Parameters in Cocurrent Mercury-Nitrogen Flow." Argonne National Laboratory, Report ANL-6625 (January 1963).

63. Neal, L. G. and Bankoff, S. G. "A High Resolution Resistivity Probe for Determination of Local Void Properties in Gas-Liquid Flow." Presented at 55th Annual Meeting of AIChE, Chicago, December 2-6, 1962.

64. Noyes, R. C. "Summary of Recent Results of Sodium Boiling Studies." Presented at Third Annual High-Temperature Liquid Metal Heat Transfer Technology Conference, Oak Ridge National Laboratory, Sept. 4-6, 1963. Proceedings to be published.

65. Petrick, M. "Two-Phase Air-Water Flow Phenomena." Argonne National Laboratory, Report ANL-5787 (March 1958).

66. Pike, R. W. "The Adiabatic, Evaporating, Two-Phase Flow of Steam and Water in Horizontal Pipe." Ph.D. Thesis Georgia Institute of Technology (1962).

67. Poppendiek, H. F. Geoscience Ltd., Solana Beach, Calif., Private communication, February 1964.

68. Poppendiek, H. F., Greene, N. D., MacDonald, F. R., Sabin, C. M., Livett, R. K. and Thompson, A. S. "Annual Technical Report on High Acceleration Field Heat Transfer for Auxiliary Space Nuclear Power Systems (AEC Contract No. AT(04-3)-409). Period Sept. 1, 1962 through August 31, 1963." Geoscience Ltd., Solana Beach, Calif., Report GLR-15.

69. Price, W. J. Nuclear Radiation Detection. McGraw-Hill, New York, 1958.

70. "Proceedings of the 1962 High-Temperature Liquid-Metal Heat Transfer Technology Meeting." Brookhaven National Laboratory, Report BNL-756 (c-35), (May 17-18, 1962).

71. "Proceedings of the 1963 High-Temperature Liquid-Metal Heat Transfer Technology Meeting." Oak Ridge National Laboratory, Sept. 4-6, 1963. To be published.

72. "Proceedings of the Symposium on Two-Phase Fluid Flow." The Institution of Mechanical Engineers, London (1962).

73. Reid, R. C., Reynolds, A. B., Diglio, A. J., Spiewak, I. and Klipstein, D. H. "Two-Phase Pressure Drops in Large-Diameter Pipes." AIChE J. Vol. 3, 321 (1957).

74. Richardson, B. L. "Some Problems in Horizontal Two-Phase, Two-Component Flow." Argonne National Laboratory, Report ANL-5949 (December 1958).

75. Ros, N. C. J. "Simultaneous Flow of Gas and Liquid as Encountered in Well Tubing." Trans. Soc. Pet.Eng. of AIME. Vol. 222, 1037 (1961).

76. Rouse, H., Editor. Advanced Mechanics of Fluids. Wiley, New York, 1959. Chapter 1.

77. "SC-18 Superscaler: Operating and Maintenance Instructions." Tracerlab, Inc., Boston, Mass. (1952).

78. Smith, C. R., Tang, Y. S. and Walker, C. L. "Slip Velocity in Two-Phase Metallic Fluids." Allison Division, General Motors Corp., Indianapolis, Indiana, Eng. Dept. Report No. 2809 (May 25, 1962).

79. Street, J. R. "A Study of Vertical Gas-Liquid Slug Flow." Ph.D. Thesis, The University of Michigan (1962).

80. Tang, Y. S., Smith, C. R. and Ross, P. T. "Potassium-Mercury Amalgam Boiling Heat Transfer, Two-Phase Flow, and Properties Investigation." Allison Division, General Motors Corp., Indianapolis,Indiana, Eng. Dept. Report No. 3549 (September 16, 1963).

81. "Taylor Transcope Recording Receiver 91J." Instructions for Taylor Instruments 3E211, Taylor Instrument Companies, Rochester, N. Y., Issue 3.

82. "Taylor Volumetric Pressure Systems." Bulletin 98365, Taylor Instrument Companies, Rochester, N. Y. (February 1961).

83. Tek, M. R. The University of Michigan, Department of Chemical and Metallurgical Engineering. Private communication, January 1964.

84. "Transaire Volumetric D-P Transmitter 205-T." Instructions for Taylor Instruments 2B204. Taylor Instrument Companies, Rochester, N. Y., Preliminary Issue (March 1959).

85. Vohr, J. H. "Flow Patterns of Two-Phase Flow--A Survey of Literature." United States Atomic Energy Commission, Report TID-11514 (Dec. 15, 1960).

86. Volk, Wm. Applied Statistics for Engineers. McGraw-Hill, New York, 1958. Chapter 8.

87. Ward, H. C., Rhodes, J. E., Ziegler, W. T. and Ross, L. W. "Analytical Investigation of Two-Phase Vapor-Liquid Ratio Measuring Systems and Two-Phase Flow Literature Survey Supplement." United States Air Force, WADC Report No. 59-230 (August 1959).

88. Weatherford, W. D., Tyler, J. C. and Ku, P. M. "Properties of Inorganic Energy-Conversion and Heat Transfer Fluids for Space Applications." United States Air Force, WADD-Tech. Report 61-96 (November 1961).

89. West, R. "Low-Energy Gamma-Ray Sources." Nucleonics. Vol. 11, 20, (February 1953).

APPENDICES

APPENDIX A

PROPERTIES OF SODIUM-POTASSIUM MIXTURE CONTAINING 8 PER CENT Na BY WEIGHT

It was pointed out in the Introduction that, due to leakage in the heat transfer section, the two-phase flows studied were for a sodium-potassium mixture containing 8% sodium by weight. This situation made it necessary to predict fluid properties using techniques valid for such mixtures. Accurate values of physical and thermal properties are essential in processing and interpretation of the two-phase flow data. This appendix summarizes the methods used to predict fluid properties important to this study.

In predicting mixture properties for engineering use, values for pure components are frequently used. Except where otherwise noted, properties for pure potassium and sodium are those reported in the compilation by Weatherford, et al. (88). The data presented in this publication were selected on the basis of mutual consistency among related properties and consistency between various fluids, in addition to consideration of the precision in the data. Values given for viscosities of saturated alkali metal vapors were estimated theoretically since no data have been reported.

In the discussion of various properties which follows, the data are presented in terms of best-fit equations. Such a presentation of property data was most advantageous to the processing of two-phase flow data on the IBM 7090 computer.

1. Density of Saturated Liquid

The Liquid Metals Handbook (43) indicates that mixture densities may be expressed in terms of a molal average of the pure-component specific volumes.

$$\frac{1}{\rho_\ell} = x_K v_K + x_{Na} v_{Na} \qquad \text{(A-1)}$$

where ρ_ℓ = density of the liquid mixture

x_K, x_{Na} = mol fraction of K and Na in the mixture, respectively

v_K, v_{Na} = specific volume of pure K and pure Na, respectively

Comparison of values predicted by Equation (A-1) with actual data showed a maximum deviation of 0.7 per cent.

Weatherford's data inserted in Equation (A-1) yields the following liquid density equation for Na-K mixtures containing 8 weight per cent Na.

$$\rho_\ell = 53.66 - 0.00829\ T \qquad \text{(A-2)}$$

where ρ_ℓ = liquid density, lb/ft^3

T = temperature, °F

In the temperature range 850-1350°F the accuracy of liquid densities thus predicted is about $\pm$ 0.3 lb/ft^3.

2. Viscosity of Saturated Liquid

The Liquid Metals Handbook recommends that viscosities of liquid Na-K mixtures be predicted by the equation of Andrade (43), which has the for

$$\mu_\ell = \rho_\ell^{1/3} B e^{C\rho_\ell/T_a} \qquad \text{(A-3)}$$

where T_a = absolute temperature. B and C are constants whose values depend on mixture composition. From a set of values given in reference (43), the constants for a mixture of 8% sodium in potassium were determined graphically. Inserting the constants and converting to engineering units, Equation (A-3) becomes

$$\mu_\ell = 242.5 \left(\frac{\rho_\ell}{62.4}\right)^{1/3} \cdot \exp\left[\frac{1273}{(T+460)} \cdot \left(\frac{\rho_\ell}{62.4}\right)\right] \qquad \text{(A-4)}$$

where μ_ℓ = liquid fiscosity, lb/ft/hr

ρ_ℓ = liquid density, lb/ft^3

T = temperature, °F

3. Specific Heat of Saturated Liquid

The Liquid Metals Handbook (43) states that specific heats for Na-K alloys can be calculated from a weighted average of pure-component values.

$$Cp_\ell = W_{Na} C_{Na} + W_K C_K \qquad (A-5)$$

where Cp_ℓ = mixture specific heat

C_{Na}, C_K = specific heat for pure Na and K, respectively

W_{Na}, W_K = weight fractions of Na and K in the alloy, respectively

Pure component data from reference (43) were inserted in Equation (A-5) to give the following equation for a Na-K mixture containing 8% Na.

$$Cp_\ell = 0.2144 + 2.462 \times 10^{-8} T^2 - 4.770 \times 10^{-5} T \qquad (A-6)$$

where Cp_ℓ = mixture liquid specific heat, Btu/lb/°F

T = temperature, °F

It should be noted that the pure-component curves for both metals exhibit a minimum, suggesting that the mixture curve should also. Equation (A-6) gives a minimum value of 0.1913 Btu/lb/°F at 968°F.

The uncertainty in Cp_ℓ is 0.4 per cent, or approximately ± 0.0008 Btu/lb/°F.

4. Vapor Pressure

A recent technological review (21) cites vapor pressure measurements up to 25 atm for NaK (presumably the eutectic mixture, 78% K by weight). The results fell only slightly below those calculated on the basis of an ideal solution. Since the mixture used in this study is much more dilute, it is

believed that suitable vapor pressure estimates are obtained using Raoult's Law. Vapor pressures for the 8-92 Na-K system were thus calculated; no attempt was made to correct for the association effects in the vapor. Figure A-1 presents the vapor pressure curve so obtained, based on Weatherford's data. The equation of the line is

$$\ell n\ P = 12.016 - \frac{17,419}{T+460} \qquad \text{(A-7)}$$

where P = vapor pressure, psia

T = temperature, °F

5. Heat of Vaporization

In the experiments the liquid was never completely vaporized. It follows that the composition of the vapor was different from that of the liquid and the latent heats of interest are for partial vaporization. Values were estimated as molal averages of the pure-component values, based on equilibrium vapor composition.

$$\lambda = y_K \lambda_K + y_{Na} \lambda_{Na} \qquad \text{(A-8)}$$

where λ = heat of vaporization for partial vaporization of mixture

λ_K, λ_{Na} = heat of vaporization of K and Na, respectively

y_K, y_{Na} = mol fraction of K and Na in equilibrium vapor, respectively

Raoult's and Dalton's Laws were combined to estimate the equilibrium vapor compositions.

$$y_K = \frac{x_K p_K^\circ}{P} \qquad \text{(A-9)}$$

where y_K = mol fraction K in vapor

x_K = mol fraction K in liquid (0.868 for the 8% Na mixture)

P = vapor pressure of mixture

p_K° = vapor pressure of pure potassium

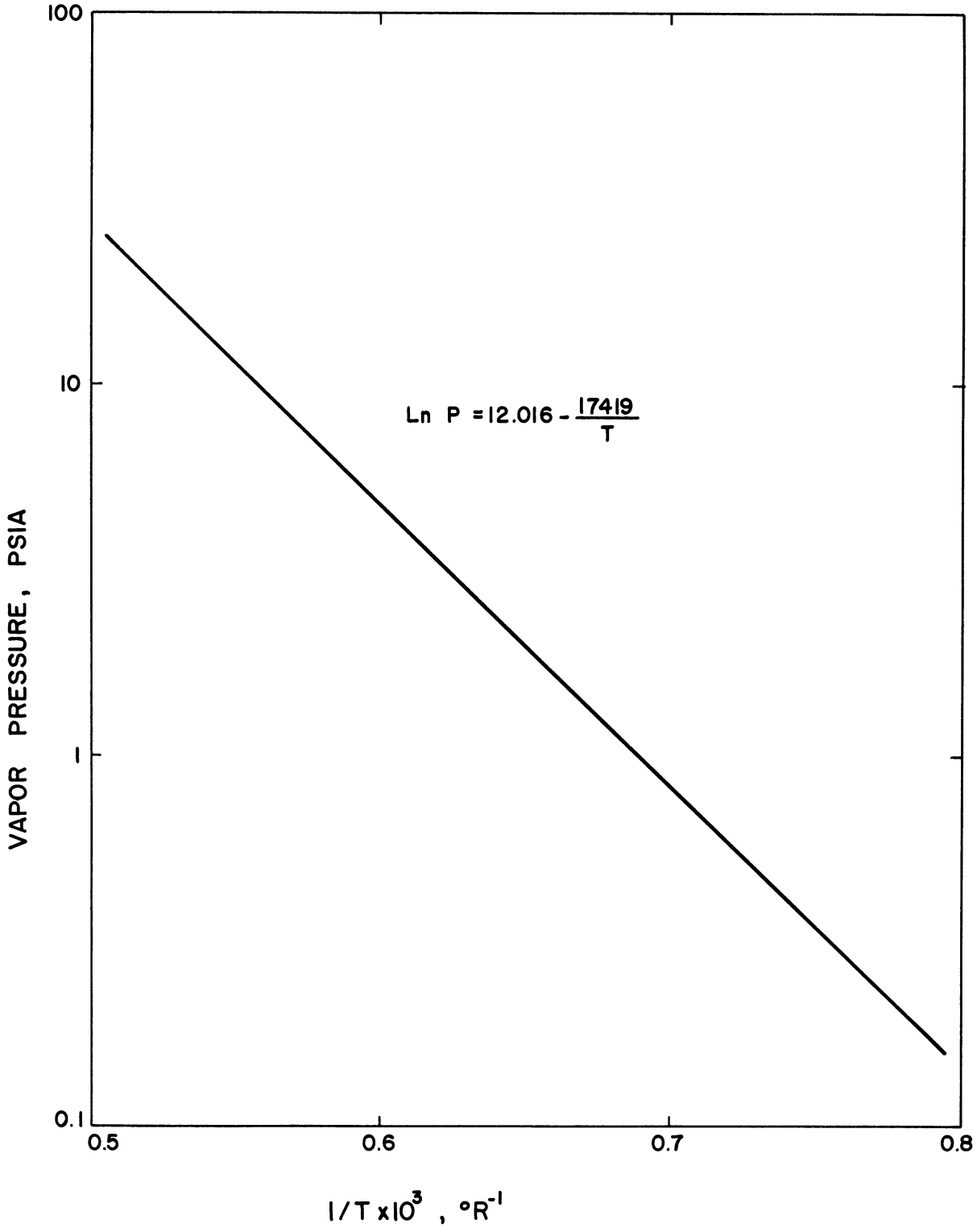

Figure A-1. Vapor Pressure of Sodium-Potassium Mixture Containing 8 Weight Per Cent Sodium

Using Equations (A-7), (A-8), and (A-9) together with Weatherford's data, the following empirical relationship is given for heat of vaporization.

$$\lambda = 969 - 0.0575\ T \quad (T \leq 1200°F)$$
$$\lambda = 993 - 0.0775\ T \quad (T > 1200°F) \qquad \text{(A-10)}$$

where λ = latent heat of vaporization of an 8-92 Na-K mixture, Btu/lb

The uncertainty in λ is about 1 per cent, or $\pm$ 10 Btu/lb.

6. Viscosity of Equilibrium Vapor

As suggested by Knudsen and Katz (46) the viscosity of the vapor mixture may be taken as

$$\mu_g = y_{Na}\ \mu'_{Na} + y_K\ \mu'_K \qquad \text{(A-11)}$$

where μ'_{Na}, μ'_K = vapor viscosity of Na and K, respectively

y_{Na}, y_K = mol fraction of Na and K in equilibrium vapor, respectively

The composition of the equilibrium vapor is expressed by Equation (A-9), and it was found that this equation could be stated empirically as

$$y_K = 1.0227 - 4.44 \times 10^{-5}\ T \qquad \text{(A-12)}$$

in terms of system temperature, °F. The pure-component theoretically predicted data from Weatherford may also be expressed as functions of temperature, °F.

$$\mu'_K = 0.02645 + 1.176 \times 10^{-5}\ T$$
$$\mu'_{Na} = 0.02890 + 1.625 \times 10^{-5}\ T \qquad \text{(A-13)}$$

Equations (A-13) give values in lb/ft/hr between 800 and 1600°F. Insertion of Equations (A-12) and (A-13) in Equation (A-11) allows estimation of desired values.

7. Density of Saturated Vapor

Densities for the equilibrium vapor were calculated using the perfect gas law.

$$\rho_g = \frac{PM}{R(T + 460)} \qquad \text{(A-14)}$$

where ρ_g = vapor density, lb/ft^3

P = vapor pressure, psia

T = temperature, °F

M = molecular weight of saturated vapor

R = 10.72 ft^3 psia/lb-mole/°R

Neglecting polymerization effects in the vapor phase, the molecular weight is taken as a molal average of monomer values.

$$M = 39.1\, y_K + 23.0\, (1 - y_K) \qquad \text{(A-15)}$$

Values of y_K are provided by Equation (A-12).

APPENDIX B

FLOW METER CALIBRATION AND ACCURACY

The primary circuit flowmeter is an MSAR Style FM-2 magnetic flowmeter, as described in Chapter III. The permanent magnet has a measured strength of 3010 gauss. The serial numbers of meter and magnet are 305 and 118, respectively.

MSAR provided theoretically-derived calibration curves for pure potassium and sodium. Prior to the heat transfer section failure, the calibration for potassium was checked. The procedure used was to fill the known volume between thermocouples TC25 and TC29, with the throttle valve closed, at various constant millivolt signals. The average meter calibration factor from eight determinations at 325°F fell within 1.7 per cent of the curve value. This result indicated that the theoretical curve was quite satisfactory. The theoretical calibration curve for a sodium-potassium mixture containing 8 weight per cent sodium is described by the following equation

$$K = 0.3193 + 2.14 \times 10^{-5} T \qquad \text{(B-1)}$$

where K = meter calibration factor, gpm/millivolt

T = temperature at flowmeter, indicated by thermocouple TS15, °F

The calibration factors given by the above equation yield mass flow rates according to the following equation.

$$\dot{m} = 8.02 \rho_{\ell} E K \qquad \text{(B-2)}$$

where 8.02 = conversion factor, 60/7.481

ρ_ℓ = liquid density at temperature indicated by thermocouple TS15, lb/ft^3

E = millivolt signal from flowmeter

The maximum error in $\dot{m}$ values may be estimated using the notion of a differential of a function of several variables, as suggested by Mickley, Sherwood, and Reed (59). Differentials are approximated by small finite differences.

$$\Delta \dot{m} = \frac{\partial \dot{m}}{\partial \rho_\ell} \Delta \rho_\ell + \frac{\partial \dot{m}}{\partial E} \Delta E + \frac{\partial \dot{m}}{\partial K} \Delta K$$

Inserting Equation (B-1),

$$\Delta \dot{m} = 8.02 \; EK \Delta \rho_\ell + \rho_\ell K \Delta E + \rho_\ell E \Delta K \qquad \text{(B-3)}$$

The millivolt signals were easily read within 0.02 mv on the potentiometer. That is,

$$\Delta E = \pm 0.02$$

The calibration curve was accurate to within 0.0005, giving

$$\Delta K = \pm 0.0005$$

From the discussion in Appendix A

$$\Delta \rho_\ell = \pm 0.3$$

represents maximum uncertainty in liquid density. Recalling that liquid density is a function of temperature, Equation (A-2), it is evident that the maximum error in $\dot{m}$, given by Equation (B-3), is dependent on two variables --temperature and flowmeter signal.

Estimates of $\Delta \dot{m}$, covering the entire experimental range of temperatures and flowmeter signals, are presented in Table B-I. Positive values were assigned to the individual errors in order to maximize $\Delta \dot{m}$. Examination of

the per cent maximum errors shows that the effect of temperature is negligible and that the worst errors occur at lowest flow rates. The tabulation suggests that the accuracy of the flow rate measurements is excellent, since the errors discussed are maximum possible values.

TABLE B-I

MAXIMUM ERROR IN TOTAL MASS FLOW RATE AS

A FUNCTION OF TEMPERATURE AND FLOWMETER SIGNAL

Temperature °F	Flowmeter Signal E Millivolts	Predicted Mass Flow Rate $\dot{m}$ lb/hr Equation (B-1)	Maximum Error in Mass Flow Rate $\Delta\dot{m}$ lb/hr Equation (B-2)	Per Cent Maximum Error in Mass Flow Rate
875	1	125	3.52	2.82
875	3	376	5.52	1.47
875	6	752	8.51	1.13
1100	1	122	3.45	2.83
1100	3	365	5.46	1.50
1100	6	730	8.47	1.16
1350	1	118	3.38	2.86
1350	3	354	5.39	1.52
1350	6	708	8.42	1.19

APPENDIX C

CALCULATION OF MIXTURE QUALITY

In presentation and discussion of the experimental results, the quality at the entrance and exit of the pressure drop section are variables of primary interest. Values were calculated using the open-system form of the First Law of Thermodynamics, assuming that thermodynamic equilibrium existed at all points in the two-phase flow.

Figure C-1 shows the open system used in calculating qualities and indicates heat transfer quantities and important thermocouples, where

Q_1 = heat supplied to preheaters (electrical), Btu/hr

Q_2 = heat loss from preheaters, Btu/hr

Q_3 = heat loss from heat transfer section, Btu/hr

Q_4 = heat loss from pressure drop section, Btu/hr

No heat input to the heat transfer section is indicated, since no sodium was being condensed during the two-phase flow runs. A discussion of the heat loss terms is given in Appendix D.

A statement of the First Law for the open system between preheater inlet and point 2 for steady flow (neglecting kinetic and potential energy terms) is

$$\dot{m}h_{\ell 25} + Q_1 = \dot{m}\left[(1-x_2)h_{\ell 2} + x_2 h_{g2}\right] + Q_2 + Q_3 + Q_4 \qquad \text{(C-1)}$$

where $\dot{m}$ = total mass flow rate, lb/hr

$h_{\ell 25}$ = enthalpy of liquid entering preheaters, based on reading of TC25, Btu/lb

$h_{\ell 2}$ = enthalpy of saturated liquid at point 2, Btu/lb

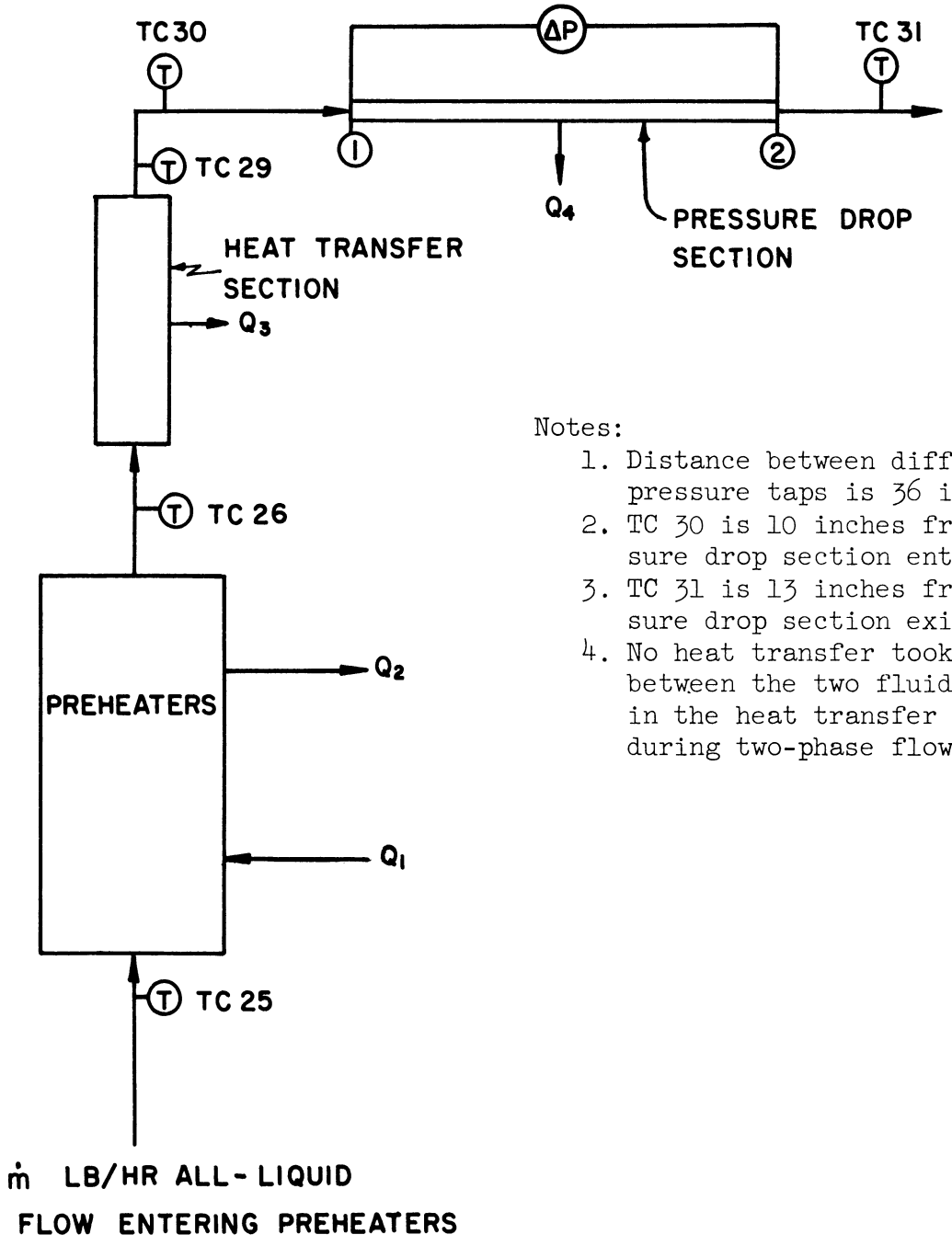

Notes:

1. Distance between differential pressure taps is 36 inches.
2. TC 30 is 10 inches from pressure drop section entrance.
3. TC 31 is 13 inches from pressure drop section exit.
4. No heat transfer took place between the two fluid circuits in the heat transfer section during two-phase flow runs.

Figure C-1. Diagram of Open System Used in Quality Calculations

h_{g2} = enthalpy of saturated vapor at point 2, Btu/lb

x_2 = quality (mass fraction vapor) at point 2

Equation (C-1) may be rearranged to give

$$\dot{m}\left[h_{\ell 2} - h_{\ell 25} + x_2(h_{g2} - h_{\ell 2})\right] = Q_1 - Q_2 - Q_3 - Q_4$$

But the liquid enthalpy change may be written as

$$h_{\ell 2} - h_{\ell 25} = \int_{TC25}^{T_2} Cp_\ell dT$$

where the Cp_ℓ temperature function is given by Equation (A-6). The difference $(h_{g2} - h_{\ell 2})$ under conditions of equilibrium is the latent heat of vaporization at point 2, λ_2. Thus, Equation (C-1) ultimately yields:

$$x_2 = \frac{1}{\lambda_2}\left[\frac{Q_1 - Q_2 - Q_3 - Q_4}{\dot{m}} - \int_{TC25}^{T_2} Cp_\ell dT\right] \qquad (C\text{-}2)$$

By similar analysis, the quality at point 1 is obtained as

$$x_1 = \frac{1}{\lambda_1}\left[\frac{Q_1 - Q_2 - Q_3}{\dot{m}} - \int_{TC25}^{T_1} Cp_\ell dT\right] \qquad (C\text{-}3)$$

where λ_1 = latent heat of vaporization at point 1. The λ values are available from Equation (A-10).

Figure C-1 indicates that thermocouples TC30 and TC31 are not located exactly at the entrance and exit of the pressure drop section. It was necessary to approximate temperatures T_1 and T_2 by use of the experimentally determined pressure gradients. The inlet and exit pressures were estimated by:

$$P_1 = P_{30} - (\Delta P/36)\,10 \qquad (C\text{-}4)$$

$$P_2 = P_{31} + (\Delta P/36)\,13 \qquad (C\text{-}5)$$

where P_{30} and P_{31} represent equilibrium pressures corresponding to the temperatures at TC30 and TC31. The term ($\Delta P/36$) represents the experimental pressure gradient, psi/inch; the factors 10 and 13 are the distances between thermocouples and appropriate points of interest. Temperatures T_1 and T_2 were calculated from P_1 and P_2 using the vapor pressure equation, Equation (A-7).

It is important to consider the accuracy of the T_1 and T_2 values obtained by the method outlined above. No definite statement can be offered regarding the accuracy of pressures or temperatures calculated by Equation (A-7), so it is assumed P and T values thus calculated are precise. Therefore, since the P_{30} and P_{31} values in Equations (C-4) and (C-5) are considered precise, the only error possible in P_1 or P_2 arises from error in the ΔP value. The worst experimental uncertainty in ΔP is about $\pm$ 0.1 psi. Then from Equation (C-4) or (C-5) approximate maximum errors are

$$\Delta P_{1 \text{ (or 2)}} \cong \pm \frac{1}{3} (0.1) = \pm 0.0333$$

The errors in the derived temperatures T_1 and T_2 are obtained from

$$\Delta T = \frac{dT}{dP} \Delta P$$

Inserting Equation (A-7),

$$\Delta T = \frac{17{,}419}{P(12.016 - \ell nP)^2} \Delta P = \frac{\pm 580}{P(12.016 - \ell nP)^2} \qquad \text{(C-6)}$$

Equation (C-6) shows that the errors in the T_1 and T_2 estimates depend on the temperature level of the measurements. This situation is shown graphically in Figure C-2. In terms of percentage these errors are small, but the important consideration is what fraction the error is of the difference ($TC30-T_1$) or (T_2-TC31). The pressure drop data in Appendix G were examined, and it became clear that the worst cases were represented by low pressure

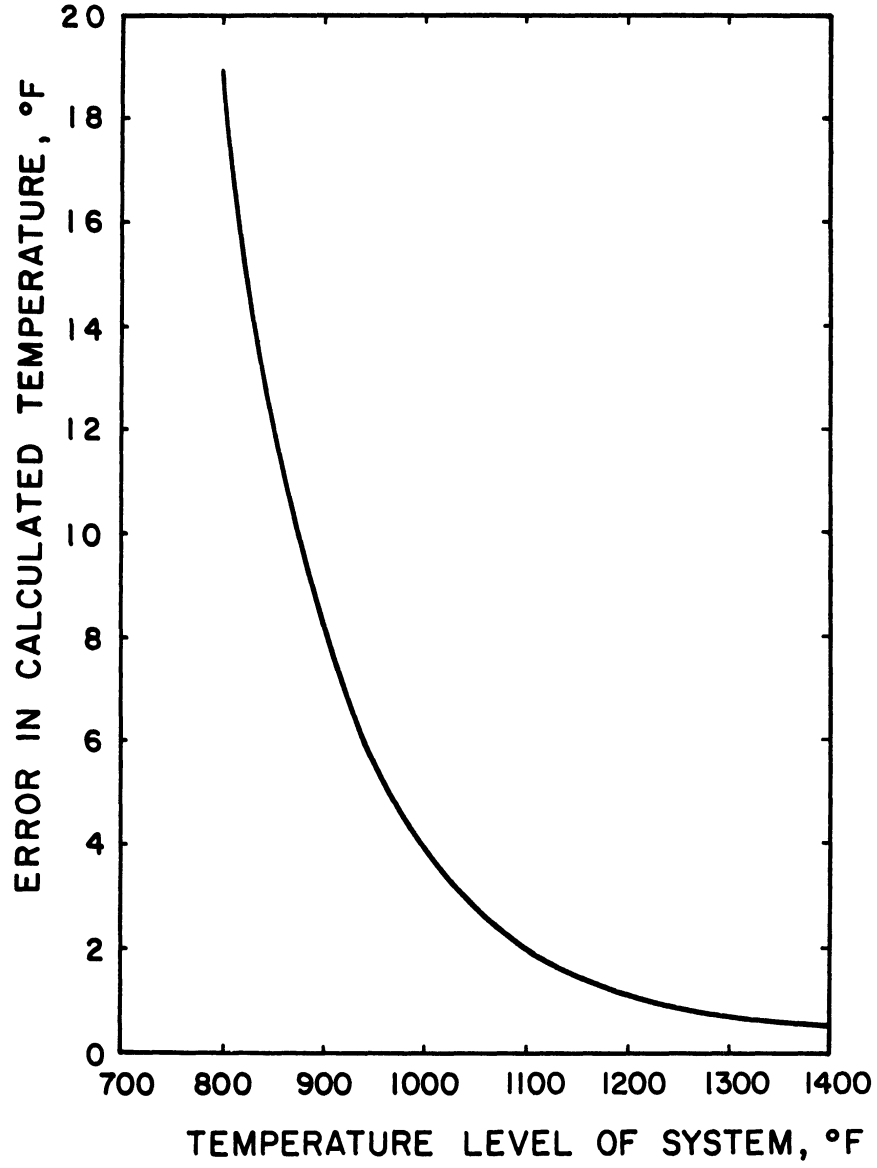

Figure C-2. Maximum Errors in Temperatures at Inlet and Outlet of Pressure Drop Section as a Function of Temperature Level

drop values, in which the corrections (to arrive at T_1 and T_2) were very small. In one typical low pressure drop case, the difference (TC30-T_1) was 1°F with an error of $\pm$ 1°F (1200°F level). Although the error represents 100 per cent of the correction, the correction itself is so small that it is within the accuracy of the thermocouple measurements.

The worst absolute values of error in T_1 and T_2, as shown in Figure C-2, occur at low temperatures. Only nine thermocouple readings were below 900°F --all on TC31. For six of these, the errors in T_2 amounted to about 30 per cent of the corrections--i.e., (T_2-TC31) was about 25 $\pm$ 8°F for these cases. For three points--Code numbers 63.2, 82.1, and 86.6--the errors were nearly 100 per cent of the correction. The uncertainties in the inlet temperatures were also very serious for these same three points. It should also be mentioned that these three points have very low pressure drops, leading to the conclusion that the high proportion of error to correction arises from a compounding of two error-increasing factors--low temperature and low pressure drop.

Fifty five thermocouple readings fell between 900 and 1000°F--ten for TC-30 and 45 for TC31. With the exception of TC30 readings for the three points mentioned above and also the TC31 reading for point number 86.7, the errors in T_1 or T_2 ranged from 10 to 50 per cent of the total correction. The majority of these cases, however, showed corrections greater than 10°F with errors less than 30 per cent of the corrections. It will be shown in Appendix E that the errors in T_1 or T_2 contribute only minor components to the errors in calculated quality values.

The validity of neglecting the potential and kinetic energy change terms in stating the First Law in Equation (C-1) was verified by calculations for a worst possible case. For this case flow was taken as 750 lb/hr with a net quality generation of 0.15 at 800°F. The potential energy change over the

103 inch height amounted to 8.3 Btu/hr; the kinetic energy change, evaluated with the aid of the void fraction correlation, amounted to 182 Btu/hr. These values are insignificant compared to the enthalpy and heat contributions.

A discussion of accuracy of calculated qualities is given in Appendix E.

APPENDIX D

HEAT LOSS CORRELATIONS

It is evident from Appendix C that knowledge of heat losses from the preheater, heat transfer section, and pressure drop section is important in the calculation of qualities.

The heat losses were obtained in all-liquid operations. Heat loss values were calculated from the First Law, which for the heat transfer and pressure drop sections reduces to an overall enthalpy change (potential and kinetic energy contributions are negligible). The following equations, with reference to Figure C-1, were used.

$$Q_2 = Q_1 - \dot{m}\,(h_{\ell 26} - h_{\ell 25}) = Q_1 - \dot{m} \int_{TC25}^{TC26} Cp_\ell dT \qquad \text{(D-1)}$$

$$Q_3 = \dot{m}\,(h_{\ell 26} - h_{\ell 29}) = \dot{m} \int_{TC29}^{TC26} Cp_\ell dT \qquad \text{(D-2)}$$

$$Q_4 = \dot{m}\,(h_{\ell 30} - h_{\ell 31}) = \dot{m} \int_{TC31}^{TC30} Cp_\ell dT \qquad \text{(D-3)}$$

The heat loss determinations were made with pure potassium in the loop --i.e., prior to the heat transfer section failure. In application of the above equations, a mean specific heat was multiplied by the temperature drop, using the data of Weatherford (88). Flow rates were determined by the method outlined in Appendix B, using the theoretical flowmeter calibration curve for pure potassium.

The heat losses were correlated as functions of appropriate temperature: preheater losses against outlet temperature (TC26); heat transfer section and pressure drop section losses against inlet temperature (TC26 and TC30, respectively). The preheater and heat transfer section losses were essentially independent of flow rate, but pressure drop section losses displayed a parametric dependence on flow rate.

Preheater losses ranged from 3000 Btu/hr at 800°F on TC26, to 10,000 Btu/hr at 1400°F. Heat transfer section losses ranged from 1400 Btu/hr to 3900 Btu/hr over the same temperature range on TC26. For a flowmeter signal of 3 millivolts, the pressure drop section losses ran from 1300 to 1500 Btu/hr for 800°F to 1400°F on TC30; for a flowmeter signal of 6 millivolts the losses from this section ran from 1900 to 2050 Btu/hr over the same temperature range. Following are the average deviations of the data from the correlation curves.

Preheater Losses:	ΔQ_2	= $\pm$ 580 Btu/hr
Heat Transfer Section Losses:	ΔQ_3	= $\pm$ 490 Btu/hr
Pressure Drop Section Losses:	ΔQ_4	= $\pm$ 130 Btu/hr

APPENDIX E

ACCURACY OF MIXTURE QUALITIES

An estimate of the uncertainty in quality at the inlet of the pressure drop section, x_1, will be given. The results of the evaluation will be approximately correct for outlet quality values, x_2.

Referring to Appendix C the inlet qualities are computed from

$$x_1 = \frac{1}{\lambda_1}\left[\frac{Q_1 - Q_2 - Q_3}{\dot{m}} - \int_{TC25}^{T_1} Cp_\ell dT\right] \qquad \text{(E-1)}$$

For the purpose of this discussion, the integral term may be written as

$$\int_{TC25}^{T_1} Cp_\ell dT = Cp_\ell\,(T_1 - TC25) \qquad \text{(E-2)}$$

The average deviation or uncertainty in x_1 is obtained from

$$\Delta x_1^2 = \left[\frac{\partial x_1}{\partial Q_1}\Delta Q_1\right]^2 + \left[\frac{\partial x_1}{\partial Q_2}\Delta Q_2\right]^2 + \left[\frac{\partial x_1}{\partial Q_3}\Delta Q_3\right]^2 + \left[\frac{\partial x_1}{\partial \dot{m}}\Delta \dot{m}\right]^2$$

$$+ \left[\frac{\partial x_1}{\partial \lambda_1}\Delta \lambda_1\right]^2 + \left[\frac{\partial x_1}{\partial T_1}\Delta T_1\right]^2 + \left[\frac{\partial x_1}{\partial Cp_\ell}\Delta Cp_\ell\right]^2 \qquad \text{(E-3)}$$

where Δx_1 = uncertainty in x_1, and the Δ terms on the right refer to the average uncertainties in the quantities involved. It is assumed that the temperature measured by TC25 is known exactly, but the equation does indicate error arising from uncertainty in T_1 (see Appendix C). This expression for error is somewhat different from the technique used in Appendix B. In this case the average error in x_1 is estimated. Strictly speaking the Δ terms on

the right should be average errors. The ΔQ's employed here are estimated average errors, while other Δ terms are maximum error values, discussed in other appendices. Since the ΔQ's make the largest contributions to the quality error, the Δx_1^2 values are good estimates of the average error.

Returning to Equations (E-1) and (E-2), the following partial derivatives are obtained.

$$\frac{\partial x_1}{\partial Q_1} = \frac{1}{\lambda_1 \dot{m}}$$

$$\frac{\partial x_1}{\partial Q_2} = \frac{\partial x_1}{\partial Q_3} = \frac{-1}{\lambda_1 \dot{m}}$$

$$\frac{\partial x_1}{\partial \dot{m}} = \frac{-(Q_1 - Q_2 - Q_3)}{\lambda_1 \dot{m}^2}$$

$$\frac{\partial x_1}{\partial \lambda_1} = \frac{-1}{\lambda_1^2}\left[\frac{Q_1 - Q_2 - Q_3}{\dot{m}} - Cp_\ell(T_1 - TC25)\right] = -\frac{x_1}{\lambda_1}$$

$$\frac{\partial x_1}{\partial T_1} = \frac{-Cp_\ell}{\lambda_1}$$

$$\frac{\partial x_1}{\partial Cp_\ell} = \frac{TC25 - T_1}{\lambda_1}$$

The power input to the preheaters is read to within 0.1 KW, so that

$$\Delta Q_1 = \pm 342 \text{ Btu/hr}$$

The results of Appendix D gave

$$\Delta Q_2 = \pm 580 \text{ Btu/hr}$$

$$\Delta Q_3 = \pm 490 \text{ Btu/hr}$$

Appendix A indicates that the following uncertainties may be used for λ_1 and Cp_ℓ:

~~$\Delta \lambda_1$ $\pm$ 10 Btu/lb~~

$$\Delta Cp_\ell = \pm 0.0008 \text{ Btu/lb/°F}$$

The maximum error in $\dot{m}$ was shown to be a function of flowrate--i.e., flowmeter signal--in Appendix B. The maximum error in T_1 was shown in Appendix C to be a function of the temperature level involved. For the purpose of this discussion, the following constant values may be taken for λ_1 and Cp_ℓ.

$$\lambda_l = 900 \text{ Btu/lb}$$

$$Cp_\ell = 0.2 \text{ Btu/lb/°F}$$

Inserting all known quantities, together with the partial derivatives, Equation (E-3) becomes.

$$\Delta x_1^2 = \frac{0.856}{\dot{m}^2} + \left[\frac{Q_1 - Q_2 - Q_3}{900\ \dot{m}^2}\ \Delta\dot{m}\right]^2 + \frac{x_1^2}{8100} + \frac{\Delta T_1^2}{20.2 \times 10^6}$$

$$+ 0.79 \times 10^{-12}\ (TC25 - T_1)^2 \qquad \text{(E-4)}$$

It will be recalled that Q_2 and Q_3 values are functions of the temperature indicated by TC26. The ΔT_1 value is a function of temperature level--i.e., the reading of TC30. A detailed study of the potassium loop's operating history revealed that the definitive operating variables are preheater power input, Q_1, and flowmeter signal, E--i.e., the values of these variables essentially set the temperature levels indicated by thermocouples TC25, TC26, TC30, etc. (10). It follows, then, that values of Δx_1 obtained from Equation (E-4) are essentially functions of Q_1 and flowmeter signal.

Table E-I presents average temperature levels for three flowmeter signals and power inputs. These data were inserted in Equation (E-4) to yield the uncertainty values presented in Table E-II. The data of Table E-I also allow calculation of mean quality levels from Equation (E-2). These quality values are also given in Table E-II. The major contribution to the uncertainty in x_1 comes from the three Q terms.

The uncertainty in calculated quality values is plotted as a function of quality level in Figure E-1. This graph indicates that for qualities below 0.01, the uncertainty rapidly increases above 25 per cent. For qualities above about 0.05 the uncertainty is essentially constant at 5 per cent. Forty-two pressure drop points (19 per cent of the data) occurred at conditions where the quality uncertainty is greater than 10 per cent--i.e., for qualities below 0.025. Four void fraction points corresponded to quality uncertainties greater then 10 per cent.

TABLE E-I

SUMMARY OF AVERAGE LOOP OPERATING DATA FOR USE IN

ESTIMATING ERRORS IN QUALITY VALUES

Flowmeter Signal E Millivolts	Preheater Power Input, Q_1								
	11 KW			15 KW			19 KW		
	TC25	TC26	TC30	TC25	TC26	TC30	TC25	TC26	TC30
1	830	1225	1180	860	1290	1260	920	1430	1430
2	650	1125	1170						
3	695	1100	1070	780	1230	1190	1025	1385	1360
6				1080	1420	1350	1110	1430	1355

TABLE E-II

ERROR IN INLET QUALITY, BASED ON AVERAGE

LOOP OPERATING CHARACTERISTICS

Flowmeter Signal E Millivolts	Preheater Power Input, Q_1								
	11 KW			15 KW			19 KW		
	x_1	Δx_1	% error	x_1	Δx_1	% error	x_1	Δx_1	% error
1	0.1655	0.0102	6.2	0.315	0.0157	5.0	0.341	0.0154	4.5
2	0.0167	0.00450	26.9						
3	0.00467	0.00286	61.3	0.0269	0.00297	11.0	0.1043	0.00399	3.8
6				0.00688	0.00152	22.1	0.0182	0.00155	8.5

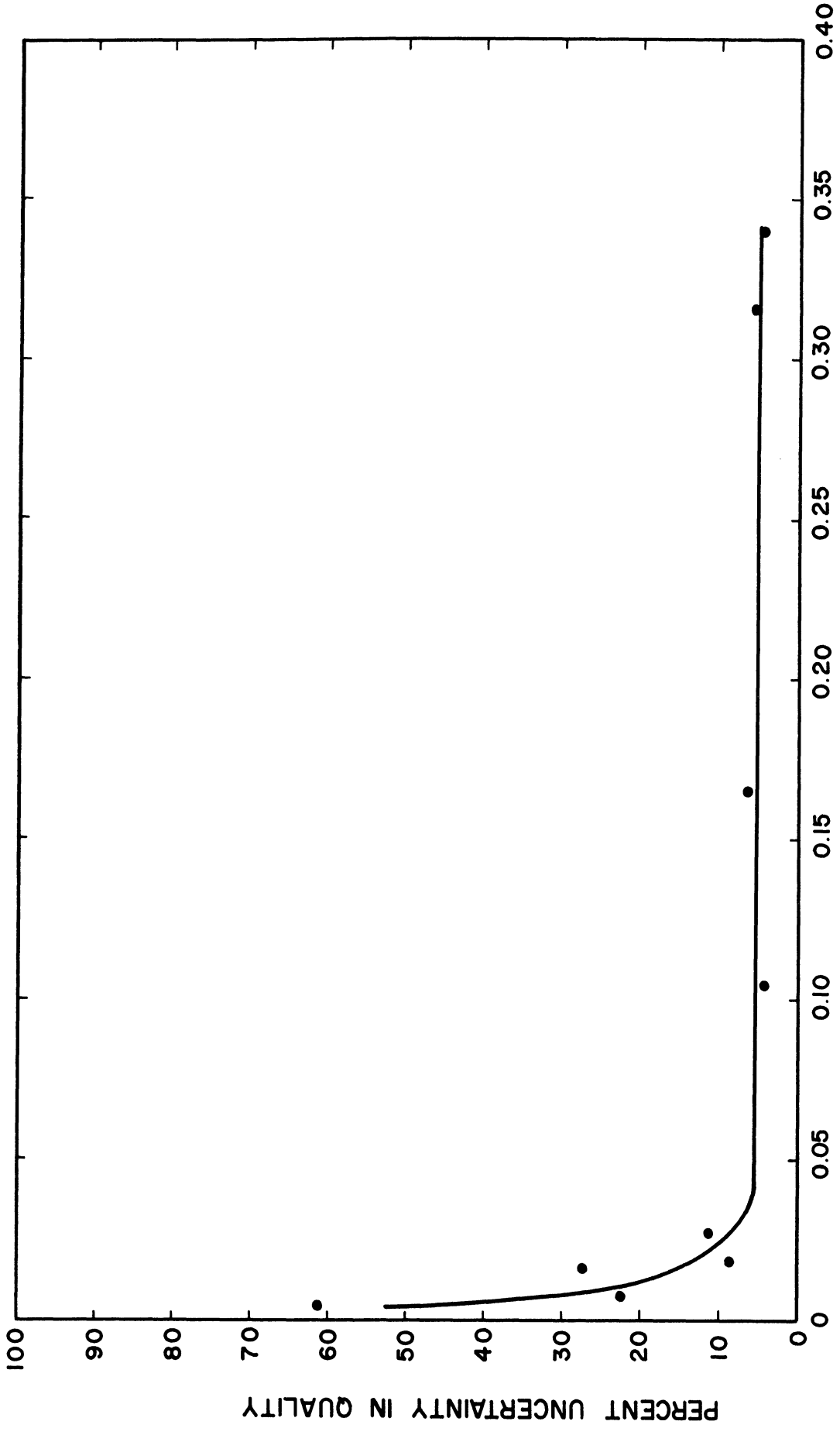

Figure E-1 Uncertainty in Calculated Qualities, Based on Average Loop Operating Characteristics

APPENDIX F

ACCURACY AND QUALITY LIMITATION OF VOID FRACTION MEASUREMENTS

In Chapter III it was pointed out that measurements of void fraction by gamma-ray attenuation are generally reliable for qualities up to about 0.20. This limitation will be illustrated in this appendix. First, however, the accuracy of the void fraction results will be examined.

Any experimental correlation between two or more variables will contain residual variance or "scatter." The void fraction data obtained in this study, together with metallic data of other investigators, have yielded the following "least-squares" straight line on log-log paper.

$$\log (1-\alpha) = - 0.2414 + 0.3421 \log X_{tt} \qquad \text{(F-1)}$$

Volk (86) shows that the variance of any average value $\hat{y}_i$ estimated by a correlation for any given $\hat{x}_i$ value is given by

$$s^2(\hat{y}_i) = s^2(\hat{y}) \left[\frac{1}{n} + \frac{(\bar{\hat{x}} - \hat{x}_i)^2}{\sum(\bar{\hat{x}} - \hat{x}_i)^2} \right] \qquad \text{(F-2)}$$

where $\hat{y}_i$ and $\hat{x}_i$ are two linearly-related variables

$\bar{\hat{x}}$ = average value of $\hat{x}$

n = number of data points

$s^2(\hat{y}_i)$ = variance of any average estimated $\hat{y}_i$ value

$s^2(\hat{y})$ = variance of estimate of correlation

$$\hat{y}_i = a + b \hat{x}_i \qquad \text{(F-3)}$$

and

$$s^2(\hat{y}) = \frac{\sum(\hat{y} - y_i)^2 - b\sum\left[(\hat{x} - \hat{x}_i)(\hat{y} - \hat{y}_i)\right]}{n - 2} \qquad \text{(F-4)}$$

The constants a and b are determined by the least-squares technique. The variance $s^2(\hat{y}_i)$ when multiplied by the appropriate values of Student's t establishes confidence ranges on the linear correlation given by Equation (F-3).

Letting $\hat{y}_i = \log (1 - \alpha)$

and $\hat{x}_i = \log X_{tt}$

the variance of any average value of $(1 - \alpha)$ predicted by Equation (F-1) may be obtained. It must be emphasized that the variance determined by this technique is due only to the scatter of the data around the best-fit correlation line. For the case in question here, a = - 0.2414 and b = 0.3421. From this technique the standard deviation of void fraction values, arising from scatter in the data, were obtained as a function of α. These $s(\alpha)$ values are plotted in Figure F-1.

The variance of a quantity which is a function of one or more variables may be derived mathematically, provided the variances of the various independent variables are known (86). Void fractions were calculated from

$$\alpha = \frac{\ell n\ N/N_\ell}{\ell n\ N_g/N_\ell} \qquad \text{(F-5)}$$

From the single-phase calibration measurements, with use of the temperature-correcting equations in Appendix I as well as density-temperature functions from Appendix A, Equation (F-5) reduces to

$$\alpha = \frac{\ell n\ N - \ell n\ 254.6 - 0.04393\ (49.09 - \rho_\ell)}{0.04393\ (\rho_\ell - \rho_g)} \qquad \text{(F-6)}$$

where the densities are taken at the temperature of the N measurement. This equation says that α is a function of N and temperature. Hence, the variance of any α value is given by (86)

$$\sigma^2(\alpha) = \left(\frac{\partial\alpha}{\partial N}\right)^2 \sigma^2(N) + \left(\frac{\partial\alpha}{\partial T}\right)^2 \sigma^2(T) \qquad \text{(F-7)}$$

where $\sigma^2(\alpha)$ = variance of calculated void fraction

$\sigma^2(N)$ = variance of gamma ray count rate

$\sigma^2(T)$ = variance of temperature measurement

In this discussion only the $\sigma^2(N)$ component of the α variance is considered, since $\sigma^2(N)$ is easily known theoretically. It will be recalled that the working beam count rate N is obtained from

$$N = N_{coll} - N_{bkg} \qquad \text{(F-8)}$$

where N_{coll} and N_{bkg} are count rates obtained for the collimated beam and in background measurement, respectively. Price (69) shows that the variance of any individual gamma-ray counting measurement is equal to the number of counts obtained. It follows, then, that

$$\sigma^2(N) = \left(\frac{\partial N}{\partial N_{coll}}\right)^2 \sigma^2(N_{coll}) + \left(\frac{\partial N}{\partial N_{bkg}}\right)^2 \sigma^2(N_{bkg})$$

so that

$$\sigma^2(N) = N_{coll} + N_{bkg} \qquad \text{(F-9)}$$

The variance in α due to variance in N, from Equations (F-6) and (F-7) is

$$\sigma_N^2(\alpha) = \left[\frac{1}{0.04393\,(\rho_\ell - \rho_g)\,N}\right]^2 \sigma^2(N) \qquad \text{(F-10)}$$

where N and $\sigma^2(N)$ are evaluated from Equations (F-8) and (F-9). The variance given by Equation (F-10) arises from natural, statistical randomness of the gamma ray emission process. The value of $\sigma_N^2(\alpha)$ was obtained for each data point. The resulting standard deviations are plotted as a function of α in Figure F-1.

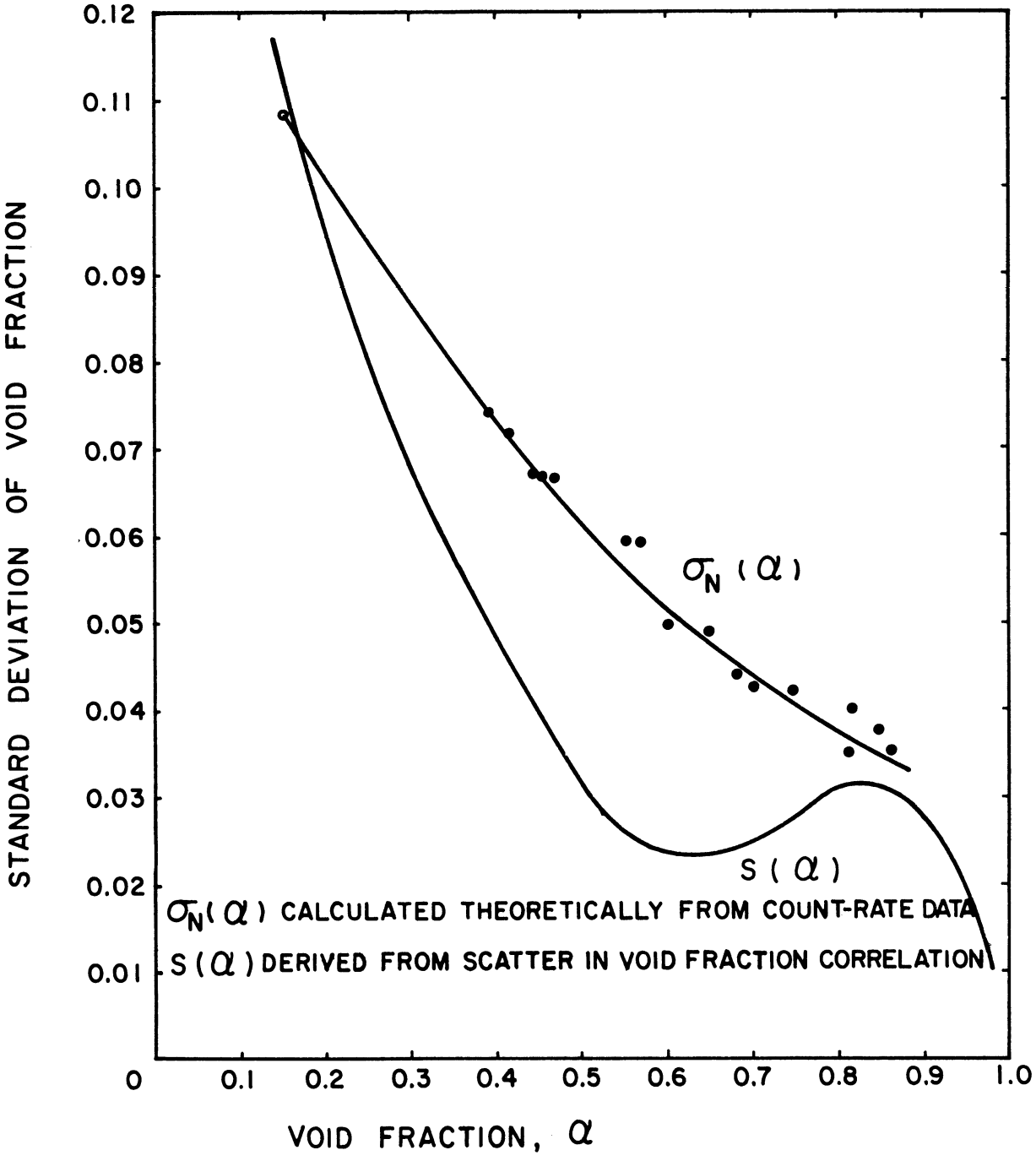

Figure F-1. Standard Deviation of Void Fraction

The important point to be gained from examination of Figure F-1 is that the scatter of the experimental data is within the statistical inaccuracy of the gamma-ray counting process. In addition, the percentage uncertainty in α values based on $\sigma_N(\alpha)$, runs from about 4 to 19 per cent (neglecting the one lone value which is about 70 per cent uncertain).

The limitation of reliability of void fraction measurements to qualities below about 0.20 can be best illustrated by consideration of the slip velocity ratio. In Chapter V this was given as

$$s = \frac{V_g}{V_\ell} = \left(\frac{x}{1 - x}\right)\left(\frac{1 - \alpha}{\alpha}\right)\left(\frac{\rho_\ell}{\rho_g}\right) \qquad \text{(F-11)}$$

This quantity, s, frequently arises in analytical investigations, as it is related to the interfacial shear force. The value of s, or sometimes only V_g, is also useful in the consideration of critical flow phenomena. In any case, the accuracy of s values is related to the accuracy of α values and also the value of x. Equation (F-11) shows s to be a function of α, x, and temperature.

Consider next the variance in s which is due only to variance in α.

$$s^2(s) = \left(\frac{\partial s}{\partial \alpha}\right)^2 s^2(\alpha) \qquad \text{(F-12)}$$

Combining Equations (F-11) and (F-12)

$$s^2(s) = \left(\frac{\rho_\ell}{\rho_g}\right)^2 \left(\frac{x}{1 - x}\right)^2 \alpha^{-4} \; s^2(\alpha) \qquad \text{(F-13)}$$

From Equation (F-13) the standard deviation in slip ratio, s(s), may be calculated as a function of x, α, and temperature.

Equation (F-11) allows one to plot s as a function of α with parametric values of x for any constant temperature. This has been done in Figure F-2 for the potassium mixture at 1200°F. The parametric quality lines are indicated, and it is quite evident that they crowd closer and closer together as x increases.

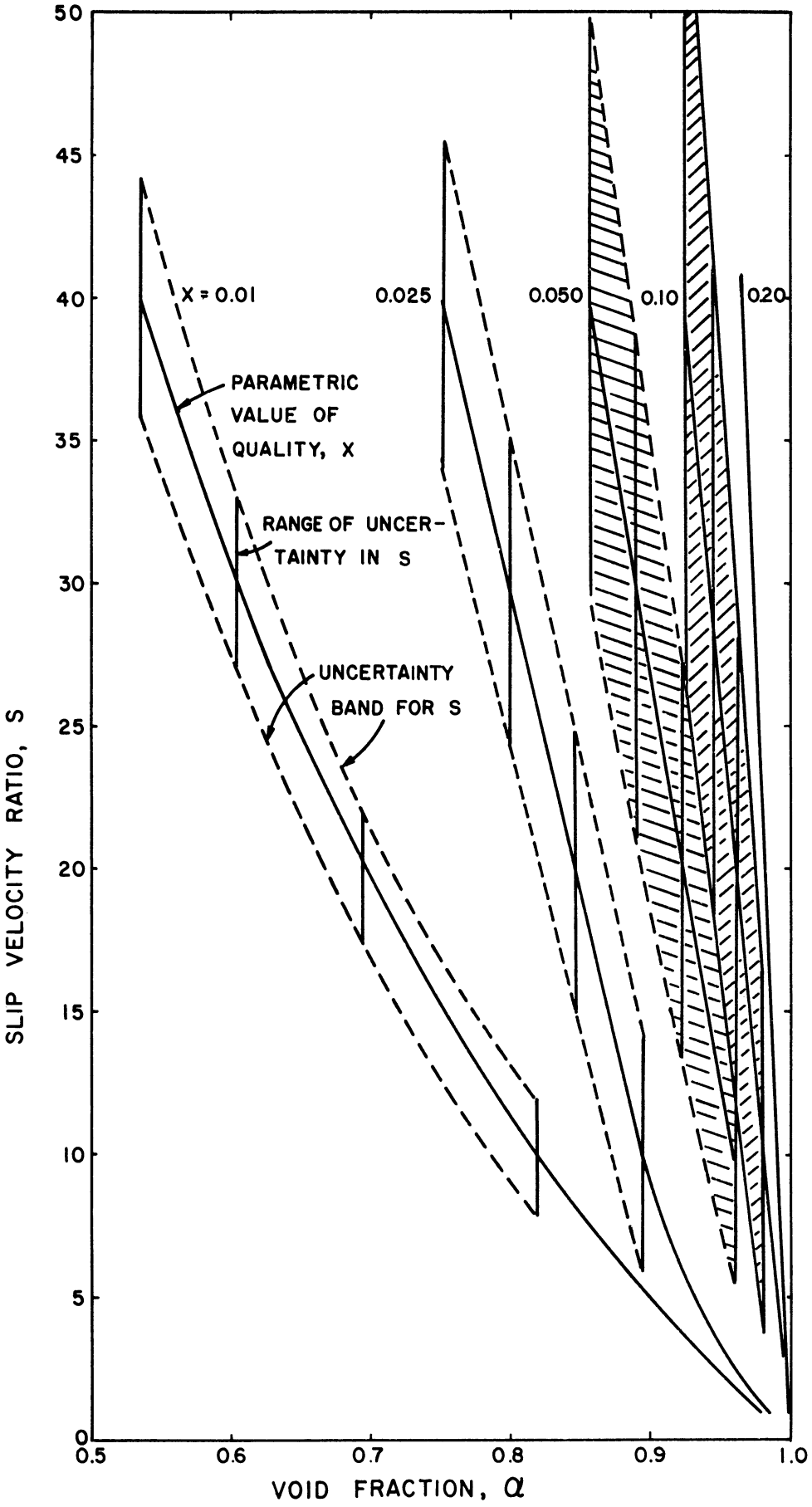

Figure F-2. Slip Velocity Ratio as a Function of Void Fraction and Quality for 8-92 Na-K at 1200°F, Showing Uncertainty in Slip Ratio

Equation (F-13) was used to calculate the standard deviation s(s) at 1200°F for various values of quality and mean slip ratio. The $s(\alpha)$ values from Figure F-1 are used in the computation--i.e., the α variances used are those due to scatter in the correlation. Computed values of s(s) are given in Table F-I. This table shows that the standard deviation (a measure of the uncertainty) in s increases rapidly with x at any mean s level. Between x values of 0.1 and 0.2 the uncertainty gets very high and the regions of uncertainty overlap. This situation is illustrated in Figure F-2, where uncertainty bands are drawn around the parametric quality lines. The bands indicate the probable range of s for any given value of α and x. As x increases, the uncertainty bands approach each other, as is emphasized by the two cross-hatched regions. It can be appreciated that for qualities greater than about 0.20 the situation becomes grossly confused due to overlap of the uncertainty bands.

This illustration of the limitation in utility of α values to the low quality region has been made at a single temperature, but the same result is obtained over the entire temperature range. The situation is improved slightly at higher temperatures. That the s(s) values increase is due to the rapid increase of the factor $\frac{x}{1 - x}$ with x in Equation (F-13). The only way to overcome the rapid increase of this factor is to substantially decrease the $s(\alpha)$ values. The gamma ray attenuation technique has not yet been sufficiently improved to effect the necessary decrease in $s(\alpha)$, or, for that matter, the theoretical standard deviation $\sigma(\alpha)$.

TABLE F-I

STANDARD DEVIATION IN SLIP VELOCITY
RATIO FOR TWO-PHASE POTASSIUM FLOWS AT 1200°F

Quality	s = 10		s = 20		s = 30		s = 40	
x	α	s(s)	α	s(s)	α	s(s)	α	s(s)
0.010	0.820	2.16	0.697	2.31	0.605	2.89	0.535	4.34
0.025	0.895	4.07	0.854	4.95	0.796	5.69	0.744	5.68
0.050	0.960	4.41	0.922	6.76	0.889	8.76	0.857	10.10
0.100	0.980	6.31	0.962	8.75	0.945	11.38	0.926	14.16
0.200	0.990	6.96	0.983	10.85	0.975	14.38	0.965	19.7
0.300	0.995	7.87	0.990	11.92	0.985	16.10	0.980	20.3

APPENDIX G

TABLES OF PRESSURE DROP RESULTS

TABLE G-I

RESULTS OF ALL-LIQUID PRESSURE DROP RUNS

CODE	Total Mass Flow, lb/hr	Average Temperature °F	Pressure Drop psi	Reynolds Number Re	Experimental Moody Friction Factor	Calculated Moody Friction Factor Equation (28)	Per Cent Difference in Friction Factor
97.120	810	305	0.1082	2.80×10^4	0.0251	0.0245	2.4
97.123	793	288	0.1082	2.66×10^4	0.0263	0.0249	5.5
97.100	661	272	0.0650	2.12×10^4	0.0226	0.0263	15.1

Average per cent difference in friction factor = 7.7

TABLE G-II

EXPLANATION OF COLUMNAR HEADINGS

CODE	Code number for data point. Number to left of decimal refers to the page number in University of Michigan Research Institute Data Book No. 3496 on which the raw data are recorded. The number to the right of the decimal refers to the time the data were taken. Parenthetic numbers refer to more than one data point at same hours.
MDOT	Total mass flow rate, lb/hr
DELP	Pressure drop, psi
X1	Quality at inlet to pressure drop section
X2	Quality at outlet of pressure drop section
XAVG	Average quality in pressure drop section, $1/2(X1 + X2)$
T1	Temperature at inlet to pressure drop section, °F
T2	Temperature at outlet of pressure drop section, °F
P1	Absolute pressure at inlet of pressure drop section, psia
DELX	Quality change across pressure drop section, $(X2 - X1)$
DP/EQDP	Ratio of experimental pressure drop to pressure drop calculated from equilibrium vapor pressures.
F	Two-phase friction factor, defined by Equation (7)
F/FG	Ratio of two-phase friction factor to single-phase Moody friction factor based on all-vapor flow at total flowrate and average section temperature.

(The numerical notation X.XXXX E $\pm$ yy is equivalent to X.XXXX . $10^{\pm yy}$.)

TABLE G-II

RESULTS OF PRESSURE DROP STUDY

IN HORIZONTAL TWO-PHASE FLOWS OF 8-92 NA-K

CODE	MDOT	DELP	X1	X2	XAVG	T1	T2	P1	DELX	DP/EQDP	F	F/FG
76.100	116	1.080	.3788	.3780	.3784	1391	1381	13.13	-.0008	1.75	.2741E-02	.1419E 00
76.200	127	1.080	.3446	.3396	.3421	1380	1394	12.46	-.0051	-1.22	.2287E-02	.1209E 00
76.300	126	1.080	.3407	.3425	.3416	1428	1405	15.84	.0018	.62	.2655E-02	.1397E 00
77.700	130	1.080	.2458	.2463	.2460	1283	1275	7.34	.0005	3.20	.1302E-02	.6975E-01
77.800	126	1.080	.2597	.2614	.2605	1278	1264	7.13	.0017	2.01	.1327E-02	.7065E-01
77.900	111	1.080	.3084	.3069	.3077	1259	1262	6.39	-.0015	-8.74	.1621E-02	.8392E-01
78.120	127	.760	.1727	.1768	.1748	1176	1156	3.81	.0041	1.62	.5167E-03	.2776E-01
78.100	131	.860	.1612	.1682	.1647	1174	1144	3.76	.0070	1.27	.5282E-03	.2858E-01
84.110	128	1.180	.3371	.3377	.3374	1358	1345	11.12	.0007	1.52	.2105E-02	.1117E 00
84.120 (2)	123	1.180	.3697	.3671	.3684	1383	1385	12.63	-.0026	-11.16	.2615E-02	.1374E 00
85.400	127	1.080	.2495	.2485	.2490	1325	1322	9.30	-.0011	6.56	.1705E-02	.9051E-01
85.500	136	1.080	.2321	.2321	.2321	1312	1305	8.64	-.0001	3.15	.1380E-02	.7448E-01
85.600	134	1.180	.2358	.2391	.2375	1313	1291	8.71	.0033	1.15	.1515E-02	.8152E-01
85.110	127	.760	.1696	.1731	.1713	1194	1175	4.30	.0035	1.53	.5793E-03	.3107E-01
86.600	130	.109	.0284	.0376	.0330	942	894	.64	.0093	.48	.1230E-04	.6777E-03
86.700	134	.109	.0454	.0583	.0518	1001	931	1.06	.0129	.23	.1706E-04	.9424E-03
86.800	134	.217	.0428	.0563	.0495	1017	952	1.21	.0135	.43	.3937E-04	.2172E-02
86.900	129	.326	.0688	.0862	.0775	1059	979	1.68	.0174	.41	.8249E-04	.4498E-02
86.100	129	.380	.0691	.0833	.0762	1045	985	1.51	.0142	.65	.9369E-04	.5109E-02
86.110	130	.272	.1441	.1486	.1464	969	954	.81	.0046	2.79	.4386E-04	.2407E-02
86.120	108	.435	.1644	.1798	.1721	1067	999	1.79	.0154	.59	.1738E-03	.9097E-02
87.100	125	.435	.1258	.1440	.1349	1102	1016	2.30	.0183	.40	.1555E-03	.8390E-02
94.600	150	.380	.1061	.1043	.1052	1399	1390	13.74	-.0017	.59	.6005E-03	.3291E-01
94.700	125	.488	.1615	.1591	.1603	1379	1374	12.37	-.0024	1.53	.1025E-02	.5397E-01
94.800	135	.434	.1424	.1402	.1413	1367	1361	11.63	-.0022	1.14	.7387E-03	.3962E-01
94.900	134	.380	.1129	.1112	.1121	1370	1361	11.83	-.0017	.70	.6542E-03	.3507E-01
94.100	133	.380	.1285	.1262	.1274	1346	1341	10.41	-.0023	1.24	.5976E-03	.3204E-01
94.110	135	.380	.1183	.1163	.1173	1355	1347	10.93	-.0019	.87	.6075E-03	.3263E-01
95.120	140	.380	.1164	.1139	.1152	1342	1338	10.19	-.0025	1.56	.5368E-03	.2908E-01
95.200	132	.244	.1035	.0987	.1011	1332	1337	9.64	-.0048	-.93	.3754E-03	.2009E-01
95.300	136	.163	.0903	.0903	.0903	1353	1334	10.82	.0000	.16	.2475E-03	.1332E-01
95.400	142	.163	.0894	.0876	.0885	1336	1326	9.87	-.0019	.31	.2131E-03	.1160E-01
95.500	130	.217	.1115	.1084	.1099	1327	1324	9.38	-.0031	1.31	.3320E-03	.1771E-01
95.600	131	.108	.0736	.0717	.0727	1330	1320	9.57	-.0018	.20	.1618E-03	.8648E-02
95.700	130	.108	.0765	.0740	.0753	1330	1323	9.57	-.0025	.28	.1662E-03	.8862E-02
95.730	127	.108	.0794	.0778	.0786	1326	1315	9.36	-.0016	.19	.1680E-03	.8921E-02
96.830	127	.054	.0466	.0471	.0469	1305	1282	8.30	.0006	.05	.7348E-04	.3911E-02
96.900	134	.054	.0426	.0432	.0429	1299	1276	8.03	.0006	.06	.6452E-04	.3474E-02
56.700	274	1.950	.1078	.1175	.1126	1293	1257	7.78	.0097	1.32	.5175E-03	.3257E-01
56.800	274	1.950	.1035	.1166	.1100	1311	1258	8.60	.0131	.86	.5430E-03	.3415E-01
56.900	249	1.950	.1316	.1420	.1368	1285	1246	7.41	.0104	1.30	.5985E-03	.3693E-01
56.110	272	1.780	.0831	.1004	.0917	1244	1181	5.85	.0173	.93	.3437E-03	.2169E-01
56.120	294	1.730	.0803	.0943	.0873	1230	1182	5.36	.0140	1.25	.2765E-03	.1773E-01
56.121	294	1.840	.0741	.0911	.0826	1247	1186	5.95	.0170	.98	.3121E-03	.2000E-01
57.100	288	1.950	.0722	.0917	.0820	1264	1192	6.59	.0195	.83	.3675E-03	.2343E-01
57.500	257	2.440	.0814	.0952	.0883	1198	1174	4.40	.0139	3.84	.4545E-03	.2840E-01
57.600	236	2.440	.0937	.1141	.1039	1226	1168	5.23	.0204	1.52	.5771E-03	.3537E-01
58.900	243	1.980	.0737	.0961	.0849	1200	1132	4.47	.0224	1.22	.3696E-03	.2285E-01
58.100	232	2.130	.0867	.1118	.0992	1220	1139	5.04	.0251	1.03	.4691E-03	.2870E-01
58.110	282	2.100	.0579	.0794	.0687	1206	1143	4.62	.0215	1.35	.3035E-03	.1935E-01

TABLE G-II Cont'd

CODE	MDOT	DELP	X1	X2	XAVG	T1	T2	P1	DELX	DP/EQDP	F	F/FG
58.113	250	2.160	.0858	.1056	.0957	1183	1134	4.00	.0198	1.93	.3617E-03	.2252E-01
58.115	270	2.100	.0598	.0860	.0729	1221	1136	5.09	.0262	.97	.3398E-03	.2146E-01
58.120	264	2.020	.0754	.0918	.0836	1161	1128	3.46	.0164	2.92	.2804E-03	.1766E-01
58.122	255	2.160	.0792	.0935	.0863	1164	1142	3.53	.0143	4.41	.3376E-03	.2110E-01
58.123	251	2.060	.0746	.0957	.0852	1187	1130	4.11	.0211	1.57	.3434E-03	.2138E-01
59.400	289	1.700	.0400	.0620	.0510	1164	1101	3.52	.0220	1.37	.1816E-03	.1167E-01
59.450	243	1.700	.0699	.0874	.0786	1138	1099	2.97	.0175	2.40	.2364E-03	.1467E-01
59.500	213	1.660	.0946	.1140	.1043	1130	1084	2.80	.0193	2.16	.2785E-03	.1683E-01
59.510	256	1.950	.0601	.0811	.0706	1147	1100	3.15	.0210	2.22	.2524E-03	.1582E-01
59.530	291	1.730	.0345	.0568	.0456	1170	1105	3.67	.0223	1.32	.1890E-03	.1215E-01
60.900	256	1.080	.0370	.0594	.0482	1104	1035	2.34	.0224	1.15	.9871E-04	.6211E-02
60.100	263	1.120	.0414	.0547	.0481	1066	1045	1.77	.0133	4.19	.8775E-04	.5561E-02
60.102	259	1.150	.0287	.0599	.0443	1136	1028	2.92	.0312	.72	.1109E-03	.6995E-02
60.104	259	1.120	.0385	.0569	.0477	1071	1029	1.83	.0185	2.22	.8685E-04	.5490E-02
60.110	258	1.080	.0362	.0574	.0468	1087	1028	2.07	.0212	1.44	.8935E-04	.5639E-02
61.100	260	.975	.0226	.0453	.0340	1102	1028	2.31	.0227	.99	.8403E-04	.5306E-02
61.200	260	.975	.0297	.0488	.0392	1060	1012	1.70	.0191	1.85	.6868E-04	.4347E-02
61.300	255	.940	.0333	.0377	.0355	1056	1064	1.65	.0044	-9.30	.8138E-04	.5120E-02
61.400	249	.940	.0463	.0554	.0509	1011	1015	1.16	.0091	-29.46	.6087E-04	.3826E-02
61.500	254	.940	.0340	.0511	.0425	1061	1019	1.70	.0170	1.97	.7073E-04	.4456E-02
61.600	260	.940	.0108	.0472	.0290	1165	1022	3.56	.0364	.41	.9761E-04	.6151E-02
61.700	260	.940	.0310	.0479	.0394	1073	1028	1.87	.0169	1.72	.7322E-04	.4629E-02
61.800	260	.795	.0301	.0478	.0389	1058	1007	1.67	.0177	1.43	.5460E-04	.3457E-02
62.840	260	.940	.0285	.0484	.0385	1062	1009	1.72	.0200	1.61	.6582E-04	.4166E-02
62.900	251	.865	.0353	.0480	.0417	1051	1024	1.59	.0127	2.89	.6619E-04	.4158E-02
62.100	259	.865	.0284	.0488	.0386	1094	1026	2.18	.0204	.98	.7224E-04	.4562E-02
63.200	267	.055	.0046	.0156	.0101	923	862	.54	.0110	.23	.1185E-05	.7627E-04
64.100	262	.271	.0133	.0270	.0202	960	911	.76	.0137	1.01	.8761E-05	.5595E-03
64.103	255	.289	.0157	.0296	.0226	962	914	.77	.0139	1.07	.1006E-04	.6392E-03
64.110	255	.307	.0164	.0303	.0234	969	921	.82	.0139	1.08	.1131E-04	.7181E-03
64.120	258	.307	.0147	.0289	.0218	971	921	.83	.0143	1.03	.1110E-04	.7067E-03
64.100	259	.325	.0152	.0293	.0223	970	922	.82	.0141	1.16	.1172E-04	.7461E-03
64.200	258	.324	.0149	.0288	.0219	972	925	.84	.0139	1.14	.1191E-04	.7582E-03
65.500	256	.588	.0179	.0336	.0257	1021	976	1.26	.0157	1.49	.3257E-04	.2060E-02
65.600	267	.595	.0165	.0336	.0250	1021	970	1.26	.0172	1.39	.2957E-04	.1888E-02
65.700	260	.595	.0165	.0347	.0256	1031	974	1.36	.0182	1.17	.3264E-04	.2072E-02
65.800	260	.612	.0176	.0349	.0263	1026	974	1.31	.0174	1.36	.3308E-04	.2101E-02
65.900	257	.595	.0162	.0334	.0248	1025	973	1.29	.0172	1.34	.3273E-04	.2072E-02
65.100	260	.612	.0168	.0350	.0259	1031	974	1.35	.0182	1.23	.3363E-04	.2135E-02
66.200	261	.993	.0263	.0457	.0360	1077	1023	1.92	.0194	1.55	.7627E-04	.4827E-02
66.300	260	.993	.0296	.0461	.0379	1060	1023	1.69	.0165	2.36	.7246E-04	.4584E-02
66.400	260	1.010	.0287	.0474	.0381	1076	1026	1.91	.0187	1.67	.7913E-04	.5002E-02
66.500	263	1.050	.0268	.0454	.0361	1077	1029	1.92	.0185	1.81	.8083E-04	.5124E-02
66.600	262	1.080	.0296	.0477	.0386	1069	1027	1.81	.0181	2.17	.8130E-04	.5150E-02
66.620	263	1.080	.0279	.0487	.0383	1083	1027	2.01	.0208	1.55	.8413E-04	.5332E-02
66.700	259	1.080	.0296	.0471	.0383	1080	1037	1.97	.0175	1.96	.8918E-04	.5633E-02
82.120(1)	253	1.010	.0256	.0469	.0362	1088	1026	2.09	.0212	1.27	.8668E-04	.5447E-02
82.100(2)	267	.091	.0004	.0127	.0065	945	882	.66	.0123	.31	.2348E-05	.1509E-03
82.300	258	.470	.0190	.0356	.0273	1009	955	1.14	.0165	1.12	.2253E-04	.1430E-02
82.400	258	.540	.0181	.0351	.0266	1015	963	1.19	.0169	1.29	.2729E-04	.1731E-02
82.120(3)	263	.950	.0260	.0444	.0352	1062	1015	1.72	.0183	1.82	.6650E-04	.4218E-02
84.100	232	1.660	.1746	.1754	.1750	1314	1310	8.73	.0008	9.38	.7392E-03	.4482E-01
91.700	241	.108	.0371	.0348	.0359	1246	1239	5.92	-.0023	.44	.3137E-04	.1926E-02
91.800	261	.108	.0264	.0245	.0255	1275	1266	7.02	-.0019	.29	.3104E-04	.1933E-02
91.900	248	.108	.0405	.0388	.0397	1292	1282	7.74	-.0017	.24	.3738E-04	.2301E-02
91.100	247	.108	.0396	.0377	.0387	1312	1303	8.67	-.0020	.24	.4159E-04	.2556E-02
91.110	247	.162	.0398	.0375	.0386	1320	1312	9.04	-.0022	.42	.6521E-04	.4004E-02
91.120	254	.650	.0852	.0854	.0853	1360	1345	11.21	.0002	.77	.2957E-03	.1821E-01
91.100	241	.542	.0943	.0927	.0935	1380	1371	12.42	-.0015	1.02	.3031E-03	.1844E-01
91.200	245	.542	.0906	.0889	.0897	1394	1386	13.35	-.0018	1.04	.3125E-03	.1906E-01

TABLE G-II Cont'd

CODE	MDOT	DELP	X1	X2	XAVG	T1	T2	P1	DELX	DP/EQDP	F	F/FG
91.300	239	.488	.0916	.0913	.0915	1409	1394	14.42	-.0003	.45	.3119E-03	.1891E-01
91.400	248	.542	.0864	.0852	.0858	1408	1397	14.33	-.0011	.70	.3237E-03	.1977E-01
92.500	249	.542	.0642	.0629	.0636	1407	1397	14.26	-.0013	.77	.3190E-03	.1951E-01
92.600	255	.488	.0613	.0572	.0592	1397	1400	13.57	-.0041	-2.80	.2710E-03	.1665E-01
92.700	252	.488	.0638	.0623	.0631	1391	1382	13.16	-.0015	.80	.2615E-03	.1605E-01
92.800	259	.488	.0625	.0616	.0620	1373	1361	11.99	-.0008	.68	.2278E-03	.1408E-01
92.900	260	.542	.0662	.0654	.0658	1369	1357	11.72	-.0008	.81	.2461E-03	.1522E-01
92.100	235	.434	.0542	.0543	.0543	1357	1341	11.03	.0001	.48	.2268E-03	.1374E-01
92.110	266	.380	.0408	.0396	.0402	1340	1330	10.08	-.0012	.69	.1442E-03	.8980E-02
92.120	254	.400	.0499	.0487	.0493	1332	1322	9.65	-.0012	.78	.1607E-03	.9914E-02
92.100	254	.412	.0525	.0515	.0520	1328	1317	9.43	-.0010	.76	.1620E-03	.9996E-02
93.400	264	.184	.0358	.0336	.0347	1323	1315	9.19	-.0022	.49	.6583E-04	.4097E-02
93.500	261	.292	.0508	.0491	.0500	1353	1343	10.78	-.0017	.54	.1223E-03	.7582E-02
93.600	252	.357	.0530	.0550	.0540	1363	1337	11.41	.0020	.24	.1622E-03	.9979E-02
93.700	251	.380	.0601	.0584	.0593	1375	1366	12.14	-.0017	.68	.1915E-03	.1176E-01
93.800	251	.400	.0614	.0597	.0605	1374	1365	12.07	-.0017	.74	.2011E-03	.1234E-01
93.900	251	.434	.0638	.0604	.0621	1369	1369	11.75	-.0034	15.42	.2177E-03	.1336E-01
93.100	251	.520	.0712	.0695	.0704	1394	1386	13.35	-.0018	.98	.2870E-03	.1759E-01
93.110	245	.520	.0740	.0725	.0732	1403	1394	13.98	-.0016	.82	.3107E-03	.1895E-01
93.120	250	.542	.0726	.0710	.0718	1406	1397	14.19	-.0016	.86	.3156E-03	.1932E-01
94.100	245	.595	.0878	.0862	.0870	1417	1408	14.98	-.0016	.93	.3795E-03	.2311E-01
94.200	245	.542	.0967	.0941	.0954	1423	1419	15.44	-.0027	1.64	.3594E-03	.2187E-01
94.300	231	.380	.0617	.0597	.0607	1394	1386	13.39	-.0020	.68	.2473E-03	.1489E-01
94.400	245	.325	.0519	.0498	.0508	1377	1369	12.22	-.0022	.68	.1735E-03	.1059E-01
50.200	388	.740	.0041	.0230	.0135	1077	1013	1.92	.0189	.99	.2484E-04	.1704E-02
50.300	362	.580	.0098	.0286	.0192	1093	1017	2.16	.0189	.61	.2398E-04	.1621E-02
50.400	368	.820	.0106	.0322	.0214	1126	1044	2.74	.0216	.66	.4013E-04	.2716E-02
50.500	389	.960	.0058	.0273	.0166	1137	1059	2.95	.0214	.76	.4571E-04	.3125E-02
50.600	393	.800	.0142	.0339	.0241	1115	1042	2.53	.0197	.76	.3281E-04	.2251E-02
51.100	359	1.630	.0256	.0454	.0355	1150	1097	3.22	.0198	1.65	.1071E-03	.7197E-02
51.110	397	1.630	.0178	.0404	.0291	1155	1091	3.32	.0227	1.37	.8718E-04	.5974E-02
51.120	388	1.700	.0233	.0393	.0313	1129	1099	2.79	.0161	3.21	.9019E-04	.6156E-02
52.400	380	2.240	.0310	.0485	.0398	1180	1144	3.92	.0175	2.68	.1661E-03	.1125E-01
52.500	370	2.240	.0293	.0510	.0401	1191	1136	4.21	.0217	1.74	.1764E-03	.1189E-01
52.600	368	2.240	.0284	.0505	.0394	1192	1135	4.24	.0221	1.68	.1787E-03	.1203E-01
52.900	383	2.600	.0402	.0606	.0504	1222	1171	5.12	.0204	1.82	.2315E-03	.1568E-01
52.100	407	2.560	.0335	.0514	.0425	1188	1156	4.12	.0178	3.31	.1751E-03	.1202E-01
53.102	407	2.550	.0306	.0495	.0400	1204	1163	4.56	.0189	2.41	.1863E-03	.1278E-01
53.200	401	3.000	.0353	.0554	.0454	1240	1193	5.71	.0201	2.07	.2731E-03	.1863E-01
53.300	390	3.000	.0372	.0573	.0473	1241	1194	5.74	.0200	2.05	.2894E-03	.1964E-01
54.850	375	2.370	.0533	.0712	.0623	1260	1203	6.44	.0180	1.26	.2686E-03	.1806E-01
54.100	404	2.370	.0425	.0626	.0526	1278	1209	7.12	.0201	.99	.2463E-03	.1680E-01
54.100	407	2.480	.0513	.0693	.0603	1300	1238	8.11	.0180	1.01	.2902E-03	.1979E-01
54.200	368	2.480	.0637	.0822	.0729	1292	1228	7.72	.0185	1.02	.3386E-03	.2264E-01
55.300	380	2.440	.0584	.0769	.0676	1300	1233	8.07	.0186	.94	.3227E-03	.2171E-01
55.340	387	2.380	.0545	.0721	.0633	1297	1234	7.94	.0176	.98	.3031E-03	.2047E-01
55.400	393	2.440	.0584	.0743	.0664	1289	1236	7.59	.0159	1.20	.2966E-03	.2009E-01
67.120	377	.650	.0085	.0251	.0168	1056	1002	1.65	.0166	1.13	.2066E-04	.1411E-02
67.123	370	.650	.0088	.0256	.0172	1056	1001	1.65	.0168	1.12	.2131E-04	.1450E-02
67.100	380	.650	.0065	.0233	.0149	1051	997	1.58	.0168	1.19	.1960E-04	.1341E-02
67.200	371	.650	.0114	.0277	.0196	1042	992	1.48	.0163	1.34	.1959E-04	.1334E-02
68.700	385	2.750	.0672	.0786	.0729	1318	1283	8.94	.0114	1.72	.4210E-03	.2834E-01
68.800	384	2.780	.0764	.0811	.0788	1290	1289	7.64	.0047	47.84	.4042E-03	.2722E-01
68.900	358	2.820	.0830	.0909	.0870	1326	1305	9.35	.0079	2.74	.5377E-03	.3564E-01
75.700	371	2.160	.0829	.0891	.0860	1333	1310	9.70	.0063	1.89	.3959E-03	.2641E-01
75.800	382	2.060	.0871	.0922	.0897	1324	1306	9.24	.0050	2.42	.3455E-03	.2320E-01
75.900	364	2.060	.0846	.0940	.0893	1351	1311	10.70	.0094	.99	.4097E-03	.2722E-01
81.300	357	2.240	.0430	.0587	.0508	1162	1138	3.48	.0157	4.28	.1749E-03	.1172E-01
81.700	364	2.460	.0410	.0632	.0521	1203	1147	4.55	.0222	1.77	.2152E-03	.1444E-01
81.800	397	2.600	.0384	.0566	.0475	1201	1164	4.48	.0182	2.75	.1992E-03	.1360E-01

TABLE G-II Cont'd

CODE	MDOT	DELP	X1	X2	XAVG	T1	T2	P1	DELX	DP/EQDP	F	F/FG
81.120	401	2.930	.0395	.0562	.0479	1217	1188	4.96	.0167	3.52	.2468E-03	.1686E-01
82.100(1)	369	2.920	.0484	.0671	.0577	1232	1190	5.43	.0186	2.35	.3040E-03	.2041E-01
83.300	362	.580	.0051	.0202	.0126	1029	983	1.34	.0151	1.39	.1699E-04	.1153E-02
69.110	494	2.960	.0394	.0552	.0473	1335	1285	9.81	.0159	1.24	.2894E-03	.2044E-01
69.120	492	3.030	.0447	.0548	.0497	1303	1284	8.25	.0101	3.45	.2752E-03	.1945E-01
69.100	507	3.060	.0388	.0494	.0441	1321	1296	9.07	.0106	2.66	.2820E-03	.2002E-01
69.140	507	3.100	.0413	.0521	.0467	1302	1281	8.18	.0108	3.33	.2618E-03	.1861E-01
69.200	507	3.060	.0435	.0542	.0488	1291	1272	7.70	.0108	3.70	.2458E-03	.1749E-01
74.300	490	2.380	.0521	.0651	.0586	1338	1292	9.97	.0130	1.05	.2415E-03	.1703E-01
74.400	508	2.380	.0475	.0616	.0546	1327	1278	9.42	.0142	1.04	.2117E-03	.1505E-01
74.500	493	2.380	.0514	.0655	.0584	1329	1279	9.47	.0141	1.03	.2261E-03	.1597E-01
83.900(1)	496	2.920	.0344	.0499	.0421	1312	1267	8.63	.0154	1.50	.2551E-03	.1806E-01
83.100(1)	495	3.070	.0461	.0568	.0515	1291	1272	7.70	.0107	3.74	.2585E-03	.1831E-01
83.800(2)	522	2.060	.0359	.0508	.0433	1311	1257	8.62	.0149	.89	.1583E-03	.1132E-01
83.900(2)	473	2.060	.0437	.0579	.0508	1316	1262	8.82	.0142	.89	.1980E-03	.1388E-01
84.120(1)	484	2.380	.0625	.0742	.0683	1326	1287	9.36	.0116	1.29	.2378E-03	.1674E-01
87.800	502	.109	.0133	.0124	.0128	1309	1298	8.52	-.0009	.21	.9971E-05	.7070E-03
87.830	501	.109	.0115	.0115	.0115	1322	1307	9.16	-.0000	.14	.1058E-04	.7490E-03
87.103	499	.163	.0178	.0148	.0163	1379	1377	12.39	-.0029	1.09	.2149E-04	.1515E-02
87.110	494	.272	.0175	.0159	.0167	1377	1370	12.24	-.0016	.61	.3586E-04	.2523E-02
87.113	481	.163	.0194	.0177	.0186	1376	1368	12.20	-.0017	.32	.2251E-04	.1576E-02
88.100	496	.651	.0294	.0284	.0289	1406	1399	14.23	-.0010	1.32	.9728E-04	.6838E-02
88.200	504	.923	.0273	.0276	.0275	1413	1402	14.66	.0004	1.21	.1360E-03	.9590E-02
88.300	491	.923	.0343	.0338	.0341	1383	1377	12.64	-.0006	2.50	.1269E-03	.8913E-02
89.300	499	.217	.0162	.0140	.0151	1332	1328	9.64	-.0022	.97	.2288E-04	.1617E-02
89.400	485	.272	.0187	.0182	.0185	1335	1323	9.79	-.0005	.45	.3020E-04	.2123E-02
89.500	498	.054	.0105	.0105	.0105	1301	1284	8.12	-.0000	.08	.4757E-05	.3369E-03
90.630	491	.054	.0123	.0114	.0118	1300	1287	8.07	-.0009	.10	.4911E-05	.3470E-03
90.700	502	.109	.0124	.0111	.0117	1301	1292	8.15	-.0013	.26	.9630E-05	.6831E-03
90.730	494	.109	.0142	.0128	.0135	1305	1296	8.33	-.0013	.25	.1018E-04	.7192E-03
70.120	624	3.070	.0312	.0441	.0377	1293	1267	7.80	.0129	2.74	.1617E-03	.1197E-01
70.100	599	3.030	.0335	.0459	.0397	1289	1264	7.62	.0124	2.96	.1703E-03	.1251E-01
73.800	625	2.440	.0300	.0419	.0360	1332	1295	9.67	.0119	1.34	.1515E-03	.1119E-01
73.900	600	2.440	.0341	.0487	.0414	1337	1267	9.90	.0146	1.02	.1627E-03	.1193E-01
73.100	622	2.440	.0263	.0421	.0342	1336	1281	9.84	.0158	.95	.1489E-03	.1099E-01
73.110	622	2.440	.0281	.0426	.0353	1331	1283	9.62	.0145	1.07	.1484E-03	.1095E-01
83.100(2)	643	2.060	.0140	.0290	.0215	1316	1262	8.82	.0150	.89	.1070E-03	.7957E-02
84.600	606	2.440	.0356	.0542	.0449	1344	1276	10.30	.0186	.75	.1582E-03	.1162E-01
84.700	606	2.490	.0379	.0500	.0439	1336	1298	9.88	.0120	1.32	.1673E-03	.1228E-01
88.400	621	.706	.0188	.0209	.0199	1383	1365	12.63	.0021	.64	.5917E-04	.4349E-02
88.500	621	.869	.0195	.0223	.0209	1380	1361	12.46	.0027	.74	.7174E-04	.5273E-02
88.600	627	1.030	.0221	.0238	.0229	1368	1356	11.71	.0017	1.46	.8007E-04	.5901E-02
88.700	629	.489	.0128	.0128	.0128	1348	1338	10.50	-.0000	.96	.3454E-04	.2550E-02
88.800	605	.869	.0178	.0196	.0187	1338	1324	9.95	.0018	1.26	.6272E-04	.4599E-02
88.900	599	.869	.0193	.0215	.0204	1333	1318	9.73	.0022	1.13	.6245E-04	.4572E-02
89.100	622	1.680	.0285	.0334	.0310	1364	1345	11.47	.0049	1.52	.1282E-03	.9436E-02
89.110	630	.977	.0083	.0102	.0093	1339	1327	10.03	.0019	1.54	.6564E-04	.4850E-02
89.120	623	.489	.0107	.0128	.0117	1317	1299	8.90	.0021	.57	.2975E-04	.2197E-02
89.100	611	.597	.0122	.0137	.0130	1304	1291	8.29	.0014	.98	.3584E-04	.2639E-02
71.110	742	1.950	.0170	.0284	.0227	1306	1269	8.35	.0114	1.23	.7529E-04	.5751E-02
72.200	714	2.580	.0216	.0376	.0296	1340	1287	10.09	.0160	1.00	.1226E-03	.9282E-02
72.300	740	2.580	.0185	.0376	.0281	1344	1278	10.32	.0191	.81	.1129E-03	.8609E-02
72.400	752	2.330	.0203	.0355	.0279	1341	1288	10.16	.0153	.90	.1005E-03	.7684E-02
72.500	746	2.580	.0196	.0351	.0273	1345	1294	10.38	.0155	1.01	.1160E-03	.8851E-02
83.400	744	2.860	.0172	.0306	.0239	1289	1259	7.62	.0135	2.35	.1029E-03	.7868E-02
84.100	722	2.380	.0391	.0548	.0469	1338	1283	9.97	.0157	.91	.1091E-03	.8279E-02

APPENDIX H

TABLES OF VOID FRACTION RESULTS

TABLE H-I

SINGLE-PHASE GAMMA RAY ATTENUATION
MEASUREMENTS FOR CALIBRATION

CODE	Flow Condition	Average Temp. °F	Uncorrected Average Count Rates, cps		Phototube Temp., °F	
			Collimated Beam	Background	Collimated Beam	Background
79.6	All Liquid	500	3802	3560	134	134
80.7	All Vapor	551	5583	3481	133	133

TABLE H-II

EXPLANATION OF COLUMNAR HEADINGS

CODE	Code number for data point. Number to left of decimal refers to the page number in University of Michigan Research Institute Data Book No. 3496 on which the raw data are recorded. The number to the right of the decimal refers to the time the data were taken. Parenthetic numbers refer to more than one data point at same hours.
MDOT	Total mass flow rate, lb/hr.
XTT	Martinelli two-phase flow parameter, given by Equation (13).
SLIP RATIO	Ratio of mean vapor velocity to mean liquid velocity, given by Equation (5).

(The numerical notation X.XXXX E $\pm$ yy is equivalent tc X.XXXX . $10^{\pm yy}$.)

TABLE H-II

RESULTS OF VOID FRACTION STUDY

IN HORIZONTAL TWO-PHASE FLOWS OF 8-92 NA-K

	EXPERIMENTAL DATA							DERIVED RESULTS		
CODE	QUALITY	TEMP F	UNCORRECTED MEAN COUNT RATE, CPS BEAM	BACKGD	PHOTUBE TEMP, F BEAM	BACKGD	MDOT	VOID FRACTION	XTT	SLIP RATIO VG/VL
51.12	.0313	1114	6014	4746	147	148	388	.7456	.301E 00	.910E 02
51.11	.0404	1123	6712	5134	140	140	397	.8603	.244E 00	.532E 02
55.4	.0633	1266	5835	4914	140	128	390	.5700	.242E 00	.169E 03
56.8	.1100	1285	6734	5192	150	148	274	.8442	.148E 00	.680E 02
56.9	.1368	1255	6844	5390	150	150	249	.8151	.109E 00	.126E 03
59.5	.0581	1130	4787	4111	132	132	291	.4170	.177E 00	.641E 03
60.11	.0468	1057	5310	4150	130	128	259	.6996	.171E 00	.257E 03
62.10	.0386	1060	4656	3951	147	145	259	.4447	.207E 00	.599E 03
63.3	.0195	879	5078	4364	140	138	267	.4712	.191E 00	.115E 04
64.10	.0214	936	5327	4393	138	137	255	.5995	.224E 00	.456E 03
64.11	.0234	945	5369	4265	139	140	255	.6820	.214E 00	.324E 03
65.10	.0259	1002	4672	4041	140	140	261	.3951	.243E 00	.747E 03
67.12	.0172	1028	4631	3935	140	140	371	.4416	.390E 00	.334E 03
68.9	.0870	1315	5570	4663	156	156	358	.5561	.201E 00	.194E 03
69.1	.0467	1292	5506	4432	140	140	507	.6470	.346E 00	.768E 02
72.4	.0273	1320	4058	3626	160	160	749	.1528	.613E 00	.386E 03
78.1	.1647	1159	5612	4160	158	158	131	.8108	.680E-01	.284E 03

**** ALL INPUT DATA HAVE BEEN PROCESSED.
AT LOC 15717

APPENDIX I

THEORY OF RADIATION ATTENUATION METHOD FOR MEASURING VOID FRACTION

Maurer (58), Petrick (65), Hooker and Popper (38), and Richardson(74) all give developments of the theory of gamma-ray attenuation as applied to measuring void fractions.

Following Maurer's discussion, the intensity of a monoenergetic beam of electromagnetic radiation emerging from an absorber is given by

$$I = I_o e^{-\left(\frac{\mu}{\rho}\right)\rho t} \tag{I-1}$$

where I_o = intensity of beam entering the absorber

t = absorber thickness

ρ = absorber density

$\left(\frac{\mu}{\rho}\right)$ = mass absorption coefficient of absorber

μ = linear absorption coefficient (dimensions are reciprocal length)

Equation I-1 is a statement of the well-known Beer-Lambert Law, in which the absorber is presumed to be homogeneous and the radiation beam is presumed to consist of parallel rays.

Referring to Figure I-1, if the incident beam has a finite size and passes through several materials, the intensity of emerging radiation will be given as:

$$I = \int_o^{y_1} \left\{ \frac{I_o}{y_1} \cdot \exp\left[-\int_o^{z_1} \left(\frac{\mu}{\rho}\right)_{z,y} \rho_{z,y}\, dz \right] \right\} dy \tag{I-2}$$

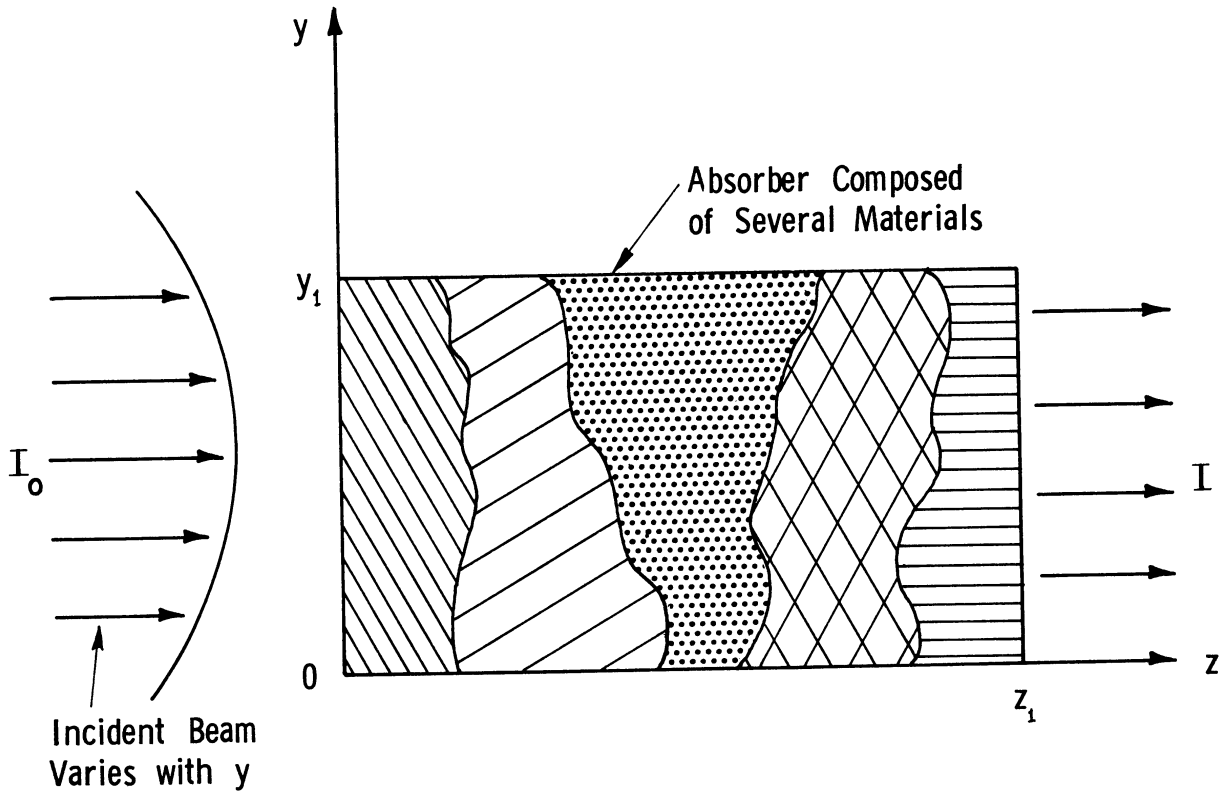

Figure I-1. Nonuniform Radiation Beam Passing Through a Nonhomogeneous Absorber

where the subscript (z,y) denotes that $\left(\frac{\mu}{\rho}\right)$ and ρ are functions of z and y. Implied in this integration is the fact that in the general two-dimensional case, the incident beam intensity I_o varies with the y coordinate. The result I is a pseudo uniformly strong beam due to the normalizing factor $1/y_1$. The case considered here is not completely general in the sense that it could be extended to three-dimensional geometry. Since the radiation is passing through a slab composed of several materials, one must deal with discontinuities in the functions $(\mu/\rho)_{z,y}$ and $\rho_{z,y}$.

Consider the more common and less complicated case where a uniform beam impinges on a laminated slab. If each of the n lamina is taken as having constant density and constant mass absorption coefficient, Equation (I-2) reduces to

$$I = I_o \cdot \exp\left[-\sum_{i=1}^{n} \left(\frac{\mu}{\rho}\right)_i \rho_i t_i \right] \qquad \text{(I-3)}$$

If density or thickness of material are the only variables, the density or thickness can be measured using the basic Equation (I-1) if I_o and (μ/ρ) are known.

$$t\rho = \frac{\ell n\ (I/I_o)}{-\ (\mu/\rho)} \qquad \text{(I-4)}$$

The value of I is measured experimentally. In practice it is often impossible to predict (μ/ρ) and I_o, so it is necessary to resort to calibration techniques which eliminate the difficulty.

Consider now the use of a gamma-ray source to measure the mean density of a two-phase fluid. A suitably collimated beam of radiation is passed through a flow channel, with the emergent beam intensity measured by a suitable detector. One way of circumventing the difficulties caused by not knowing I_o and (μ/ρ) is to take readings with all-vapor and all-liquid flows. Let

I_ℓ = intensity of emergent beam with all-liquid flow

I_g = intensity of emergent beam with all-vapor flow

Then

$$I_\ell = I_o \cdot \exp\left[- (\mu/\rho)\, \rho_\ell t_\ell - (\mu/\rho)_s\, \rho_s t_s \right] \qquad \text{(I-5)}$$

$$I_g = I_o \cdot \exp\left[- (\mu/\rho)\, \rho_g t_g - (\mu/\rho)_s\, \rho_s t_s \right] \qquad \text{(I-6)}$$

The subscript s refers to the solid channel wall through which the beam must pass. By dividing Equations (I-5) and (I-6), taking logarithms and rearranging,

$$(\mu/\rho) = \frac{\ell n\, (I_g/I_\ell)}{t\, (\rho_\ell - \rho_g)} \qquad \text{(I-7)}$$

In single-phase flows it is clear that $t_\ell = t_g$, which appear as t in Equation (I-7). Implied in Equation (I-7) is the fact that for a given absorber the mass absorption coefficient (μ/ρ) is essentially constant at given gamma energies, regardless of physical state of the absorber. Thus, Equation (I-7) is valid for a single chemical species.

If a two-phase mixture occupies the channel, the emergent beam intensity can be written in the same form as Equations (I-5) and (I-6).

$$I = I_o \cdot \exp\left[- (\mu/\rho)\, \bar{\rho}\, t - (\mu/\rho)_s\, \rho_s t_s \right] \qquad \text{(I-8)}$$

where $\bar{\rho}$ represents the mean mixture density.

In order to eliminate I_o from Equation (I-8), Equation (I-5) or (I-6) may be used. Since in the potassium experiments all-liquid flows are easier to achieve than all-vapor flows, Equation (I-5) is divided into Equation (I-8)

$$\ell n\, I/I_\ell = - (\mu/\rho)\, \bar{\rho}\, t + (\mu/\rho)\, \rho_\ell t$$

Inserting the value of (μ/ρ) from Equation (I-7),

$$\ell n\left(I/I_\ell\right) = \ell n\ (I_g/I_\ell)\left[(\rho_\ell t - \bar{\rho}t)\ \frac{1}{t\ (\rho_\ell - \rho_g)}\right]$$

Finally,

$$\frac{\ell n\ (I/I_\ell)}{\ell n\ (I_g/I_\ell)} = \frac{\rho_\ell - \bar{\rho}}{\rho_\ell - \rho_g} \qquad \text{(I-9)}$$

From Equation (I-9) the mean mixture density is obtained from the emergent beam intensity I. In addition, it is necessary to establish the single-phase intensities I_g and I_ℓ from calibration runs.

It is easy to transform Equation (I-9) to make the void fraction α the dependent variable rather than the mean density $\bar{\rho}$. The void fraction by definition is the volume fraction occupied by vapor at a point (small region) in the two-phase flow. In measuring mean mixture densities by radiation attenuation, it is necessary to pass the rays through the entire channel or at least through some chord of the channel. Because of this technique, the void fractions obtained are not point values but are mean values occurring at the channel's axial location where the test equipment is placed. Hence, in this discussion the term "void fraction" will refer to the mean values so obtained. Let

α = void fraction

A = cross sectional flow area at a given channel position

For purposes of the following discussion, the void fraction may be thought of as the fraction of flow cross section occupied by vapor. Then

mass of liquid at a section per unit length = $\rho_\ell(1-\alpha)A$

mass of vapor at a section per unit length = $\rho_g \alpha A$

total mass at a section per unit length = $\bar{\rho}A$

By mass balance

$$\bar{\rho}\ A = \rho_\ell\ (1-\alpha)\ A + \rho_g\ \alpha\ A$$

so that

$$\bar{\rho} = \rho_g \alpha + \rho_\ell (1-\alpha) \tag{I-10}$$

Insertion of Equation (I-10) into Equation (I-9) yields

$$\alpha = \frac{\ell n\ I/I_\ell}{\ell n\ I_g/I_\ell} \tag{I-11}$$

Equation (I-11) is valid for data processing to obtain void fractions as long as the two phases are sufficiently mixed to behave in pseudo-homogeneous fashion. This relationship is also valid for separated phase distributions, if the phases are distributed with respect to the gamma-ray beam as in Figure (I-2a) (38, 65, 74). Here the separated phases exist as lamina oriented perpendicular to the radiation beam.

The separated phase distribution of Figure (I-2a) represents one extreme case. Another extreme case is given in Figure (I-2b) where the phases exist as lamina oriented in the direction of the radiation beam. It can be readily shown (23, 65, 74) that the overall attenuation is expressed by

$$\alpha = \frac{I - I_\ell}{I_g - I_\ell} \tag{I-12}$$

Comparing the two extreme separated phase distributions given in Figure I-2, with results expressed by Equations (I-11) and (I-12), it is apparent that the expression used for data processing depends strongly on how the phases are oriented with respect to the radiation beam.

Detector count rates, N, rather than beam intensities can be used in Equations (I-11) and (I-12). Some investigators (38, 65, 74) have used a recorded voltage signal rather than count rates in their equations.

In utilizing Equation (I-11) or Equation (I-12) to calculate void fractions, care must be taken to account for temperature effects. Put more explicitly, if the single-phase emergent intensities are determined at flow

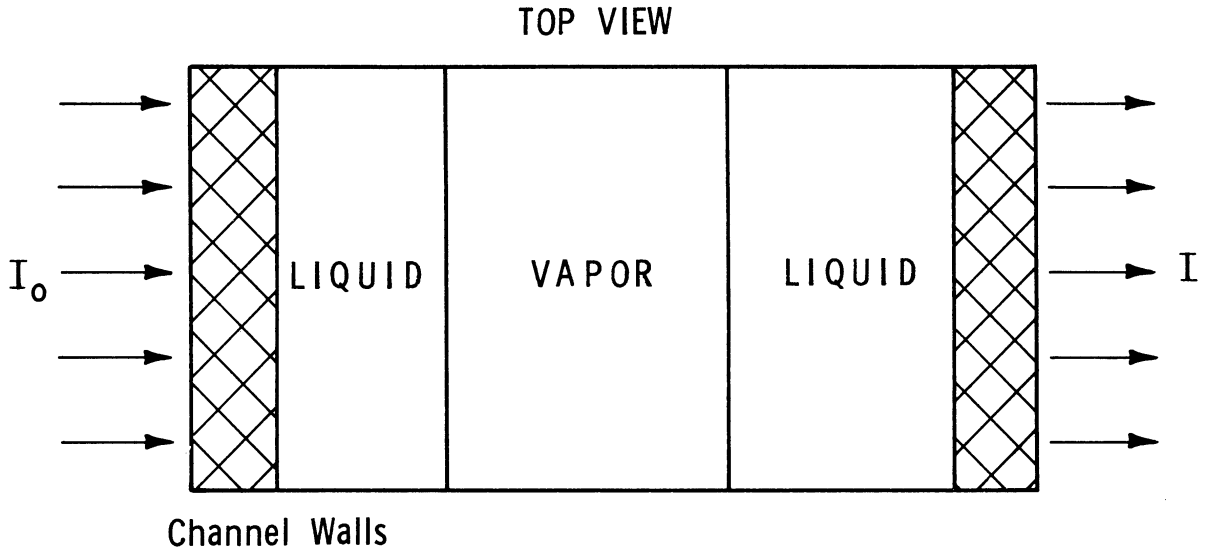

(a) Separated Phase Distribution Giving Overall Radiation Attenuation Same as for Homogeneous Mixture

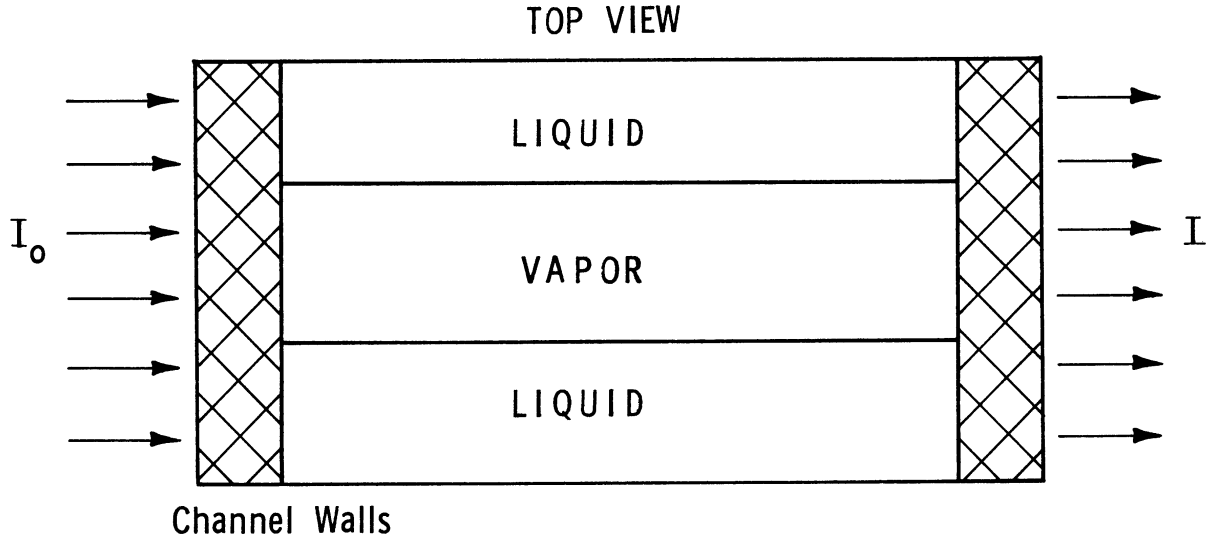

(b) Separated Phase Distribution Giving Overall Radiation Attenuation Completely Different from Homogeneous Mixture

Figure I.2. Two Extreme Cases of Separated Phase Distribution.

temperatures different from the two-phase flow temperatures, the calculated void fractions will be in error. Egen, Dingee, and Chastain (23) made a thorough analysis showing clearly how to compensate for effects arising from different temperatures. The following discussion is based on their work.

As an example, assume that a two-phase system is flowing essentially homogeneously so that the void fraction is given by

$$\alpha = \frac{\ell n\ (I/I_\ell)}{\ell n\ (I_g/I_\ell)} \qquad \text{(I-11)}$$

To be strictly correct the I's in Equation (I-11) must all be measured at the same temperature. For an all-liquid flow at temperature T_o, the emergent beam intensity is obtained from Equation (I-5) as

$$(I_\ell)_{T_o} = I_o \exp\left\{ -\left[\left(\frac{\mu}{\rho}\right)\rho_\ell t_\ell\right]_{T_o} - \left[\left(\frac{\mu}{\rho}\right)_s \rho_s t_s\right]_{T_o}\right\} \qquad \text{(I-13)}$$

where the subscript T_o indicates the temperature dependence of the densities and mass absorption coefficients. Likewise for an all-vapor flow, Equation (I-6) gives

$$(I_g)_{T_o} = I_o \exp\left\{ -\left[\left(\frac{\mu}{\rho}\right)\rho_g t_g\right]_{T_o} - \left[\left(\frac{\mu}{\rho}\right)_s \rho_s t_s\right]_{T_o}\right\} \qquad \text{(I-14)}$$

For single-phase flows $t_\ell = t_g = t$. Dividing Equations (I-13) and (I-14) and taking logarithms,

$$\ell n\ (I_g/I_\ell)_{T_o} = t\ (\mu/\rho)_{T_o} \cdot (\rho_\ell - \rho_g)_{T_o} \qquad \text{(I-15)}$$

This equation may be extended immediately to any flow temperature T. Thus,

$$\ell n\ (I_g/I_\ell)_{T} = t\ (\mu/\rho)_{T} \cdot (\rho_\ell - \rho_g)_{T} \qquad \text{(I-16)}$$

Now, the mass absorption coefficient at a given gamma energy is essentially independent of temperature over appreciable temperature ranges (23). It is

reasonable, then, to take (μ/ρ) as a constant. By dividing Equations (I-15) and (I-16) one obtains, upon rearrangement

$$\ell n\ (I_g/I_\ell)_T = \left[\ell n\ (I_g/I_\ell)_{T_o}\right] \cdot \left[\frac{(\rho_\ell-\rho_g)_T}{(\rho_\ell-\rho_g)_{T_o}}\right] \tag{I-17}$$

It is convenient to let

$$C = \frac{\ell n\ (I_g/I_\ell)_{T_o}}{(\rho_\ell - \rho_g)_{T_o}} \tag{I-18}$$

The constant C can be obtained from a single I_g/I_ℓ measurement at temperature T_o. Of course, it is assumed that fluid densities are known as functions of temperature. Using Equation (I-18), Equation (I-17) becomes

$$\ell n\ (I_g/I_\ell)_T = C\ (\rho_\ell - \rho_g)_T \tag{I-19}$$

Equations (I-18) and (I-19) establish the denominator of Equation (I-11) as a function of temperature with only one measurement of I_g/I_ℓ necessary. Egen and co-workers (23) substantiated Equation (I-17) experimentally with water-steam data.

Consider next the numerator of Equation (I-11). Here also the I_ℓ value must be corrected to the same flow temperature as the I measurement. Recalling Equation (I-13) it readily follows that

$$\frac{(I_\ell)_{T_o}}{(I_\ell)_T} = \exp\left\{ -\left[\left(\frac{\mu}{\rho}\right) \rho_\ell t_\ell\right]_{T_o} -\left[\left(\frac{\mu}{\rho}\right)_s \rho_s t_s\right]_{T_o} +\left[\left(\frac{\mu}{\rho}\right) \rho_\ell t_\ell\right]_T +\left[\left(\frac{\mu}{\rho}\right)_s \rho_s T_s\right]_T \right\}$$

For the solid channel wall both the density and mass absorption coefficient may be taken as constant. Then

$$\ell n\ \frac{(I_\ell)_T}{(I_\ell)_{T_o}} = t\cdot(\mu/\rho)\cdot\left(\rho_{\ell_{T_o}} - \rho_{\ell_T}\right) \tag{I-20}$$

It is valid to divide Equation (I-20) by Equation (I-15) which will eliminate the (μ/ρ) term assuming it is constant

$$\frac{\ell n \dfrac{(I_\ell)_T}{(I_\ell)_{T_o}}}{\ell n (I_g/I_\ell)_{T_o}} = \frac{\rho_{\ell_{T_o}} - \rho_{\ell_T}}{(\rho_\ell - \rho_g)_{T_o}}$$

By inserting Equation (I-18) and rearranging

$$(I_\ell)_T = (I_\ell)_{T_o} \cdot \exp\left[C \cdot \left(\rho_{\ell_{T_o}} - \rho_{\ell_T} \right) \right] \qquad \text{(I-21)}$$

Equation (I-21) is the desired result, as it corrects the all-liquid calibration value obtained at temperature T_o to the temperature T of the two-phase flow. This, then, is the correction necessary in the numerator of Equation (I-11).

The two single-phase calibration values I_g and I_ℓ in general are obtained at different temperatures, but to utilize Equation (I-18) both single-phase values are desired at the same calibration temperature T_o. The I_ℓ value can be adjusted quite easily to correspond to the temperature at which I_g is obtained. Assume that $(I_g)_{T_o}$ and $(I_\ell)_T$ are known and it is desired to adjust $(I_\ell)_T$ to $(I_\ell)_{T_o}$. From Equation (I-21), taking logarithms

$$\ell n (I_\ell)_{T_o} = \ell n (I_\ell)_T + C (\rho_{\ell_T} - \rho_{\ell_{T_o}})$$

Inserting the value of C from Equation (I-18) and rearranging,

$$\ell n (I_\ell)_{T_o} = \frac{\ell n (I_\ell)_T + \dfrac{\rho_{\ell_T} - \rho_{\ell_{T_o}}}{(\rho_\ell - \rho_g)_{T_o}} \ell n (I_g)_{T_o}}{1 + \dfrac{\rho_{\ell_T} - \rho_{\ell_{T_o}}}{(\rho_\ell - \rho_g)_{T_o}}} \qquad \text{(I-22)}$$

Equation (I-22) provides the necessary adjustment in I_ℓ to allow evaluation of $(I_g/I_\ell)_{T_o}$ from calibration runs at two different temperatures. Equations (I-18) and (I-19) can then be easily applied.

In obtaining the temperature correction expressions, it should be noted that no assumptions were made as to phase distribution effects, except for the purpose of example. Thus, the corrective terms could be applied or adapted to any other valid data processing equation.